Dissertation zur Erlangung des Doktorgrades

der Fakultät für Chemie und Pharmazie

der Ludwig-Maximilians-Universität München

Receptor-targeted dual pH-triggered intracellular protein transfer

Meng Lyu

aus

Weifang, Shandong, China

2022

To my family

致家人

Try not to become a man of success but rather try to become a man of value.

—— Albert Einstein

Table of Contents

1 Introduction

1.1 Protein therapeutics

Proteins are large, extraordinary biomolecules with tertiary or quaternary structures that impart important functions such as selectivity, specificity, and high potency to the body. So many different types of proteins such as enzymes, cytokines, IFNs, and antibodies are participating in various biological pathways and have diverse functionalities.[1] Also, proteins are key macromolecules responsible for the crucial building, functioning, and maintenance tasks in life. However, protein malfunction is a common cause of many disorders, making protein an attractive therapy method.[2, 3]

About protein therapeutics, diphtheria serum therapy developed in the 1890s by Behring, the first laureate of the Nobel Prize in Medicine and Physiology, dates back to the earliest antibody-based therapeutics. The late 20th century was a turning point in the rapid development of protein therapy due to a few key biotechnology developments.[4] Since insulin was approved as the first recombinant anti-diabetic protein to replace its natural counterpart that can be deficient in diabetes in 1982, the development of protein-based drugs has been the focus of great interest.[5] Then, other recombinant proteins were discovered as therapeutics to replace the natural proteins deficient in the body (e.g., growth hormone) or augment existing pathways (e.g., interferon-α and erythropoietin). In 1986, muromonab-CD3, a murine monoclonal antibody targeting CD3 on T cells, was developed as the first monoclonal antibody therapy and approved by the FDA for use during organ transplant to reduce acute rejection.[6, 7]

Over the last decades, this area has witnessed the impressive therapeutic potential of protein drugs widely varying in type and activity. Nowadays, protein therapeutics are the fastest-growing segment of the biopharmaceutical industry that is rapidly gaining importance in medicine, and more than 130 recombinant protein therapeutics have been approved (around 25 new approvals annually) by the US Food and Drug Administration

(FDA). With prediction, the global biopharmaceutical market value will reach $389 million by 2024.[8]

Protein therapeutics, including monoclonal antibodies, cytokines, transcription factors, enzymes, and peptides, play an essential role against cancer, infectious diseases, cardiovascular disorders, immunological diseases, and metabolic disorders, resulting in brilliant successes.[9-11] Compared with chemotherapy, the critical function of protein therapeutics in treating diseases that lack effective therapeutic options relies on the unique advantages of (i) abundant species; (ii) complex set of biological functions; (iii) high specificity; (iv) fewer adverse effects; (v) excellent biocompatibility and biodegradability; and (vi) inherent amino, carboxyl, and hydroxyl groups for chemical conjugations.[12]

Proteins, in contrast to genetic drugs, act on their targets in a way that is both more direct and more specific. This allows them to regulate biological processes in a way that eliminates the risk of permanent gene mutation, off-target effects brought on by persistent gene expression, and the possibility of cancer development.[11]

1.2 Major challenges of protein therapeutics

The progress path toward clinical application of proteins is neither straightforward nor uncomplicated, for example, due to the limited administration routes, low bioavailability of proteins in circulation, and host immune responses that may result in the inactivation of proteins before reaching their sites of action.[13] Therefore, biotechnologists have employed tremendous efforts to overcome the delivery drawbacks[2, 14, 15] to protect them from denaturation and degradation, facilitate tumor-targeted delivery, and control the protein release/activity in targeted sites.[16, 17]

Most protein medicines now available on the market were created based on extracellular targets. These extracellular targets include cell membrane proteins (PD1, HER2, CD20, etc.) and secretory proteins (TNFα, IL12, VEGF, etc.).[11, 18] Despite the success of current protein products that mostly address extracellular targets, efficient cytosolic delivery of

bioactive proteins still remains a major challenge.[19-21] Because proteins are macromolecular in nature and are endowed with a hydrophilic feature, they are generally incapable of passing through membranes. Nevertheless, cytosolic protein delivery is also an extremely important topic in the field of molecular cell biology and cutting-edge biotechnology because more than 70% of the proteins encoded by the genome are located inside cells.[22]

In order to remedy this flaw, carriers or modifications that can facilitate the transport of proteins across cell membranes are required. As a result, in recent years a growing amount of focus has been placed on the development of methods that are both simple and effective for protein cytosolic delivery.[23]

1.3 Strategies for intracellular protein delivery

To overcome these shortcomings of protein therapeutics, several physical methods have been developed*,* mainly based on the *in vitro* induction of transient and rapid cell membrane permeabilization such as electroporation,[24, 25] acoustic fields,[26] membrane perforating nanowires,[27] or microfluidic constrictions.[28, 29] But due to the shortcomings of the physical methods such as inefficient, not scalable, and cytotoxic, it is hard to translate *in vivo* intracellular delivery of protein therapeutics.[30]

With the development of nanotechnology, a new generation to replace the physical methods of delivery strategies with multiple functions (e.g., tumor targeting, deep tumor penetration, and effective cellular uptake) was come up to address these limitations. Among them, non-covalent and covalent modification strategies attracted widespread attention.[31]

1.3.1 Strategy of non-covalent modification for intracellular protein delivery

The emergence of nanotechnology shed light on carrier-dependent protein delivery,[21] where attention has been dedicated to numerous platforms such as inorganic nanoparticles,[32-36] nanogels,[37, 38] polymers,[23, 39-47] lipid nanoparticles,[16, 48, 49] cell-derived

vesicles,[50] and cell-penetrating peptides (CPPs).[17, 51-56] These carriers usually bind with cargo proteins via non-covalent interactions. A perfect delivery carrier should protect the cargo protein from degradation and support an easy cellular entry followed by a controllable release inside the cell.

Roder, R. et al.[34] present the coordinative interaction of oligohistidine-tags (His-tags) with metal-organic framework nanoparticles (MOF NPs) and use for delivery biomacromolecules H_6-peptides (e.g., H_6-PEG12 and H_6-KLK) and H_6-proteins (e.g., H_6-cytochrome c and H_6-GFP). The results demonstrate that biomacromolecules can be anchored on the outer surface of MOF NPs in a self-assembly process and successful transported into living cells. This study provides a diverse functionalization of MOF NPs with a high potential for co-delivery of various proteins.

Ju, E. et al.[36] first reported that gold nanoclusters (AuNCs) can self-assemble with Streptococcus pyogenes Cas9 (SpCas9) protein under physiological conditions, and the complexes (SpCas9-AuNCs) efficiently deliver SpCas9 protein into the cell nucleus. SpCas9-AuNCs could be disassembled at a lower pH 4.5 but are stable at a higher pH 7.4. SpCas9 is delivered into cells and the cell nucleus, where it performs its cleavage function, through the assembly disassembly process. Furthermore, the E6 oncogene was effectively knockout by self-assembled SpCas9-AuNCs nanoparticles after the HPV18 E6 sgRNA transfected into cervical cancer cells. Consequently, this causes the tumor-suppressing protein p53 to resume its normal activity and induces apoptosis in cervical cancer cells but had little effect on the normal cells. Because of their unique characteristics, SpCas9-AuNCs are an intriguing biomaterial for the treatment of cancer.

Nanogels are water-rich nanoscale three-dimensional polymer networks. Because of this, it is simple for nanogels to encapsulate hydrophilic proteins and peptides inside their own matrix.

It was stated that Su, S. et al.[37] had developed a straightforward and generic formulation that could produce protein nanogels (NG) of uniform sizes and an unusually high protein loading. These nanogels loaded cytochrome c and were rapidly constructed by

successively crosslinking and modifying lysine amines with both mono- and bis substituted maleamic anhydrides. The NG has been designed to have a tandem pH-programmed and traceless release personality. It is stable under typical physiological settings and protects the crosslinked cargo cytochrome c very well against breakdown by serum fouling, proteolytic enzymes, and heat. However, it can rapidly charge inversion at the slightly acidic tumor microenvironment for tumor internalization, and then traceless release of cytochrome c in a further acidulated pH in the endosome. The results show that the NG has strong cytotoxicity against cancer cells and efficient cellular uptake *in vitro*. When given intravenously via the tail vein, NG has an unusually high anticancer effectiveness *in vivo* without causing systemic toxicity or adverse effects. This study presents a universal platform for the formulation of therapeutic proteins and paves the way for vast prospects for the systemic, cytosolic, and traceless distribution of nanomedicines based on protein.

There are several ways to create polymers with exact compositions and topologies, including ring-opening metathesis polymerization, reversible addition-fragmentation chain transfer polymerization, and atom transfer radical polymerization. For the sake of particular applications, the polymers are readily modifiable using functional ligands. Moreover, it has been found that polymers, particularly cationic polymers, have a high capacity in both cellular uptake and endosomal escape.[23]

Lee, Y. et al.[39] developed an efficient method based on charge-conversional polyionic complex (PIC) micelles with citraconic amide or cis-aconitic amide for cytoplasmic protein delivery. The results show that without introducing any cross-links, raising the charge density of the protein greatly increased the stability of the PIC micelle under physiological salt levels. Then, the charge-conversion in endosomes induced the dissociation of the PIC micelles to result in efficient endosomal release. Furthermore, the combination of the lengthy circulation period of the PIC micelles and the controlled release activity of the charge-conversional moiety that was found in the charge-conversional PIC micelles has the potential to make these micelles very useful for the delivery of proteins *in vivo*. It has the potential to be ideal for the intracellular delivery of proteins with a large molecular weight that cannot pass through the cell membrane.

Zhang, P. et al.[42] used sequence-defined oligoaminoamide oligomers as a carrier for intracellular protein delivery. They found that a PEGylated with folate-receptor targeted two-arm oligomer (containing two oleic acids at the end of both arms) shows an excellent nuclear import of nlsEGFP (which contains a nuclear localization sequence) with high cellular uptake and effective endosomal escape in folate-receptor-positive KB carcinoma cells. In addition, it was shown that KB tumor cells were killed at a high rate when ribonuclease A was used as the therapeutic cargo protein. In conclusion, the sequence-defined oligoaminoamide oligomers modified by oleic acid are unique and promising nanocarriers for intracellular protein delivery and cancer treatment.

Lipid nanoparticles (LNPs) are special nanocarriers based on lipid that formulates with four different lipid excipients namely: ionizable lipids, helper phospholipids, cholesterol, and poly (ethylene glycol) (PEG) Lipid. As a delivery vehicle, LNP benefits from the inclusion of various excipients since each one serves a distinct purpose.[57]

Hirai, Y. et al.[49] established an approach to producing Lipid nanoparticles (LNPs) based on the pH-sensitive, charge-reversible lipid dioleoylglycerophosphate-diethylenediamine (DOP-DEDA), which achieved effective protein transport into cells. In order to prevent adverse effects caused by the interaction of the lipid with cationic lipids (e.g., cytotoxicity, including the lung surfactant effect), it was engineered to have a negative charge in the extracellular environment with neutral pH. However, once the lipid is carried into endosomes and exposed to an environment with a lower pH, it becomes positively charged and has the ability to interact with endosomal membranes, which can lead to membrane rupture. The results show that the encapsulation of green fluorescent protein (GFP) could reach almost 80% into LNPs and still maintain its active structure in cells indicating that the LNP system was successful in facilitating the endocytic reception of the cargo as well as its escape from the endosomes. Therefore, the DOP-DEDA-based LNP system holds promise as a carrier for the intracellular delivery of biologically active proteins.

Exosomes, which play a role in intercellular communication, are extracellular vesicles that are naturally produced by cells and come from their internal endocytic compartments and multi-vesicular bodies. It was thought of as a natural carrier for the transportation of protein.

Yim, N. et al.[50] developed a novel protein carrier for intracellular delivery of target proteins, named 'exosomes for protein loading via optically reversible protein-protein interactions' (EXPLORs). They were able to effectively load cargo proteins into newly generated exosomes by integrating an endogenous mechanism of exosome synthesis with a reversible protein-protein interaction module that was regulated by blue light. It has been shown that treatment with protein-loaded EXPLORs leads to a considerable increase in the intracellular levels of cargo proteins as well as the activity of these proteins in recipient cells both *in vitro* and *in vivo*. When compared to other approaches for protein-loaded exosomes, the loading capacity and delivery efficiency of this novel delivery system are better. It offers tremendous benefits for both clinical and scientific applications.

1.3.2 Strategy of covalent modification for intracellular protein delivery

As alternative strategy to physical delivery and nanoformulation with polymer-based carriers, direct genetic[58-60] or chemical[17, 61-63] covalent conjugation of proteins with domains facilitating cellular translocation[30, 64, 65] has been considered. For such conjugates, a bioreversible status of covalent bonds between protein cargo and delivery domain is highly desirable, allowing dynamic changes during the delivery process[66-68] and an intracellular release of native protein without being affected by the transport units.

Since the first covalent linkage of poly (ethylene glycol) (PEG) to bovine serum albumin (BSA) reported by Abuchowski and co-workers in the 1970s,[69] the PEG-based protein conjugates have shown the greatest clinical and commercial success. As extensively reviewed,[70-72] the conjugation of proteins to PEG, also known as "PEGylation," results in an increase in the hydrodynamic volume of the proteins, inhibits quick renal clearance, and lengthens the serum half-life through altering the quantity, size, and branching extent of PEG molecules attached.[73] Therefore, the conjugation of well-defined polymer/peptide to proteins, which has been effectively employed in the development of therapeutic

medications, is defined as a promising method to overcome the limitations posed by proteins.[74] Moreover, protein-polymer/peptide conjugates are hybrid molecules that can take use of the complementary behaviors of both elements and should be able to get beyond some of their inherent constraints.[74, 75]

In comparison to noncovalent interactions, covalent binding offers plentiful desirable pharmacological benefits, including increased potency and efficiency, prolonged duration of action, improved therapeutic index, complete target inactivation, and the ability to inhibit intractable targets.[76, 77] which is widely used in therapeutics, biomedicine, nanotechnology, bioengineering, catalysis, and sensing,[78, 79] and the protein or peptide can impart (bio)functional properties to the bioconjugate.

The introduction of functional groups onto proteins by covalent modification is an alternate strategy that could be used for the subsequent conjugation of other sections. Bifunctional linkers are often utilized when attaching polymer/peptide to proteins to prevent difficulties associated with poor reactivity when the ample protein and polymer/peptide are brought together. In particular, pH-labile linkages have been introduced for this purpose, disintegrated at either the mild acidic conditions in tumor tissue and/or in the slightly more acidic intracellular endolysosomal compartments.[39, 43, 80-86]

Bifunctional crosslinkers like azidomethyl-methylmaleic anhydride (AzMMMan) have represented such a step forward in developing protein conjugates.[43, 87] As shown by Kevin Maier et al.,[87] besides forming an acid-labile amide bond with lysine amino groups, AzMMMan can be used for different click chemistries: copper-catalyzed azide-alkyne cycloaddition (CuAAC), Staudinger ligation, and copper-free (strain-promoted) azide-alkyne cycloaddition with dibenzocyclooctyne (DBCO)-modified molecules. Based on this AzMMMan traceless linker, our group demonstrated efficient intracellular RNase A protein delivery.[61] For this purpose, RNase A was reversibly modified with polyethylene glycol (PEG)-folate for folate receptor targeting, and with the pH-responsive influenza HA2-derived negatively charged peptide INF7 for endosomal release, which in combination favored a high transduction efficiency. Most recently, an exciting report by Lieser et al. showed a similar approach, delivering epidermal growth factor receptor (EGFR)-targeted

conjugates of the fluorescent protein mCherry, demonstrating distinct effects of four different conjugated endosomal escape peptides.[63]

1.4 Aim of this thesis

Recent years have seen an explosive growth in the discovery of protein-based therapies in almost all areas of medical practice. However, owing to the difficulties of transporting active proteins into cells, most of the protein therapies now available work either extracellularly or on the cell membrane.[88] Therefore, the precise delivery of therapeutic proteins into cells is essential for both basic biology therapeutic research and clinical applications because proteins delivered intracellularly have quick effects and have been effectively proven as a viable treatment method for a variety of diseases.[89] Nowadays, research efforts have concentrated heavily on developing efficient delivery systems for proteins because of the potential impact of intracellular protein therapies. Many strategies have been discovered to overcome this natural barrier and enhance protein transport intracellularly.[90] Nevertheless, several serious drawbacks still restrict the use of the applications, including inefficiency, poor targeting, and inadequate endosomal escape ability. To address these limitations, our previous work demonstrated efficient intracellular RNase A protein delivery based on pH-sensitive AzMMMan traceless linker.[61] For this purpose, positively charged protein RNase A (isoelectric point pI = 9.6) was reversibly modified with polyethylene glycol (PEG)-folate for folate receptor targeting, and with the pH-responsive influenza HA2-derived negatively charged peptide INF7 for endosomal release, which in combination favored a high transduction efficiency. However, this delivery system only moderately worked for the slightly negatively charged (pI ~ 6.0) enhanced green fluorescent protein (eGFP). Apparently, the positive charges of the RNase A cargo protein contributed to the delivery process.

Thus, the aim of this thesis was to develop a more effective receptor-targeted dual pH-triggered intracellular protein delivery system, to make it broader applicable for proteins of various isoelectric points. For this purpose, the negatively charged protein eGFP was selected as a model protein to investigate intracellular protein delivery. Meanwhile, different functional units including PEG_{2kDa}-GE11 peptide for active targeting to the EGFR

and/or (N- or C-terminal) melittin as a cationic endosomal escape domain were selected to be conjugated with octa-arginine-cysteine (R_8C) by disulfide linkages to enhance the cellular uptake and endosomolytic ability. These two functional units had to be covalent modified to eGFP through pH-sensitive traceless cleaved AzMMMan linker and evaluated for targeted intracellular protein transfer. Octa-arginine is a well-known cationic CPP, mediating cellular uptake by macropinocytosis and other endocytotic mechanisms.[52, 54, 91-94] Melittin is a cationic bee venom-derived 26-amino acid peptide with high lytic activity both at neutral and endosomal pH; its activity can be synthetically modulated by including an N-terminal or C-terminal cysteine for conjugation.[95-97] Peptide GE11 has been used in numerous applications[63, 98-105] as ligand for active targeting to the EGFR overexpressed on the surface of many cancer types.

Furthermore, charge reversal by reversible acylation of melittin with dimethylmaleic anhydride (DMMAn) had been previously applied to abolish its lytic activity in the extracellular environment, albeit the endosomal escape activity was recovered upon endosomal acidification.[84, 96, 106] Therefore, in order to achieve dual pH-triggered, the charge reversal had to be considered in this delivery system. Inspired by this and taking into account the necessity of charge-switch characteristic for tumor-selective targeting,[107] the melittins within the cationized eGFP conjugates were masked with tetrahydrophthalic anhydride (TPAn), which are supposed to be rapidly hydrolyzed at extracellular tumor pH ~ 6.5, leading to the desired charge conversion within the tumor before cell entry[108, 109] but remains attached at normal pH 7.4.

The efficiency of the delivery system had to be investigated with eGFP modified with different ratios of the two functional units for biochemical stability and in collaboration with a team colleague, for cellular uptake, effect on cell viability. In addition, analogous conjugates of pro-apoptotic cytochrome c (Cyt C) had to be synthesized and to be evaluated for biological activity in an apoptosis assay.[110]

2 Materials

2.1 Chemicals

2,3-Dimethylmaleic anhydride (DMMAn) was obtained from Alfa Aesar (Kandel, Germany). N-Bromosuccinimide, benzoyl peroxide, 1,2-dichlorobenzene, petroleum ether, 5,5-dithio-bis-(2-nitrobenzoic acid) (DTNB), dimethyl sulfoxide (DMSO), dibenzocyclooctin-N-hydroxysuccinimidyl ester (DBCO NHS ester), 2,4,6-trinitrobenzenesulfonic (TNBS) acid solution, 3,4,5,6-tetrahydrophthalic anhydride (TPAn), cytochrome c (Cyt C) from equine heart (≥ 95%), coomassie brilliant blue R250, triisopropylsilane (TIS), 1,2-ethanedithiol (EDT), 1-hydroxybenzotriazole (HOBt), 3-(4,5-dimethylthiazol-2-yl)-2,5-diphenyiltetrazolium bromide (MTT), and super-DHB (sDHB) were obtained from Sigma-Aldrich (Munich, Germany). Sodium chloride (NaCl) and dichloromethane (DCM) were purchased from Bernd Kraft GmbH (Duisburg, Germany). Fmoc-amino acids, 2-chlorotrityl chloride resin, N,N-dimethylformamide (DMF), N-methyl-2-pyrrolidone (NMP), N,N-diisopropylethylamine (DIPEA), and trifluoroacetic acid (TFA) were purchased from Iris Biotech (Marktredwitz, Germany). n-Hexane and methyl tert-butyl ether (MTBE) were obtained from Brenntag (Mühlheim an der Ruhr, Germany). 2-(1H-Benzotriazol-1-yl)-1,1,3,3-tetramethyluronium-hexafluorophosphate (HBTU) was obtained from Multi-SynTech (Witten, Germany). Sodium sulfate (Na_2SO_4) was purchased from ORG Laborchemie GmbH (Bunde, Germany). Sodium azide (NaN_3) was purchased from Acros Organics (New Jersey, USA). Ethyl acetate, acetone, and acetonitrile were purchased from VWR International GmbH (Ismaning, Germany). Triethylamine was purchased from Grüssing GmbH (Filsum, Germany). ω-2-Pyridyldithio polyethylene glycol α-succinimidylester (OPSS-PEG$_{2kDa}$-NHS) was purchased from Rapp Polymere GmbH (Tübingen, Germany). Sodium dodecyl sulfate (SDS) was purchased from Carl Roth Gmbh & Co. Kg (Karlsruhe, Germany). Peptide R_8C, the peptide ligand GE11 (IVNQ PTYG YWHY), and N-terminally cysteine-modified melittin (N-melittin, CIGA VLKV LTTG LPAL ISWI KRKR QQ) were purchased from GL Biochem (Shanghai, China). C-terminally cysteine-modified melittin (C-melittin, GIGA VLKV LTTG LPAL ISWI KRKR QQC) was generated by automated solid-phase assisted peptide synthesis using a Syro Wave

synthesizer (Biotage, Uppsala, Sweden). Sephadex G-10 material was supplied by GE Healthcare (Freiburg, Germany).

2.2 Cell lines

Name	Description	Application
KB	Human cervix carcinoma cell lines (a HeLa subclone)	EGFR over expression
N2A	Mouse neuroblastoma cell lines	EGFR no/low expression
HeLa-Gal8-mRuby3	Human cervix carcinoma cell lines	Galectin8-mRuby3 fusion protein expression

3 Methods

3.1 Synthesis of 3-(bromomethyl)-4-methyl-2,5-furandione (BrMMMan)

The BrMMMan synthesis was performed according to our previous work with some modifications.[43, 87] First, DMMAn (5.04 g, 40.0 mmol), N-bromosuccinimide (4.56 g, 25.6 mmol), and benzoyl peroxide (64 mg, 0.36 mmol) were dissolved in 1,2-dichlorobenzene (250 mL, dried over molecular sieve UOP Type 3A) in a 500 mL round-bottom flask. The mixture was refluxed for 5 h (hour) at 110–120°C under anhydrous and anaerobic conditions. Then, an additional amount of benzoyl peroxide (64 mg, 0.36 mmol) was added to the room temperature (RT) cooled mixture, followed by refluxing for a further 5 h. After the reaction, the residue was filtered and washed 2× with 1,2-dichlorobenzene (25 mL, dried over molecular sieve UOP Type 3A). Subsequently, the organic phase was washed 2× with water (100 mL) and 1× with saturated NaCl solution (100 mL). Lastly, the organic layer was dried using Na_2SO_4 and then concentrated by a rotary evaporator under vacuum (Buchi, Flawil, Switzerland) to harvest a yellow oil. To remove the benzoyl peroxide, the yellow oil was chromatographed on a silica gel column (0.035-0.07 mm, 60A), eluting with a mixture of petroleum ether:ethyl acetate (8:2 v/v). The crude product of BrMMMan was then concentrated under the vacuum of a rotary evaporator. The impurities of DMMAn and di-(bromomethyl)-1,5-furandione (DiBrMMMan) were removed by distillation according to the boiling point ranges. For this, the crude product of BrMMMan was heated to 110–120°C under 7 mbar to remove the DMMAn. Upon increasing the temperature to 140°C, BrMMMan was separated out as light-yellow oil (yield 83.5%). The DiBrMMMan was left in the still pot. The purified structure was confirmed by ^{1}H NMR.

3.2 Synthesis of 3-(azidomethyl)-4-methyl-2,5-furandione (AzMMMan)

AzMMMan was prepared based on our previously published protocol with minor modifications.[43, 87] Briefly, BrMMMan (310.5 mg, 1.5 mmol) was dissolved in 10 mL of acetone (dried over molecular sieve UOP Type 3A) and then NaN_3 (97.5 mg, 1.5 mmol)

was added. To obtain AzMMMan, the suspension was stirred for 24 h at 37°C, filtered, and rotary evaporated. Finally, AzMMMan was purified by silica gel column chromatography using petroleum ether:ethyl acetate (7:3 v/v) followed by concentrating in a rotary evaporator under vacuum to yield 89.3% of an oil. The desired structure was confirmed by ^{1}H NMR.

3.3 Expression and purification of enhanced green fluorescent protein (eGFP)

This work was performed by Miriam Höhn (Pharmaceutical Biotechnology, LMU München). eGFP containing a nuclear localization signal (nls) and a His-tag was produced according to our previously established protocol in E. coli BL2 (DE3) plysS.[43, 87] Bacteria were cultured in TB medium under constant shaking to reach an optical density of 0.75 at 600 nm. Then, eGFP expression was induced by isopropyl β-D-1-thiogalactopyranoside (IPTG, at final concentration 1 mM) and incubation for a further 16 h at 32°C. After harvesting by centrifugation (4000 rpm, 5 min), the cell pellet was lysed through ultrasonication. eGFP was purified by nickel chromatography using a gradient from a binding buffer (50 mM sodium hydrogen phosphate (Na_2HPO_4), 300 mM NaCl, and 20 mM imidazole) to elution buffer (50 mM Na_2HPO_4, 500 mM NaCl, and 250 mM imidazole). The eGFP was dialyzed against phosphate-buffered saline (PBS) buffer (pH 7.3) at 4°C overnight and finally concentrated with ultracentrifugal filter units (10 kDa).

3.4 Modification of eGFP with AzMMMan

eGFP was modified with AzMMMan as previously described.[87] Briefly, eGFP (5 mg, 0.158 µmol) was dissolved in HEPES buffer (990 µL, 500 mM, pH 9.0), and the AzMMMan (5 mg, 0.03 mmol) diluted in 10 µL acetonitrile was dropped slowly to the protein solution. After 2 h incubation under constant shaking (600 rpm, RT), free AzMMMan were removed by size exclusion chromatography (SEC) using Äkta purifier system equipped with Sephadex G-10 column with PBS buffer (pH 8.0) as a mobile phase (1 mL/min). The eGFP-AzMMMan was concentrated with ultracentrifugal filter units (10 kDa) which was

then quantified by measuring the absorbance (λ 488 nm) using an extinction coefficient of 55000 $M^{-1}cm^{-1}$.

3.5 Modification of cytochrome c (Cyt C) with AzMMMan

Cyt C was modified with AzMMMan as previously described. Briefly, Cyt C (2.5 mg, 0.2 µmol M.W. 12384) was dissolved in HEPES buffer (990 µL, 500 mM, pH 9.0) and the AzMMMan (5 mg, 30 µmol) diluted in 10 µL acetonitrile was dropped slowly to the protein solution. After 2 h incubation under constant shaking (600 rpm, RT), free AzMMMan were removed by SEC using Äkta purifier system equipped with Sephadex G-10 column with PBS buffer (pH 8.0) as a mobile phase (1 mL/min). The Cyt C-AzMMMan was concentrated with ultracentrifugal filter units (10 kDa) which was then quantified by measuring the absorbance (λ 410 nm) using an extinction coefficient of 106000 $M^{-1}cm^{-1}$.

3.6 Modification of eGFP with TPAn

Briefly, eGFP (5 mg, 0.158 µmol) was dissolved in HEPES buffer (990 µL, 500 mM, pH 9.0), TPAn (10 equiv of amine) was slowly added, and the mixtures were incubated for 4 h under constant shaking (600 rpm, RT). Then, the free TPAn were removed by SEC using Äkta purifier system equipped with Sephadex G-10 column with PBS buffer (pH 8.0) as a mobile phase (1 mL/min). The eGFP-TPAn was concentrated with ultracentrifugal filter units (10 kDa) which was then quantified by measuring the absorbance (λ 488 nm) using an extinction coefficient of 55000 $M^{-1}cm^{-1}$.

3.7 Synthesis of DBCO-R_8C

R_8C (4.1 mg, 3.0 µmol) was dissolved in 800 µL DMSO (anhydrous, amine-free, $\geq$ 99.9%) including 2 µL triethylamine with dropwise addition of DBCO NHS ester (2.5 mg, 6.2 µmol) in DMSO (anhydrous, amine-free, $\geq$ 99.9%) and reacted for 2 h under argon with constant shaking (600 rpm, RT). After dialyzing against water (pH 6.5) for 24 h at 4°C and freeze-drying, DBCO-R_8C was analyzed by MALDI-TOF-MS, UV spectrum, and high-performance liquid chromatography (RP-HPLC).

3.8 Synthesis of C-terminally cysteine-modified melittin

C-terminally cysteine-modified melittin (C-melittin) was synthesized using a 2-chlorotrityl chloride resin preloaded with Fmoc-Cys(trt)-OH (resin loading). Then, the sequence of C-melittin (GIGA VLKV LTTG LPAL ISWI KRKR QQC) was synthesized by automated solid-phase assisted peptide synthesis (SPPS) using a Syro Wave synthesizer. The reagents for the synthesizer were separated out into their own bottles and organized in the following fashion: 8 equiv of DIPEA in NMP, 4 equiv of HBTU in DMF, 4 equiv of HOBt were dissolved in NMP together with 4 equiv of the respective Fmoc-amino acid. The double coupling procedure was repeated for 12 minutes at 50°C. The deprotection of the Fmoc was achieved by 4 × 10 min incubation with 20% (v/v) piperidine in DMF. Following each phase of coupling and deprotection, an additional step consisting of washing with DMF for 5 cycles and then incubating for 1 min was carried out. After the C-melittin was synthesized by the automated synthesizer, the cleavage and purification steps were performed manually. Briefly, C-melittin cleavage off the resin by incubated with TFA/TIS/H_2O/EDT (94/1/2.5/2.5 v/v/v/v) for 45 min. Then the cleavage solution was added to 40 mL of precooled n-hexane / MTBE (1:1) solution immediately for precipitation. The precipitation of C-melittin was dried and then dissolved with water. The purification of C-melittin was performed by SEC using an Äkta purifier system based on a Sephadex G-10 column and 10 mM hydrochloric acid (HCl) in H_2O/ACN (7/3 v/v) as elution buffer. The pooled fractions containing the C-melittin were combined, snap-frozen, freeze-dried and analyzed by MALDI-TOF-MS.

3.9 Synthesis of (N/C)-melittin-TNB

N-melittin (5.8 mg, 2 μmol, containing an N-terminal cysteine) was reacted with DTNB (3.96 mg, 10 μmol) in 3.0 mL reaction buffer (0.1 M Na_2HPO_4 with 1 mM EDTA, pH 6.5) for 2 h under argon with constant shaking (600 rpm, RT). The solution was purified by SEC with elution buffer (acetonitrile:water 3:7 v/v containing 10 mM HCl as mobile phase with flow rate 1 mL/min). The collected product was lyophilized and analyzed by MALDI-TOF-MS, UV, and RP-HPLC. C-melittin-TNB (based on melittin with a C-terminal cysteine) was obtained analogously.

3.10 Synthesis of OPSS-PEG$_{2kDa}$-GE11

Peptide GE11 (3.1 mg, 2.0 µmol) was dissolved in 500 µL DMSO (anhydrous, amine-free, ≥ 99.9%), and then reacted with OPSS-PEG$_{2kDa}$-NHS (10 mg, 5.0 µmol) in 100 µL DMSO (anhydrous, amine-free, ≥ 99.9%) for 3 h with constant shaking (600 rpm, RT). The OPSS-PEG$_{2kDa}$-GE11 was dialyzed against water (pH 7.4) for 24 h at 4°C. The solution containing pure product was lyophilized, and the residue was analyzed by MALDI-TOF-MS, ^{1}H NMR, and RP-HPLC.

3.11 Synthesis of DBCO-R$_8$C-S-S-PEG$_{2kDa}$-GE11 and DBCO-R$_8$C-S-S-(N/C)-melittin

DBCO-R$_8$C (2.5 mg, 1.5 µmol) was dissolved in 500 µL HEPES buffer (500 mM, pH 6.5). Afterward, OPSS-PEG$_{2kDa}$-GE11 (3.5 mg, 1 µmol) or (N/C)-melittin-TNB (3.1 mg, 1 µmol) was dissolved in 500 µL HEPES buffer (500 mM, pH 6.5) and dropped slowly to the DBCO-R$_8$C solution in distinct tubes. Subsequently, the mixtures were incubated for 24 h with constant stirring (600 rpm, RT). The pure products were obtained after dialysis (for 24 h at 4°C) against water (pH 7.4) and lyophilization. The characterizations of DBCO-R$_8$C-S-S-PEG$_{2kDa}$-GE11 were analyzed by UV spectrum and RP-HPLC, and the characterization of DBCO-R$_8$C-S-S-(N/C)-melittin by MALDI-TOF-MS.

3.12 Synthesis of different eGFP conjugates

eGFP-AzMMMan (modified with 22 molar equivalents (equiv) of AzMMMan) was diluted in 500 µL of HEPES buffer (500 mM, pH 9.0). Afterward, DBCO-R$_8$C-S-S-(N/C)-melittin and DBCO-R$_8$C-S-S-PEG$_{2kDa}$-GE11 at different molar ratios (N/C-melittin:PEG$_{2kDa}$-GE11 22:0, 16:6, 11:11, 6:16, 0:22 equiv) was added to the protein solution and reacted for 4 h under constant shaking (600 rpm, RT). Then, the products were purified by ultrafiltration (10 kDa). Afterward, TPAn (10 equiv of amine) was slowly added, and the mixtures were incubated for a further 4 h under constant shaking (600 rpm, RT). The eGFP conjugates A–E (**Table 1**) were then obtained by ultrafiltration (10 kDa). Their concentration was

calculated by measuring the absorbance (λ 488 nm) of eGFP using an extinction coefficient of 55000 $M^{-1}cm^{-1}$.

3.13 Synthesis of Cyt C conjugate

Cyt C-AzMMMan (modified with 16 molar equivalents of AzMMMan) was diluted in 500 µL of HEPES buffer (500 mM, pH 9.0). Afterward, DBCO-R_8C-S-S-N-melittin and DBCO-R_8C-S-S-PEG$_{2kDa}$-GE11 at a molar ratio of 4:12 (based on the best candidate of eGFP conjugate D) were added to the protein solution and reacted for 4 h under constant shaking (600 rpm, RT). Then, the products were purified by ultrafiltration (10 kDa). Afterward, TPAn (10 equiv of amine) was slowly added, and the mixtures were incubated for a further 4 h under constant shaking (600 rpm, RT). The Cyt C conjugate was then obtained by ultrafiltration (10 kDa). Their concentration was calculated by measuring the absorbance (λ 410 nm) of Cyt C using an extinction coefficient of 106000 $M^{-1}cm^{-1}$.

3.14 Kinetics of pH-dependent cleavage eGFP-AzMMMan and eGFP-TPAn analyzed by TNBS assay

The eGFP-AzMMMan and eGFP-TPAn were dialyzed against 500 mM HEPES buffer (pH 7.4, 6.5 or 5.5) for 24 h at 37°C with stirring. Samples were taken at indicated time intervals, and their exposed amino groups from eGFP were measured by the TNBS assay.

3.15 pH-sensitive charge reversal of eGFP conjugates or Cyt C conjugate analyzed by zetasizer/TNBS assay

eGFP conjugates or Cyt C conjugate were prepared in HEPES buffer (500 mM, pH 9.0) followed by adjusting pH value to 7.4 or 6.5. Then, they were dialyzed against 500 mM HEPES buffer (pH of 7.4 or 6.5) for 24 h at 37°C with stirring. Samples were taken at timed intervals, and their exposed amino groups were measured by the TNBS assay. Zeta potential of eGFP conjugates was measured by Zetasizer Nano ZS (Malvern Instruments, Worcestershire, Germany).

3.16 Traceless release of eGFP or Cyt C from TPAn-free eGFP conjugates or TPAn-free Cyt C conjugate by TNBS assay

The eGFP conjugates (A–E without TPAn) or Cyt C conjugate (without TPAn) were dialyzed against 500 mM HEPES buffer (pH 7.4 or 6.5) for 24 h at 37°C with stirring. Samples were taken at indicated time intervals, and their exposed amino groups from eGFP or Cyt C (the lysine amino groups of melittin were subtracted as background) were measured by the TNBS assay.

3.17 Stability and traceless release of eGFP conjugates by SDS-PAGE assay

Before SDS-PAGE, the eGFP conjugates were pre-incubated in HEPES buffer (500 mM, pH 7.4 for stability or pH 5.5 for traceless release studies) for 24 h at 37°C. They were then loaded on 3.5% stacking gel (pH 8.8) and 12.5% separating gel (pH 6.8) with the optimized loading buffer containing only SDS. The gels ran in running buffer at 100 V for 2 h. After electrophoresis, gels were stained with Coomassie-Blue solution (acetic acid:ethanol:H_2O, 1:2:7, v/v/v with 0.3% w/v Coomassie brilliant blue R250), and destained by acetic acid:ethanol:H_2O (1:2:7, v/v/v) solution for several times, and photographed.

3.18 Cell culture

The human EGFR-overexpressing cervix carcinoma cell lines, KB cells (a HeLa subclone) were grown in RPMI-1640, and HeLa-Gal8-mRuby3 cells (stably expressing Galectin8-mRuby3 fusion protein) and neuroblastoma N2A cells were grown in Dulbecco's Modified Eagle Medium (DMEM). The cell culture was performed at 37°C in a CO_2-humidified incubator. The culture mediums were supplemented with 10% fetal bovine serum (FBS), 4 mM-stable glutamine, 100 U/mL penicillin, and 100 µg/mL streptomycin.

3.19 Cellular uptake of eGFP conjugates by flow cytometry assay

This experiment was performed by Mina Yazdi (PhD student at Pharmaceutical Biotechnology, LMU München). Details can be found in Lyu M,* Yazdi M,* Lin Y, Höhn M, Lächelt U, Wagner E. , Receptor-Targeted Dual pH-Triggered Intracellular Protein Transfer, ACS Biomater. Sci. Eng. 2022, doi:10.1021/acsbiomaterials.2c00476. (*These authors contributed equally)

3.20 Intracellular fate of eGFP conjugates by confocal laser scanning microscopy (CLSM) assay

This experiment was performed by Miriam Höhn (Pharmaceutical Biotechnology, LMU München) and Mina Yazdi (PhD student at Pharmaceutical Biotechnology, LMU München). Details can be found in Lyu M,* Yazdi M,* Lin Y, Höhn M, Lächelt U, Wagner E. , Receptor-Targeted Dual pH-Triggered Intracellular Protein Transfer, ACS Biomater. Sci. Eng. 2022, doi:10.1021/acsbiomaterials.2c00476. (*These authors contributed equally)

3.21 Cell viability by 3-(4,5-dimethylthiazol-2-yl)-2,5-diphenyltetrazolium bromide (MTT) assay

This experiment was performed by Mina Yazdi (PhD student at Pharmaceutical Biotechnology, LMU München). Details can be found in Lyu M,* Yazdi M,* Lin Y, Höhn M, Lächelt U, Wagner E. , Receptor-Targeted Dual pH-Triggered Intracellular Protein Transfer, ACS Biomater. Sci. Eng. 2022, doi:10.1021/acsbiomaterials.2c00476. (*These authors contributed equally)

3.22 Apoptosis assay of Cyt C conjugate

This experiment was performed by Mina Yazdi (PhD student at Pharmaceutical Biotechnology, LMU München). Details can be found in Lyu M,* Yazdi M,* Lin Y, Höhn M, Lächelt U, Wagner E. , Receptor-Targeted Dual pH-Triggered Intracellular Protein

Transfer, ACS Biomater. Sci. Eng. 2022, doi:10.1021/acsbiomaterials.2c00476. (*These authors contributed equally)

3.23 Analytical reversed phase High-performance liquid chromatography (RP-HPLC)

The purity of the synthesized ligands (DBCO-R_8C, N/C-melittin-TNB, OPSS-PEG_{2kDa}-GE11, and DBCO-R_8C-PEG_{2kDa}-GE11) was analyzed by analytical RP-HPLC using a VWR Hitachi Chromaster RP-HPLC system (5160 pump module, 5260 auto sampler, 5310 column oven, 5430 diode array detector). A linear gradient with aqueous (contains 0.1% TFA) and acetonitrile (contains 0.1% TFA) was used for elution through a C18-column (YMC column, HS-302, HS12S05-1546WT, 150 × 4.6 mm I.D., S-5 μm, 12 nm, YMC Europe GmbH, Dinslaken, Germany).

3.24 MALDI-TOF-MS Spectrometry

Matrix solution (1 μL, 10 mg/mL sDHB (super-DHB: 9:1 (w/w) mixture of 2,5-dihydroxybenzoic acid and 2-hydroxy-5-methoxybenzoic acid)) in TA30 (ACN/H_2O (3:7) with 0.1% (v/v) TFA) was spotted on an MTP AnchorChip (Bruker Daltonics, Bremen, Germany). After crystallizing the matrix, the sample solution (1 μL, 1 mg/mL) was added to the matrix spots. Then, the sample spots were analyzed in positive or negative reflector mode using an Autoflex II mass spectrometer (Bruker Daltonics, Bremen, Germany).

3.25 Ultraviolet-visible (UV-Vis) spectroscopy

The synthesized ligands (DBCO-R_8C, N/C-melittin-TNB, and DBCO-R_8C-PEG_{2kDa}-GE11) were analyzed by UV-Vis absorbance at the wavelength of 200 nm–900 nm. The concentrations of eGFP and Cyt C were determined by measuring UV-Vis absorbance at wavelengths of 488 nm or 410 nm. All the measurements were performed by Cary 3500 UV-Vis Spectrophotometer (Agilent Technologies, Mulgrave, Australia).

3.26 ^{1}H NMR

The ^{1}H NMR spectra were carried out by the use of a Jeol JNMR-GX (400 MHz). All spectra were recorded without TMS as an internal standard and therefore all signals were calibrated to the residual proton signal of the deuterated chloroform ($CDCl_3$) or deuterium oxide (D_2O) solvent. Chemical shifts are reported in ppm. The spectra were analyzed using the NMR software MestreNova (MestReLab Research).

3.27 Size-exclusion chromatography (SEC)

The purification by SEC was using the ÄKTA purifier 10 system (GE Healthcare Bio-Sciences AB, Uppsala, Sweden) combined with a P-900 solvent pump module, a UV-900 UV/Vis multi-wavelength detector, a pH/C-900 conductivity module, and a Frac-950 automated fraction collector. The desired fractions were collected, pooled, and then concentrated or lyophilized.

3.28 Statistical Analysis

All statistical analyses were performed by Origin 8.5 and/or GraphPad Prism 7 softwares. Data were expressed as means ± standard deviation (SD). Differences between two groups were assessed using an unpaired, two-sided Student t-test. Significant differences between the groups were presented as follows: $*p < 0.05$, $**p < 0.01$, and $***p < 0.001$.

4 Results and Discussion

This part was adapted from:

Lyu M,* Yazdi M,* Lin Y, Höhn M, Lächelt U, Wagner E. , <u>Receptor-Targeted Dual pH-Triggered Intracellular Protein Transfer</u>, ACS Biomater. Sci. Eng. 2022, doi:10.1021/acsbiomaterials.2c00476. (*These authors contributed equally)

4.1 Design of the delivery system

Scheme 1 describes the synthetic design of reversibly masked and targeted-eGFP conjugates (**Scheme 1a**) and the hypothesized process for dual pH-responsive intracellular delivery of eGFP (**Scheme 1b**). eGFP conjugates are covalently modified with two different pH-responsive maleic acid-based linkers cleavable in a traceless manner: (i) AzMMMan (azidomethylmethylmaleic anhydride)[87] for direct modification of eGFP lysine amino groups cleavable at endosomal pH ~ 5.5, and providing an azide group for click modification with other delivery domains; and (ii) TPAn (tetrahydrophthalic anhydride),[108, 109] for masking the lysine amino groups of melittin domains and causing a charge reversal of the protein conjugate from positive to negative charge.

The TPAn linkages are already cleaved when conjugates reach a mildly acidic extracellular microenvironment (pH ~ 6.5), as present in a tumor microenvironment. Unmasking of the TPAn protected negatively charged eGFP conjugates results in a charge reversal to positively charged eGFP conjugates, exposing PEG-linked GE11 peptides as specific EGFR targeting ligands, cationic octa-arginines as general cell transduction domains, as wells as membrane-destabilizing melittin peptides. Following selective cellular endocytosis of eGFP conjugates, the endosomal pH ~ 5.5 triggers further decomposition of AzMMMan linkages, melittin-triggered endosomal disruption, and cytosolic traceless release of free eGFP.
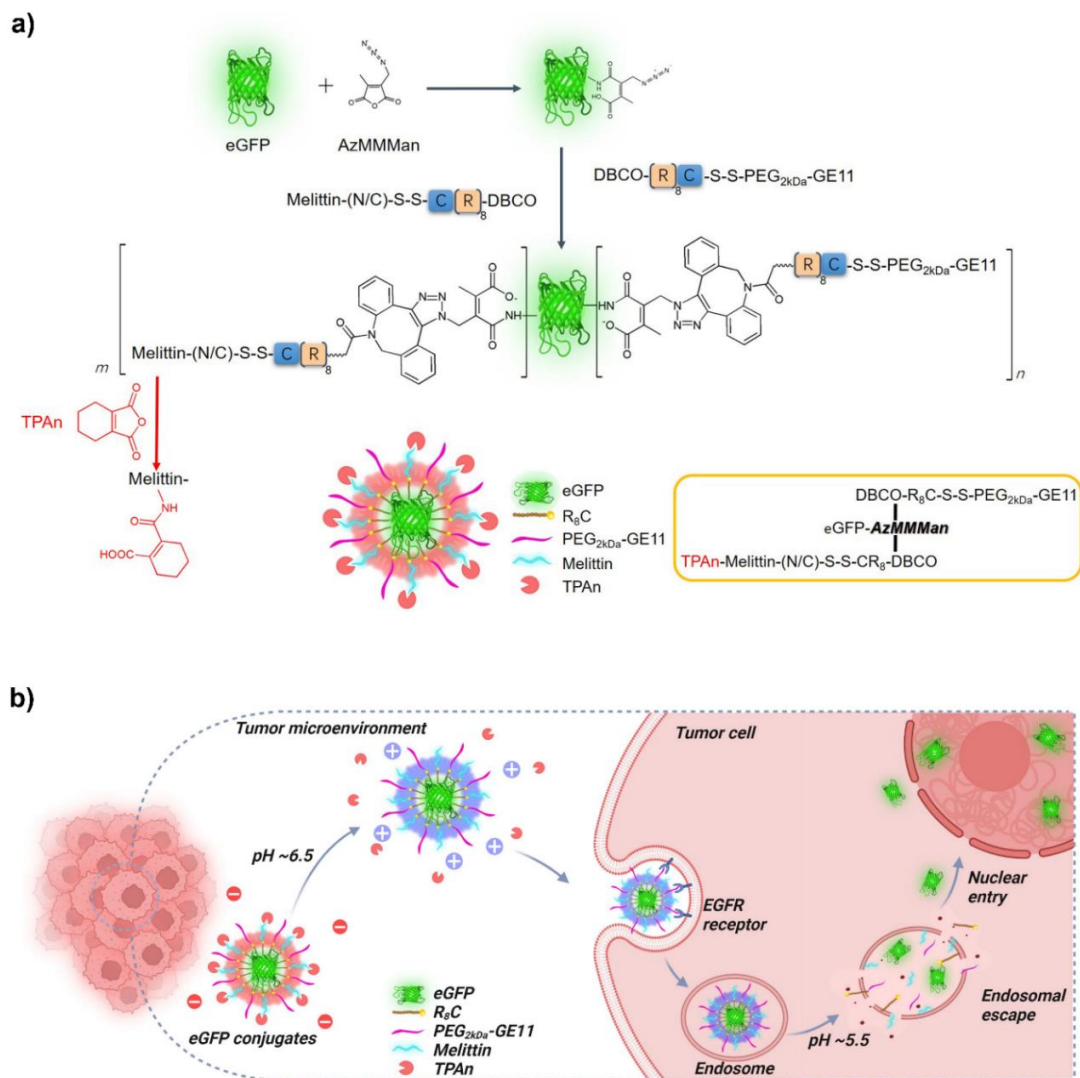
Scheme 1. Targeted dual pH-responsive intracellular delivery of eGFP. **a)** Synthesis of eGFP conjugates: eGFP was covalently modified with acidic traceless linker AzMMMan. Using copper-free click chemistry, cell-penetrating peptides DBCO-R_8C were coupled which were then additionally linked through disulfide bond with targeting ligand PEG$_{2kDa}$-GE11 or with the endosomal disruptive peptide melittin. Either N- or C-terminally cysteine-extended melittin (N/C-melittin) was integrated. The amino groups of melittin were masked by TPAn to provide a pH (6.5)-sensitive charge reversal. **b)** When reaching a mildly acidic extracellular microenvironment (pH ~ 6.5), the TPAn protecting negatively charged eGFP conjugates are unmasked for GE11-targeted selective cellular uptake of eGFP conjugates, which is followed by endosomal pH (~ 5.5)-triggered further decomposition of AzMMMan linkages, and melittin-triggered endosomal disruption both leading to traceless cytosolic release of eGFP. Graphics created with BioRender.com
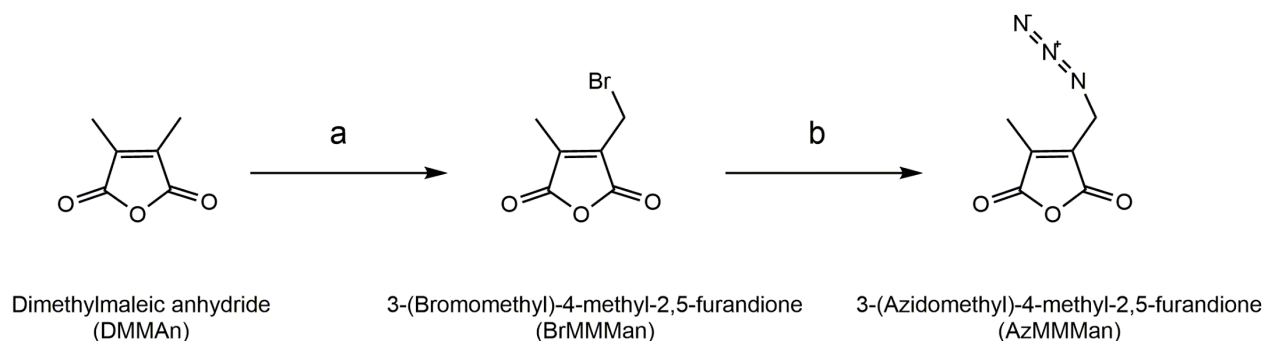
eGFP was used as our model protein because of its negative charge and its fluorescence property, which facilitate monitoring of the cellular uptake process.[111] Key steps of the conjugate synthesis (**Scheme 1a**) were as follows. First, the lysine amino groups of eGFP were covalently modified with the AzMMMan linker. The TNBS assay demonstrated that at least 22 out of the 26 primary amines of eGFP conjugates (25 lysines plus one terminal amino group) were modified with AzMMMan. To synthesize the functional side-chain units, DBCO-modified R_8C, which was either linked with (N/C)-melittin-TNB (N- or C- terminally DTNB-cysteine modified melittin) or with OPSS-PEG_{2kDa}-GE11 via disulfide bonds. Cationic R_8C was incorporated into the linking domains to enhance the cell-mediated internalization of anionic eGFP.[112] Subsequently, DBCO-R_8C-S-S-PEG_{2kDa}-GE11 and DBCO-R_8C-S-S-N/C-melittin were reacted with the eGFP-AzMMMan conjugate core by copper-free click chemistry at different ratios (**Scheme 1a**). Numerous studies have found the ligand-based cell surface receptor targeting as suitable to increase the specificity of the delivery to the tumor sites.[113-116] With respect to its proven role in EGFR-mediated delivery, peptide GE11[63, 98-105, 117, 118] was selected for the purpose of active targeting in the current work. Utilizing the pH difference between the healthy tissues and slightly acidic tumor tissues, charge reversal systems have demonstrated improved tumoral delivery efficiency.[119-121] As illustrated in **Scheme 1a,** the positively charged amino groups of N/C-melittin were masked with TPAn, converting them into anionic residues. At the tumor site (pH ~ 6.5), the TPAn is cleaved off, reverting to the original positive charge which facilitates binding of the unmasked eGFP conjugates to cell membranes (**Scheme 1b**). In addition to cellular binding and uptake, unmasking the membrane-destabilizing property of melittin for the endosomal escape prevents lysosomal-mediated protein degradation.[106, 122] By using the proposed methodology, the different eGFP conjugates A (only melittin-TPAn units), E (only PEG_{2kDa}-GE11 units), and B to D containing both delivery units, were generated to be evaluated regarding their efficiency (**Table 1**).

Table 1. Different eGFP conjugates A–E were synthesized by incorporating various molar equivalents (equiv) of the functional delivery units.

eGFP conjugates	DBCO-R$_8$C-S-S-(N/C)-Melittin-TPAn (equiv)	DBCO-R$_8$C-S-S-PEG$_{2kDa}$-GE11 (equiv)
A	22	0
B	16	6
C	11	11
D	6	16
E	0	22

4.2 Characterization of pH sensitive AzMMMan

The AzMMMan was synthesized as described in **Scheme 2** and then characterized by ^{1}H NMR (**Figure 4.1 and 4.2**). The results show that the AzMMMan was synthesized successfully with a high purity.

Dimethylmaleic anhydride (DMMAn)   3-(Bromomethyl)-4-methyl-2,5-furandione (BrMMMan)   3-(Azidomethyl)-4-methyl-2,5-furandione (AzMMMan)

Scheme 2. Synthesis of acid-labile traceless linker AzMMMan. a: N-bromosuccinimide, benzoyl peroxide, dichlorobenzene. b: Sodium azide, acetone.

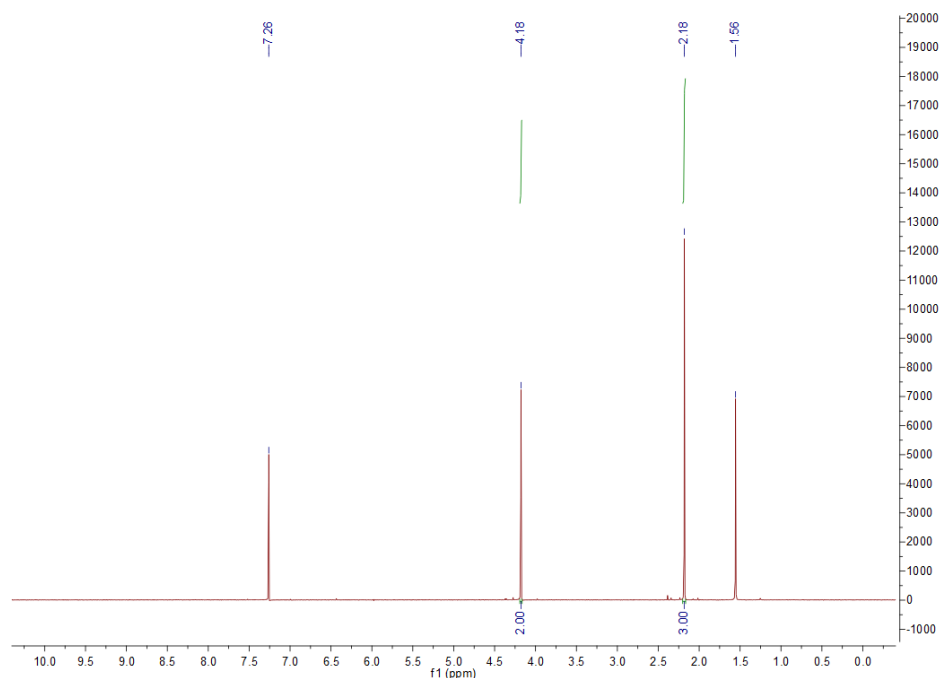**Figure 4.1** ^{1}H NMR (400 MHz, CDCl$_3$) of BrMMMan. δ (ppm) 2.18 (s, 3H, -CH$_3$ BrMMMan, 4.18 (s, 2H, -CH$_2$ BrMMMan).
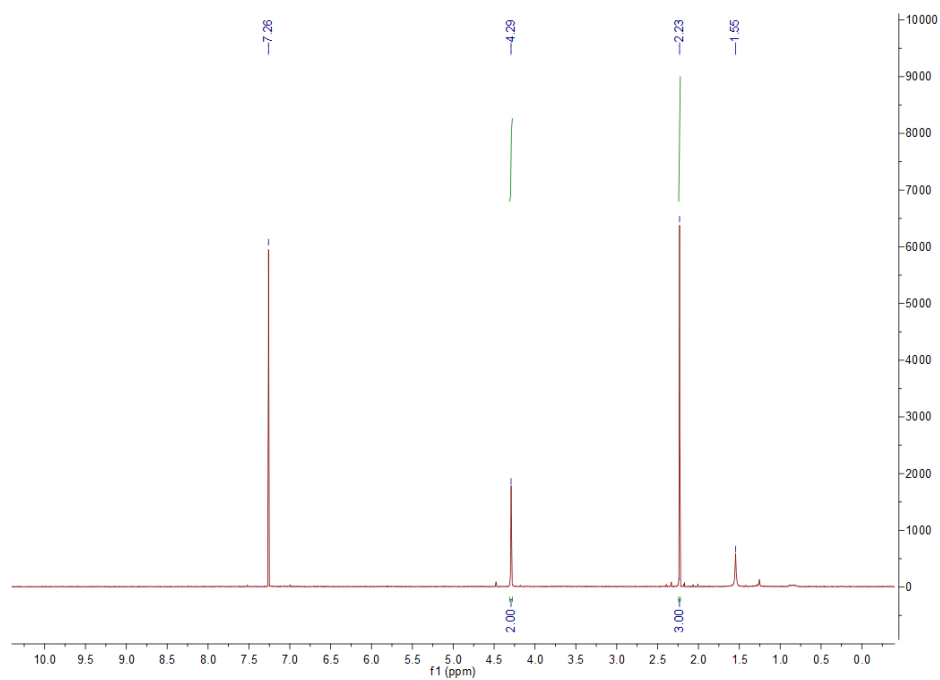

Figure 4.2 ^{1}H NMR (400 MHz, CDCl$_3$) of AzMMMan. δ (ppm) 2.23 (s, 3H, -CH$_3$ AzMMMan), 4.29 (s, 2H, -CH$_2$-N$_3$ AzMMMan).

4.3 Characterization of DBCO-modified R$_8$C

The DBCO-modified R$_8$C was synthesized and characterized by UV spectra, RP-HPLC, and MALDI-TOF-MS.

Successful DBCO NHS eater modification of R$_8$C could be confirmed by UV spectroscopy, due to the characteristic absorbance of DBCO moiety at 309 nm. As seen in **Figure 4.3**, the DBCO-R$_8$C has a specific absorbance around 309 nm comparing to non-modified R$_8$C. Therefore, we can confirm that we got the aim product DBCO-R$_8$C.
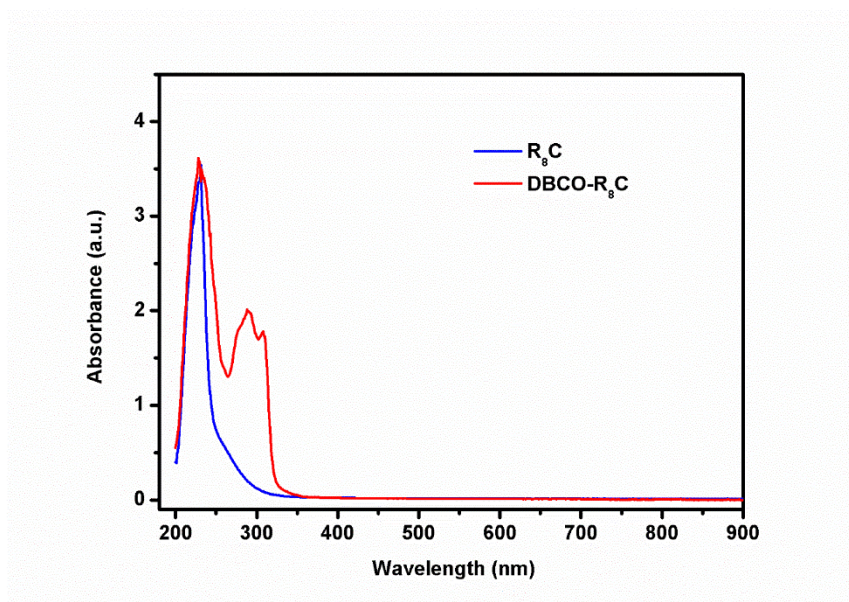
Figure 4.3 UV spectra of R$_8$C and DBCO-R$_8$C.

To further confirm the DBCO-R$_8$C was successfully synthesized and its purity, we analyzed it using RP-HPLC. According to the results in **Figure 4.4**, the appearance time of pure R$_8$C at a wavelength of 218 nm was 7.7 min, the appearance time of pure DBCO NHS ester was 20.7 min, whereas the appearance time of DBCO-R$_8$C was 12.3 min with a single peak, which means the pure DBCO-R$_8$C has been synthesized with high purity.
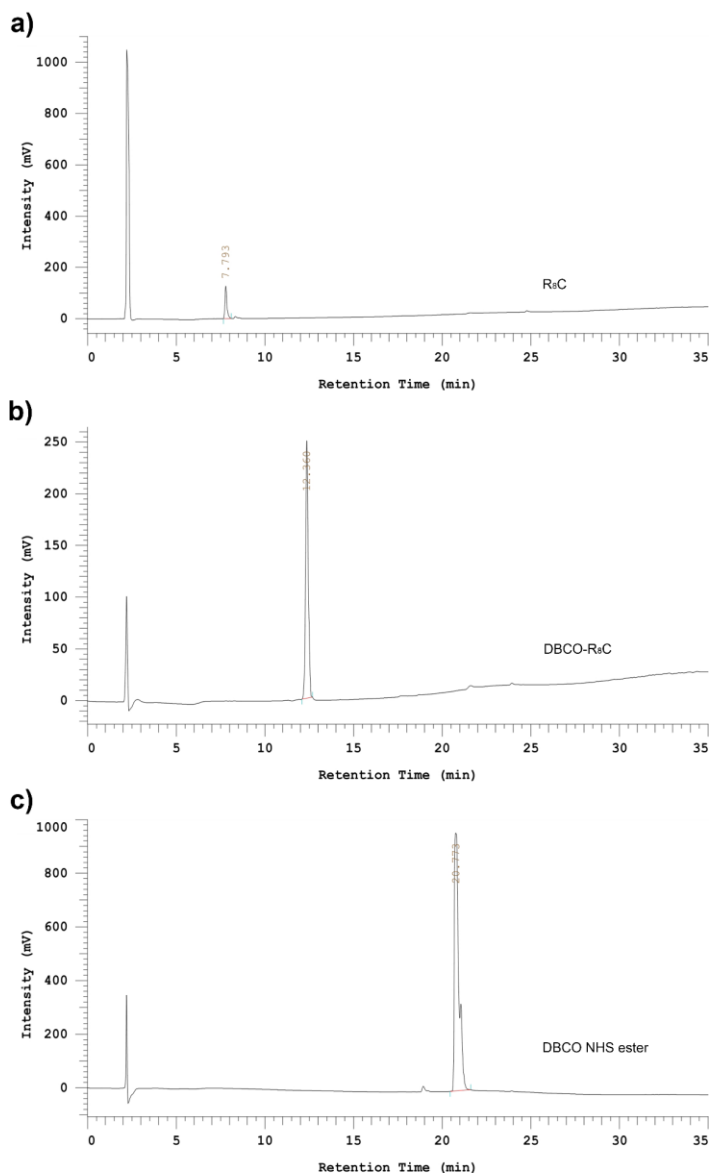
Figure 4.4 Analytical RP-HPLC chromatograms of **a)** R_8C, **b)** DBCO-R_8C, and **c)** DBCO NHS ester. The analysis was carried out using a C18 column (5 µm, 150 × 4.6 mm) and a water/acetonitrile gradient (95:5–0:100 in 35 min) containing 0.1% TFA. For the detection at 218 nm was monitored.

As shown in **Figure 4.5**, the MALDI-TOF-MS confirmed that the pure DBCO-R_8C was obtained.
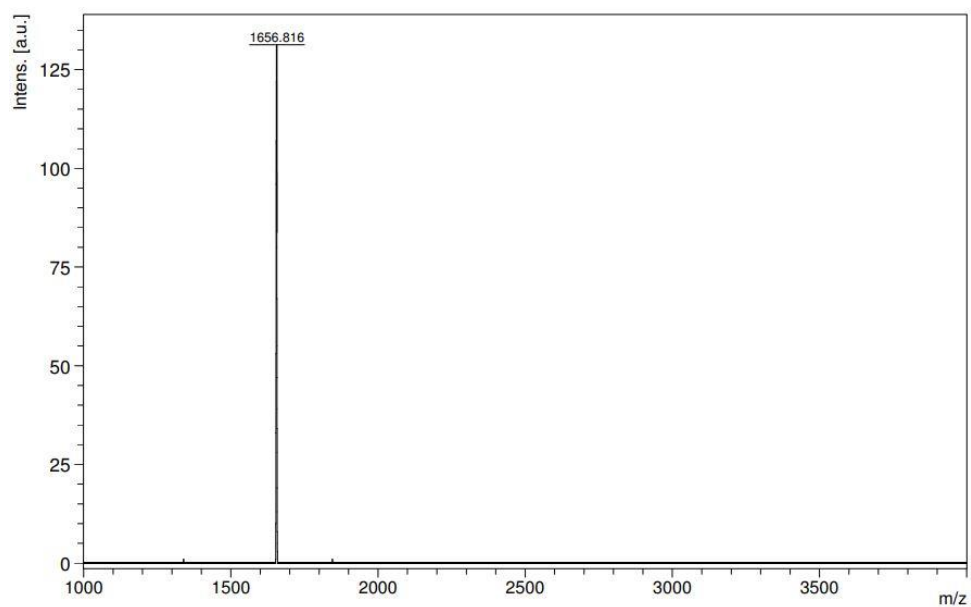
Figure 4.5 MALDI-TOF-MS spectrum of DBCO-R$_8$C.

4.4 Characterization of N-melittin-TNB

The N-melittin-TNB were synthesized and characterized by UV spectra and RP-HPLC.
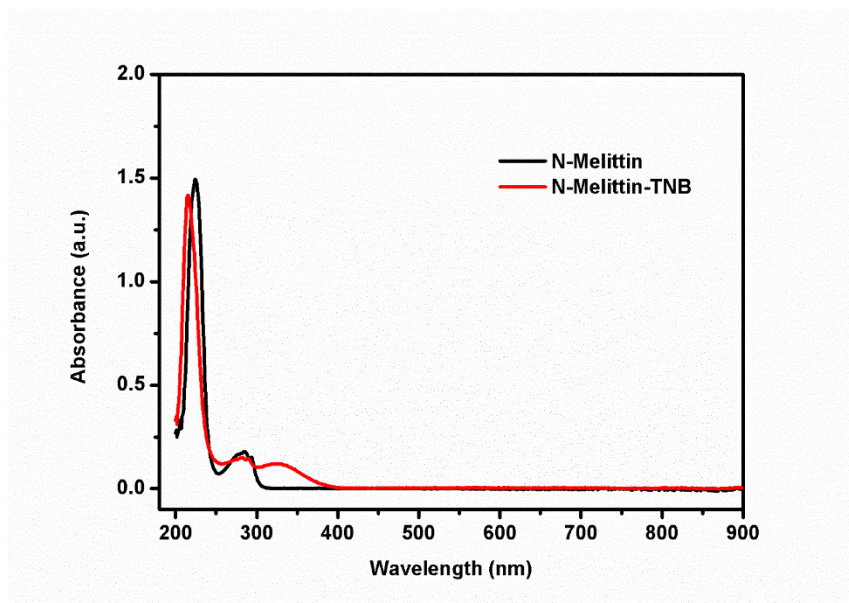
Figure 4.6 UV spectra of N-melittin and N-melittin-TNB.

The DTNB modified N-melittin was successful synthesized and confirmed by UV spectroscopy, since N-melittin-TNB has an additional absorbance around 320 nm comparing to non-modified N-melittin (**Figure 4.6**).

Figure 4.7 Analytical RP-HPLC chromatograms of **a)** N-melittin, **b)** N-melittin-TNB, and **c)** DTNB. The analysis was carried out using a C18 column (5 μm, 150 × 4.6 mm) and a water/acetonitrile gradient (95:5–0:100 in 35 min) containing 0.1% TFA. For the detection at 218 nm was monitored.

RP-HPLC analysis was performed to establish the N-melittin-TNB was successfully synthesized and its purity. As shown in the **Figure 4.7**, it took 17.5 min for pure N-melittin to show up at a wavelength of 218 nm, while it took 18.5 min for pure DTNB to show up. However, it only took 18.0 min for N-melittin-TNB to show up with a single peak, which means that it was synthesized with high purity.

4.5 Characterization of C-melittin-TNB

The C-melittin-TNB were synthesized and characterized by UV spectra and RP-HPLC.
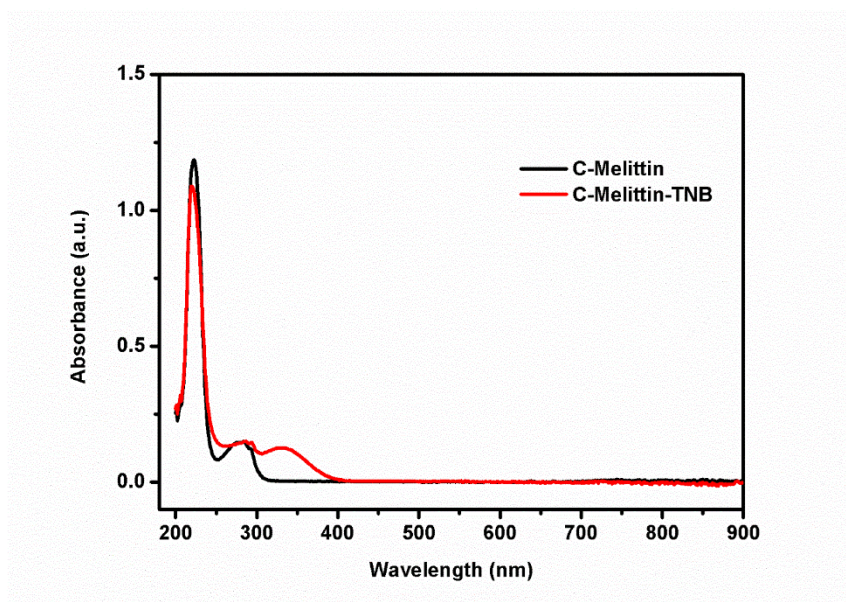
Figure 4.8 UV spectra of C-melittin and C-melittin-TNB.

As seen in the **Figure 4.8**, we can see that the C-melittin-TNB has a special absorbance around 320 nm comparing to non-modified C-melittin. This indicated that the C-melittin-TNB was obtained.

Using RP-HPLC, we confirmed that the C-melittin-TNB was effectively synthesized and of high purity. According to the results in **Figure 4.9**, at a wavelength of 218 nm, the appearance time of pure C-melittin was 19.4 min, and the appearance time of pure DTNB was 18.5 min. The appearance time of C-melittin-TNB after synthesis and purification was

19.0 min with a single sharp peak, which also shows that C-melittin-TNB has been synthesized with excellent purity.
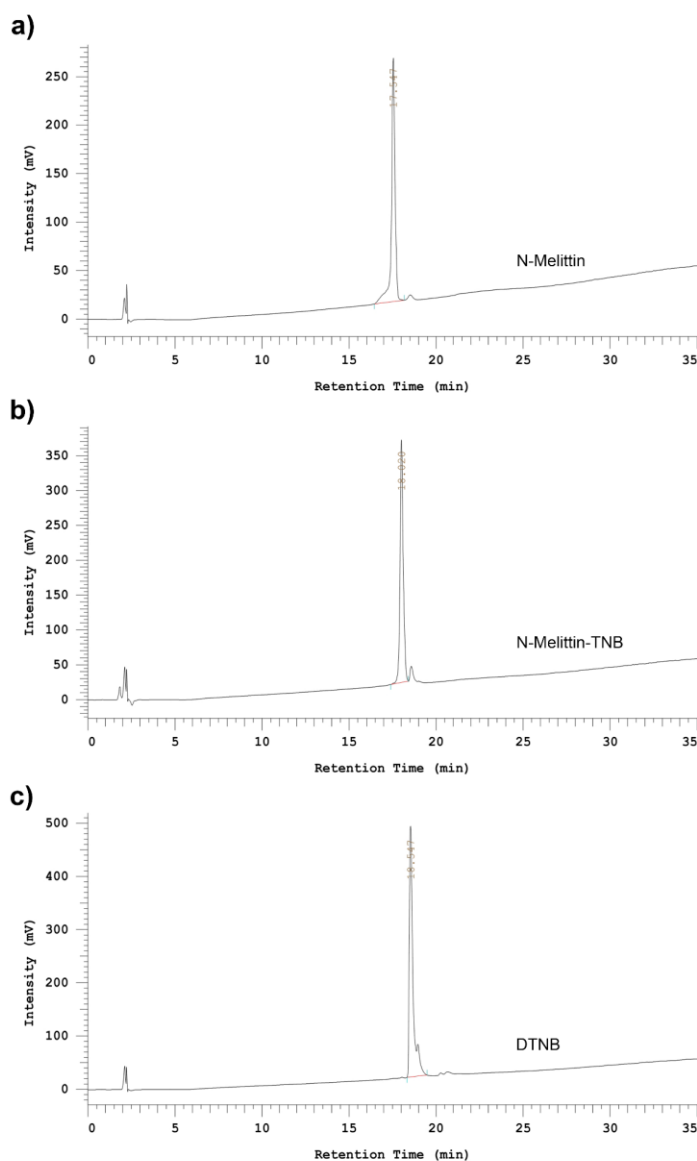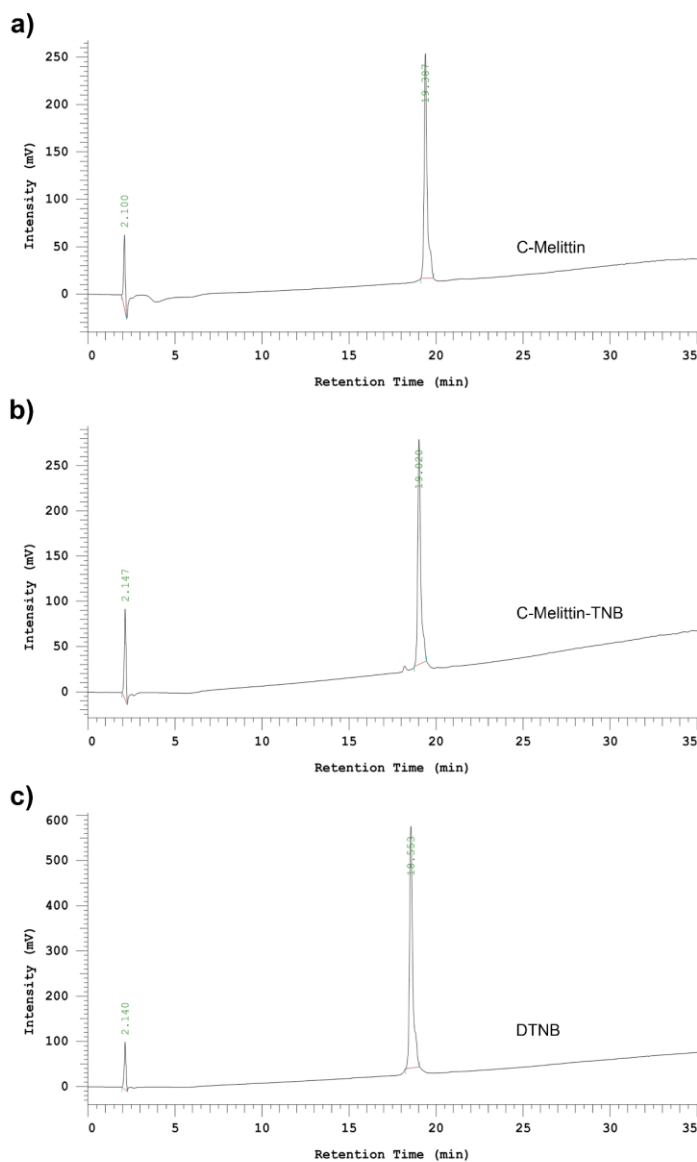

Figure 4.9 Analytical RP-HPLC chromatograms of **a)** C-melittin, **b)** C-melittin-TNB, and **c)** DTNB. The analysis was carried out using a C18 column (5 µm, 150 × 4.6 mm) and a water/acetonitrile gradient (95:5–0:100 in 35 min) containing 0.1% TFA. For the detection at 218 nm was monitored.

4.6 Characterization of OPSS-PEG$_{2kDa}$-GE11

The OPSS-PEG$_{2kDa}$-GE11 were synthesized and characterized by ^{1}H NMR and RP-HPLC.
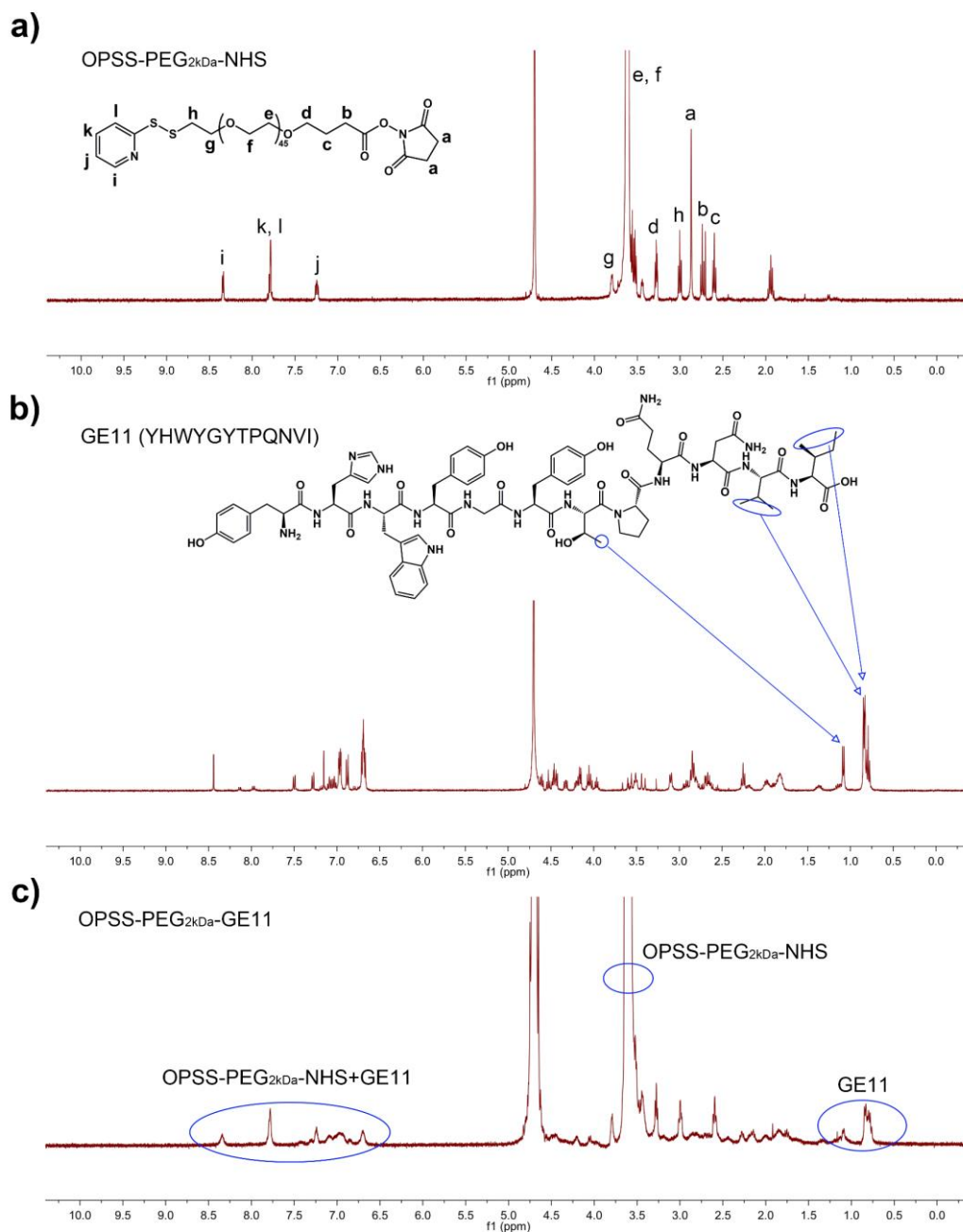
Figure 4.10 ^{1}H NMR (400 MHz, D$_2$O) of **a)** OPSS-PEG$_{2kDa}$-NHS, **b)** GE11, and **c)** OPSS-PEG$_{2kDa}$-GE11.

As seen in the **Figure 4.10a**, the typical signal of -(CH$_2$CH$_2$O)- on OPSS-PEG$_{2kDa}$-NHS can be observed at δ 3.58 ppm. The peaks at δ 7.25, 7.75, and 8.30 ppm correspond to the protons at the pyridine ring. The peak at δ 2.80 ppm was from the two -CH$_2$- on the succinimide part. The -CH$_3$- of GE11 can be observed at δ 0.75–1.15 ppm (**Figure 4.10b**). From the ^{1}H NMR data of OPSS-PEG$_{2kDa}$-GE11 (**Figure 4.10c**), we can see the typical signals of -(CH$_2$CH$_2$O)- and the pyridine ring on OPSS-PEG$_{2kDa}$-NHS at δ 3.58 ppm, δ 7.25, 7.75, and 8.30 ppm and GE11 peptide at δ 0.75–1.15 ppm. The peak at δ 2.80 ppm was missing, indicating that the succinimide part on OPSS-PEG$_{2kDa}$-NHS was replaced by GE11 peptide. All these results demonstrated that the OPSS-PEG$_{2kDa}$-GE11 was successfully obtained.

We performed an RP-HPLC analysis on the OPSS-PEG$_{2kDa}$-GE11 in order to get further evidence that it was effectively synthesized and that its purity had been maintained. According to the results in **Figure 4.11**, the appearance time of pure GE11 at a wavelength of 280 nm was 13.6 min, the appearance time of pure OPSS-PEG$_{2kDa}$-NHS was 24.8 min, whereas the appearance time of OPSS-PEG$_{2kDa}$-GE11 was 21.6 min with a single peak, which signifies that the OPSS-PEG$_{2kDa}$-GE11 was synthesized with good purity.
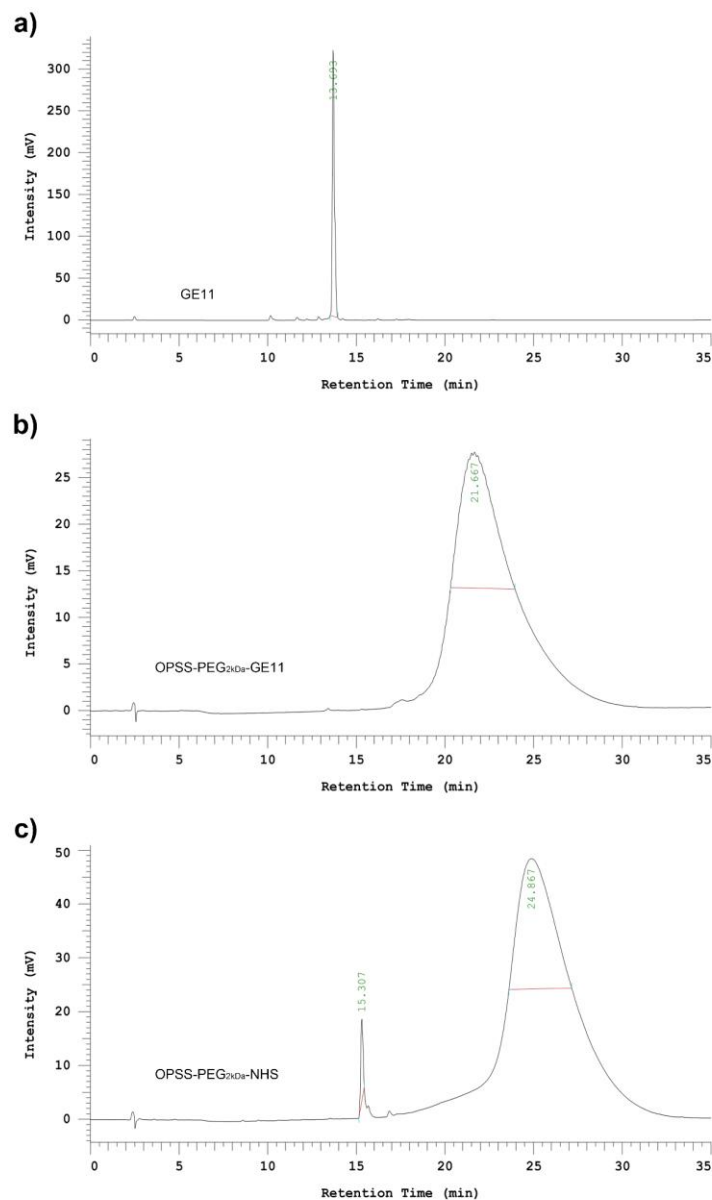
Figure 4.11 Analytical RP-HPLC chromatograms of **a)** GE11, **b)** OPSS-PEG$_{2kDa}$-GE11, and **c)** OPSS-PEG$_{2kDa}$-NHS. The analysis was carried out using a C18 column (5 µm, 150 × 4.6 mm) and a water/acetonitrile gradient (95:5–0:100 in 35 min) containing 0.1% TFA. For the detection at 280 nm was monitored.

4.7 Characterization of DBCO-R$_8$C-S-S-PEG$_{2kDa}$-GE11

The DBCO-R$_8$C-S-S-PEG$_{2kDa}$-GE11 were synthesized and characterized by UV spectra and RP-HPLC.
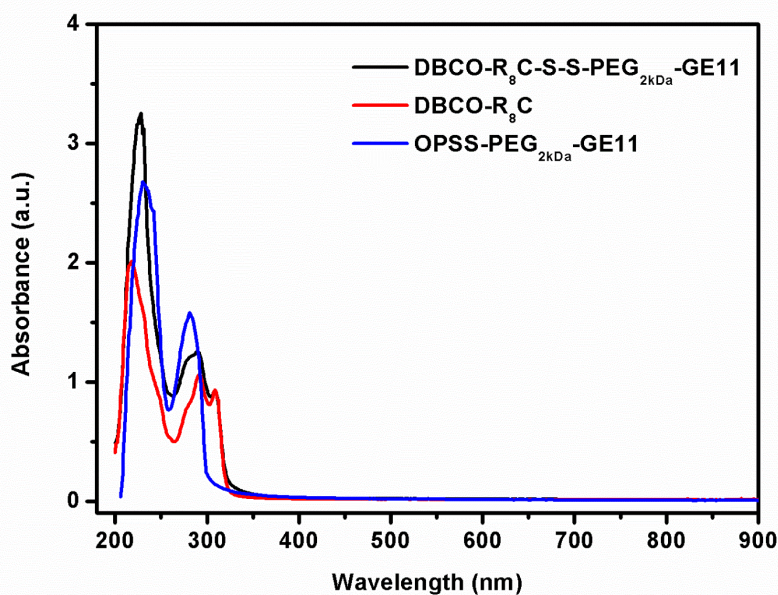
Figure 4.12 UV spectra of DBCO-R$_8$C-S-S-PEG$_{2kDa}$-GE11, DBCO-R$_8$C, and OPSS-PEG$_{2kDa}$-GE11.

Firstly, we characterized the DBCO-R$_8$C-S-S-PEG$_{2kDa}$-GE11 via UV spectra. As displayed in **Figure 4.12**, the OPSS-PEG$_{2kDa}$-GE11 has absorbance at 218 nm and 280 nm. Nevertheless, DBCO-R$_8$C has an additional absorbance at 309 nm. Therefore, when DBCO-R$_8$C and DBCO-R$_8$C-S-S-PEG$_{2kDa}$-GE11 have the same intensity peak at 309 nm, the absorbance of DBCO-R$_8$C-S-S-PEG$_{2kDa}$-GE11 at 218 nm and 280 nm were higher than the absorbance of DBCO-R$_8$C. These increased intensities were relied on the PEG$_{2kDa}$-GE11. Consequently, this signifies that the product has been synthesized.

Using RP-HPLC, we conducted an analysis on the DBCO-R$_8$C-S-S-PEG$_{2kDa}$-GE11 to further establish that it was effectively synthesized as well as its purity. As shown in the **Figure 4.13**, it took 12.3 min for pure DBCO-R$_8$C to turn up at a wavelength of 280 nm,

while it took 21.6 min for pure OPSS-PEG$_{2kDa}$-GE11 to turn up. However, it only took 20.2 min for DBCO-R$_8$C-S-S-PEG$_{2kDa}$-GE11 to turn up with a single peak, which means that it was synthesized with high purity.
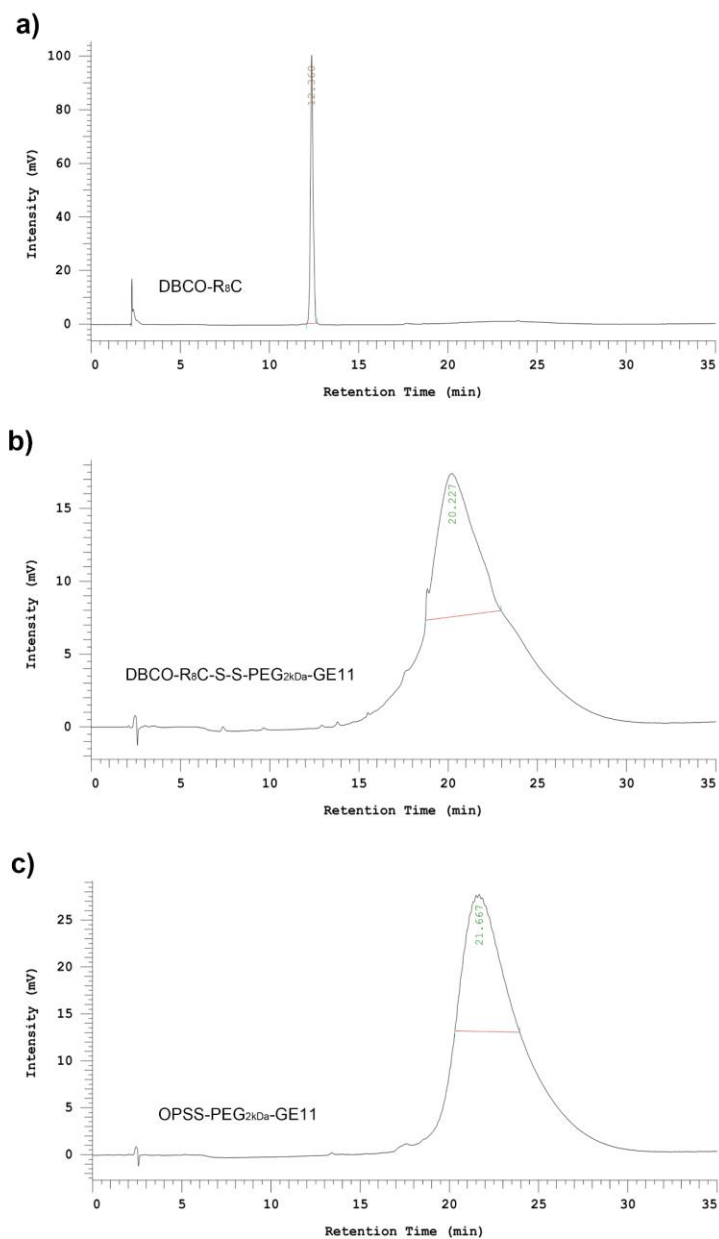
Figure 4.13 Analytical RP-HPLC chromatograms of **a)** DBCO-R$_8$C, **b)** DBCO-R$_8$C-S-S-PEG$_{2kDa}$-GE11, and **c)** OPSS-PEG$_{2kDa}$-GE11. The analysis was carried out using a C18 column (5 μm, 150 × 4.6 mm) and a water/acetonitrile gradient (95:5–0:100 in 35 min) containing 0.1% TFA. For the detection at 280 nm was monitored.

4.8 Characterization of DBCO-R$_8$C-S-S-N/C-melittin

The DBCO-R$_8$C-S-S-N/C-melittin were synthesized and characterized by MALDI-TOF-MS.

As shown in **Figure 4.14**, the MALDI-TOF-MS confirmed that the pure DBCO-R$_8$C-S-S-N/C-melittin were obtained.
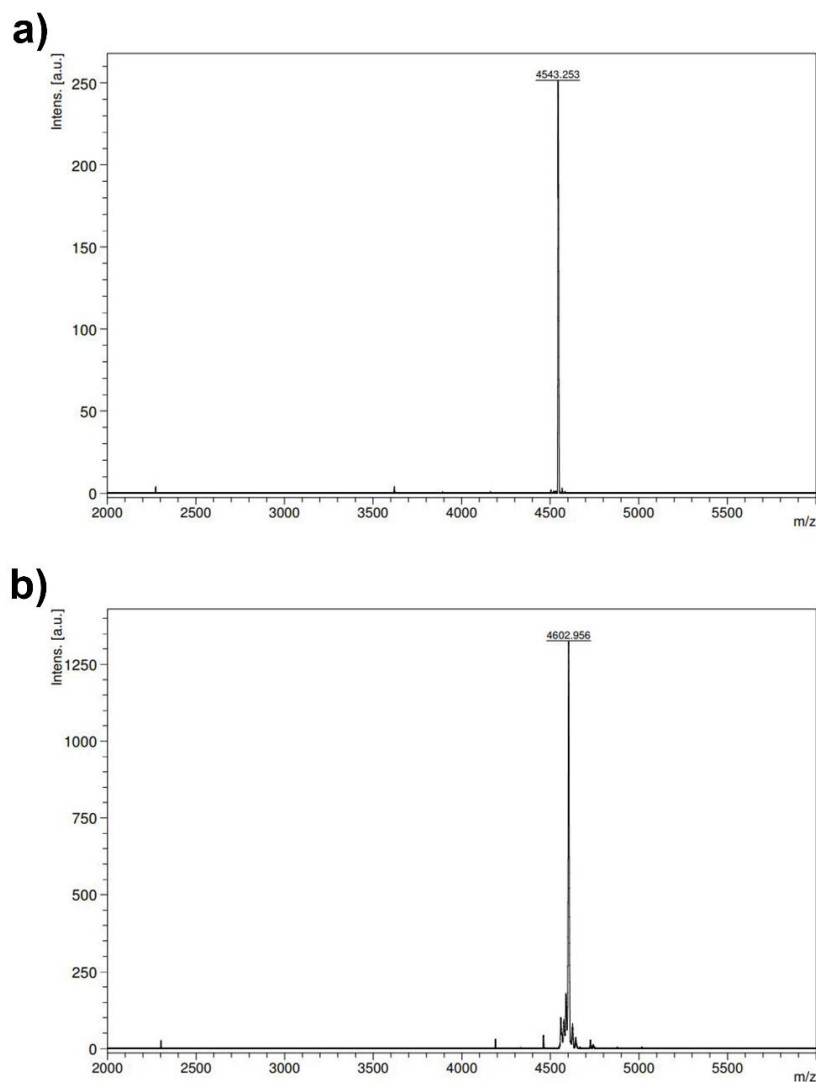
Figure 4.14 MALDI-TOF-MS spectra of **a)** DBCO-R$_8$C-S-S-N-melittin and **b)** DBCO-R$_8$C-S-S-C-melittin.

4.9 Stability and release profiles of eGFP conjugates

An efficient delivery strategy may require an optimum compromise between stability and release kinetics. High stability in the extracellular environment and favorable release triggered by local and intracellular stimuli are principle scopes in the current delivery models.[37, 123, 124] Hence, the stability/release profiles of the new eGFP conjugates were investigated with SDS-PAGE technique, albeit without reducing DDT or β-mercaptoethanol in the loading buffer, to avoid disulfide bond cleavage affecting the eGFP conjugate stability.[125] Since unmodified eGFP was the control for our stability/release studies, the effect of our optimized protocol on its gel migration was compared with the standard protocol. **Figure 4.15a** illustrates the electrophoretic pattern of free eGFP in the absence (sample I) and presence (sample II) of reducing agents in the loading buffer. Higher protein mobility was observed under non-reducing (sample I) than reducing SDS-PAGE, resulting in a lower MW band (~ 25 kDa) than the actual MW at ~ 30 kDa. This indicates that in optimized non-reducing SDS-PAGE, the disulfide bonds remain intact, leading to the compact conformation of the protein and higher electrophoretic mobility.[126] The gel mobility was also measured for monomer subunits DBCO-R_8C-S-S-PEG_{2kDa}-GE11, DBCO-R_8C-S-S-N-melittin, and DBCO-R_8C-S-S-C-melittin, as shown in samples III–V, respectively (**Figure 4.15a**).

To investigate whether eGFP conjugates are stable at physiological pH, we incubated them in HEPES buffer (pH 7.4) for 24 h at 37°C before evaluation by SDS-PAGE (**Figure 4.15b, c**). The gel revealed a different banding pattern of eGFP conjugates compared with unmodified protein. A slight shift of gel bands toward lower migration was found by increasing the PEG_{2kDa}-GE11 chains in the eGFP conjugates. In parallel with our observation, it has been reported that PEG can alter the physical characteristic and subsequent gel mobility.[127] As shown in the gels, no band was detected corresponding to the eGFP or functional units, suggesting the stability of all eGFP conjugates A–E at pH 7.4 (**Figure 4.15b, c**).
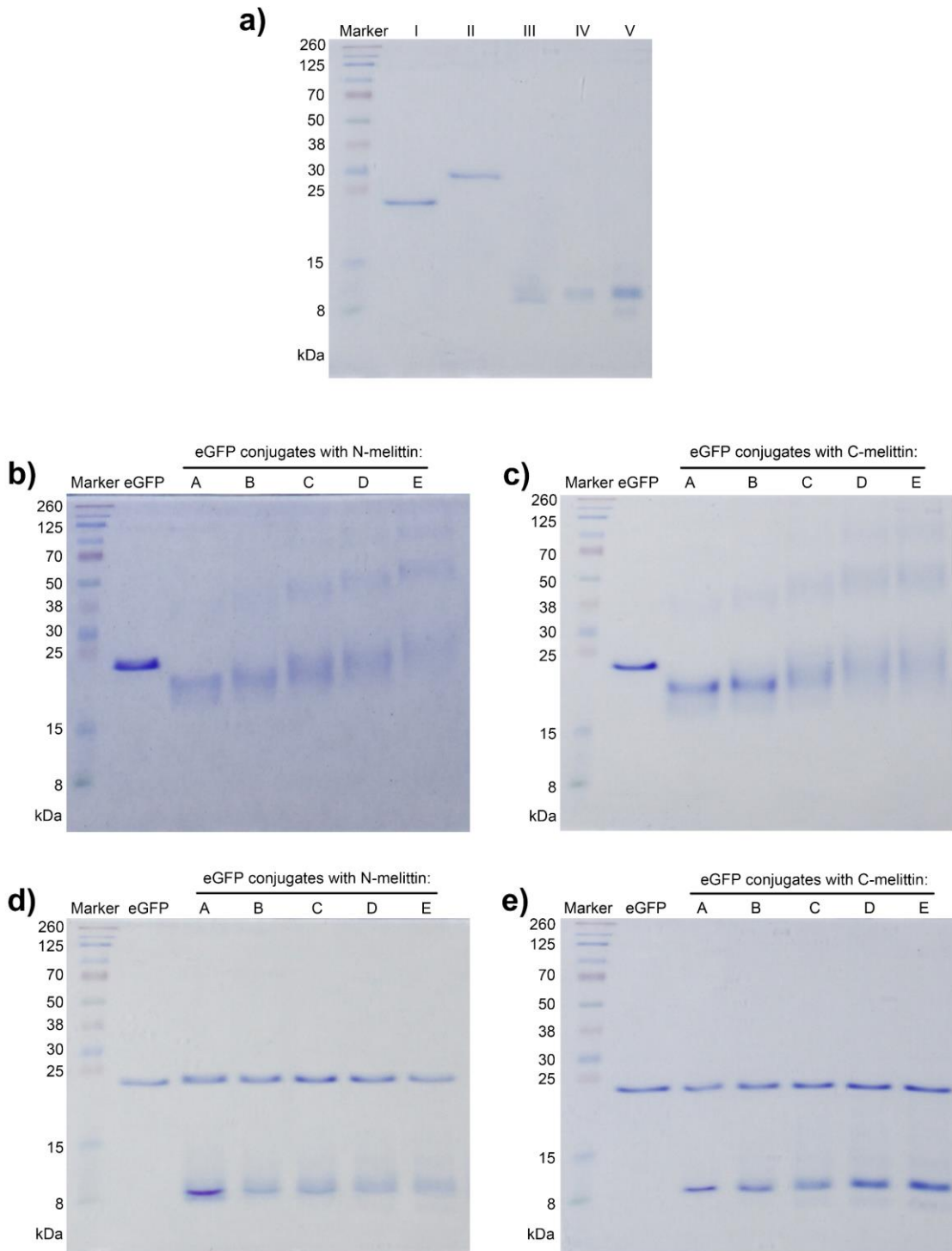
Figure 4.15 The stability and traceless release of eGFP conjugates A–E (with N- or C- melittin) by SDS-PAGE. **a)** The gel mobility was detected for free eGFP in I) non-reducing loading buffer (containing SDS alone) and II) reducing loading buffer (containing SDS+DTT+β-mercaptoethanol), alongside for III) DBCO-R_8C-S-S-PEG$_{2kDa}$-GE11, IV) DBCO-R_8C-S-S-N-melittin, and V) DBCO-

R$_8$C-S-S-C-melittin in non-reducing loading buffer. The stability of eGFP conjugates with **b)** N-melittin and **c)** C-melittin was studied after incubation in HEPES buffer (pH 7.4) for 24 h at 37°C. The pH-dependent traceless release of eGFP from conjugates with **d)** N-melittin or **e)** C-melittin was monitored after incubation in HEPES buffer (pH 5.5) for 24 h at 37°C.

Also, no significant difference was observed between the eGFP conjugate stability including N-terminally (**Figure 4.15b**) or C-terminally cysteine-containing melittin (**Figure 4.15c**). We hypothesized that covalent modification of the eGFP conjugates should be reversible upon exposure to endosomal-like acidic pH, leading to traceless release of original eGFP. To test this, eGFP conjugates were incubated for 24 h in pH 5.5 HEPES buffer at 37°C, and the released protein was then monitored using SDS-PAGE. As follows from the results, clear bands corresponding to the MWs of eGFP and functional units were observed for each eGFP conjugate, demonstrating the pH-responsive traceless cleavage of protein (**Figure 4.15d, e**). From the SDS-PAGE findings, it can be concluded that eGFP can be released tracelessly in the acidic endosome but is stable under physiological pH.

4.10 pH-dependent cleavage kinetics of eGFP-AzMMMan and eGFP-TPAn

In the dual pH-sensitive delivery system that we have designed, the order of pH response is essential to ensure that the protein can be traceless released into the cytoplasm. Specifically, TPAn triggers charge reversal in response to pH 6.5, and AzMMMan releases protein at a more acidic pH 5.5 is required.

Therefore, we did a 24 h-monitoring of the exposed amino groups from eGFP-AzMMMan and eGFP-TPAn through TNBS assay at different pH to confirm this. As seen in **Figure 4.16**, the results showed that both eGFP-AzMMMan and eGFP-TPAn were quite stable with only about 17% cleavage after 24 h at physiological pH 7.4. There was a little bit increased ratio of exposed amino groups from eGFP-AzMMMan at pH 6.5. In contrast, at pH 6.5 the amino groups exposure ratio of eGFP-TPAn was over 98% within 4 h indicating that nearly all the TPAn were cleaved from eGFP. Furthermore, we can see that the eGFP-TPAn also more sensitive than eGFP-AzMMMan at pH 5.5 which the amino groups

exposure ratio up to 90% took 4 h from eGFP-AzMMMan but only took 2 h from eGFP-TPAn.
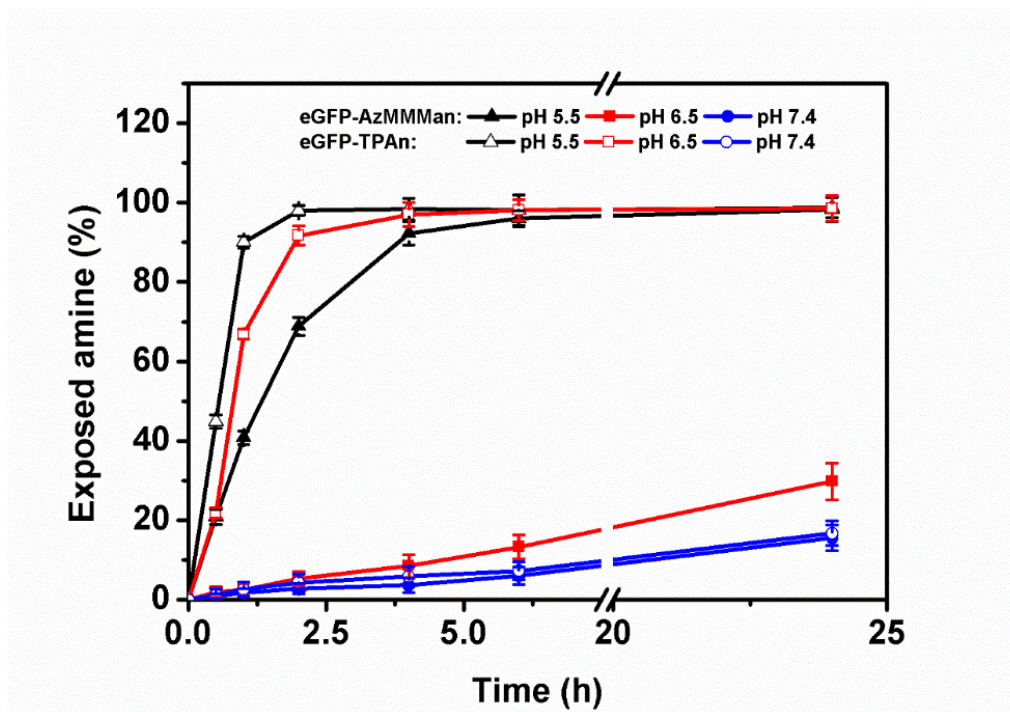
Figure 4.16 pH-dependent cleavage kinetics of eGFP-AzMMMan and eGFP-TPAn. The exposed amino changes of eGFP in HEPES buffer (pH 7.4, 6.5 or 5.5) at different incubation time points at 37°C were detected using TNBS assay (n = 3, mean ± SD).

These findings demonstrated that the TPAn was more sensitive than AzMMMan in acidic pH, and both of them are stable at physiological pH. Hence, the dual pH-sensitive delivery system was appropriate for transporting proteins.

4.11 Dual pH-responsivity of eGFP conjugates

The pH-responsive systems play fundamental roles in controllable cargo delivery by taking advantage of the pH difference between healthy tissues (pH ~ 7.4), extracellular tumor microenvironment (pH ~ 6.5), and endosomes (pH ~ 5.5).[128] A dual pH-response process may take place in an intelligent stepwise manner: the first step in the extracellular environment at the tumor site for a charge conversion-promoted cellular uptake, and the

second one in endosome for a traceless cargo release, both collaboratively ensuring the efficiency of protein delivery.[37, 129, 130]

With charge-reversal properties, delivery can benefit from the overall negative charge of the masked eGFP-octa-arginine/melittin conjugates avoiding undesired nonspecific cationic bio-interactions outside the target area on the one hand, and after unmasking the positive charge of conjugates enhancing desired cell penetration on the other hand. For demonstrating the pH-triggered charge reversal feature, we measured the zeta potential of eGFP conjugates in response to the acidic pH. Prior to the experiment, eGFP conjugates were incubated for 4 h at 37°C in HEPES buffer (pH 7.4 or 6.5). As shown in **Figures 4.17a** (including N-melittin) and **4.17b** (including C-melittin), eGFP conjugate A (only melittin-TPAn units, lacking PEG$_{2kDa}$-GE11 units) showed a low positive zeta potential at around +6 mV attributed to the presence of R$_8$C domains.
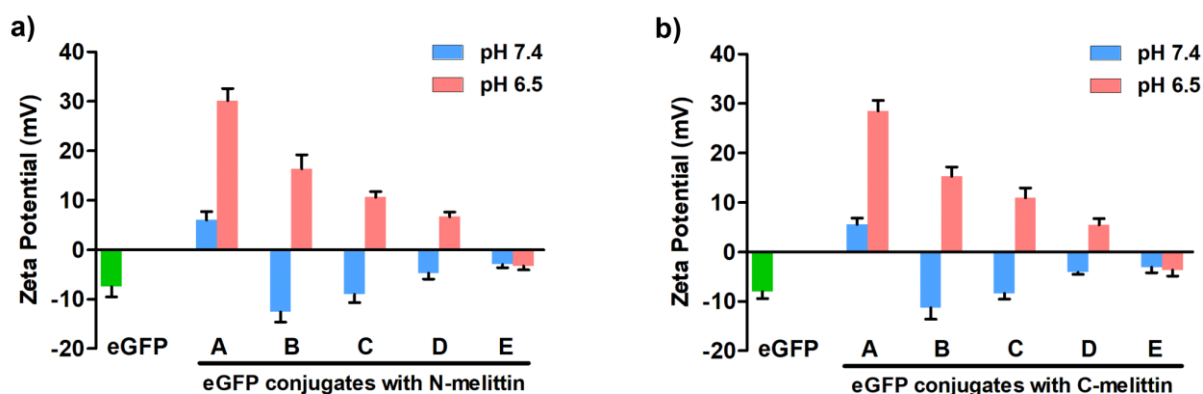
Figure 4.17 The pH-sensitive charge reversal of eGFP conjugates A–E. Zeta potential of eGFP conjugates with **a)** N-melittin-TPAn and **b)** C-melittin-TPAn were measured by electrophoretic light scattering (ELS) after incubation in HEPES buffer (pH 7.4 or 6.5) for 4 h at 37°C (n = 3, mean ± SD).

At acidic pH of 6.5, the surface charge of eGFP conjugate A experienced a dramatic increase to around +30 mV. The eGFP conjugates B, C, and D had negatively charged surfaces at pH 7.4, while after incubation in pH 6.5 HEPES buffer their zeta potential

increased to +16, +11, and +7 mV, respectively. No change was evident in the zeta potential of eGFP conjugate E (only PEG$_{2kDa}$-GE11 units) under pH 7.4 and pH 6.5, and it kept its zeta potential at around −3 mV even after acidic pH exposure. Clearly, the charge shifting from low positive to more positive charge (eGFP conjugate A) and from negative to positive charge (eGFP conjugate B–D) ensure the charge reversal phenomenon resulting from TPAn cleavage from melittin in response to the pH stimulus. Covalent masking of melittin by TPAn replaces the positively charged amino groups by negatively charged carboxyl groups for a reversible surface charge shielding at physiological pH. The positive surface charge of the eGFP conjugates after charge reversal highly depends on the melittin content. Accordingly, eGFP conjugate A exhibited the highest and eGFP conjugates D the lowest positivity after charge reversal. In the eGFP conjugate E, no change in zeta potential occurs due to the absence of melittin.

To further demonstrate the occurrence of charge reversal, we performed a 24-hour monitoring measurement for amino groups exposure ratio of the eGFP conjugates in pH 7.4 and 6.5 at 37°C through TNBS assay. As shown in the **Figure 4.18**, the results showed that the amino groups exposure ratio of eGFP conjugates A to D were increased over 90% in the first 4 h and the ratio over 95% after 24 h incubation at pH 6.5. It means that the charge reversal happened at pH 6.5 and most of the amino groups were exposed within 4 h. Meanwhile, at pH 7.4, we can see that the amino groups exposure ratio of eGFP conjugates A to D were no more than 6% in the first 4 h and less than 15% after incubated 24 h. This results also indicated that the eGFP conjugates are very stable at physiological pH within 24 h.
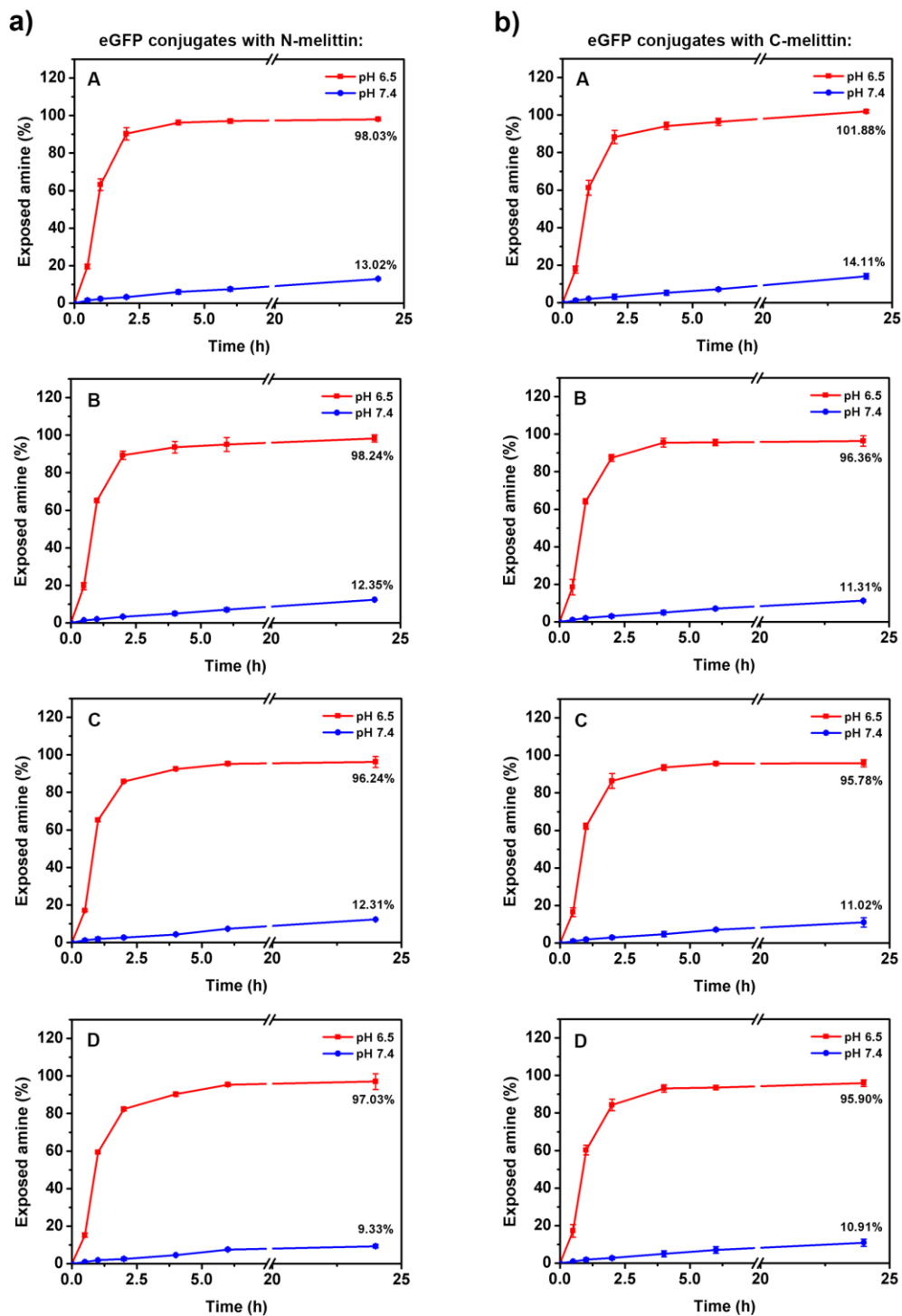
Figure 4.18 The exposed amino changes of eGFP conjugates (A–D) with **a)** N-melittin and **b)** C-melittin in HEPES buffer (pH 7.4 or 6.5) at different incubation time points at 37°C were detected using TNBS assay (n = 3, mean ± SD).

Furthermore, the traceless release of eGFP by reversal of the AzMMMan linkage at a slightly more acidic endosomal pH of 5.5 was also determined by TNBS assay. To avoid any complication by melittin-TPAn unmasking, this experiment was carried out with eGFP conjugates A–D with N-melittin but lacking TPAn, and conjugate E (lacking melittin). eGFP conjugates were subjected to a 24 h-monitoring of unmasked eGFP amino groups released at pH 5.5, 6.5, or 7.4 at 37°C (**Figure 4.19**).
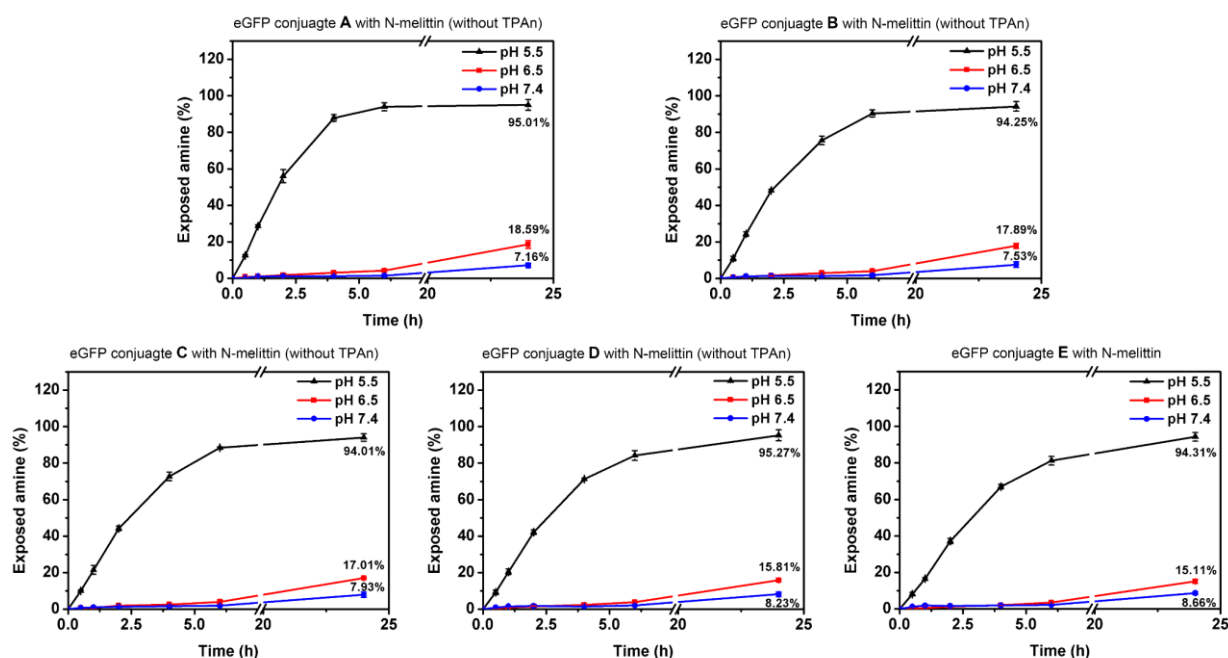
Figure 4.19 The pH-sensitive traceless release of eGFP. Traceless release of eGFP from analogs of conjugates A–D (with N-melittin but without TPAn masking) and conjugate E was evaluated upon incubation at different pH (5.5, 6.5, and 7.4) at 37°C via TNBS assay (n = 3, mean ± SD).

When using the TNBS assay to detect the exposed amino groups of eGFP, the lysine amino groups of melittin were subtracted as background. For all eGFP conjugates, the unmasking of amino groups was low both at pH 7.4 and 6.5; even after 24 h it did not exceed 10% at pH 7.4 and 19% at pH 6.5. Within the same period but at pH 5.5, more than 94% of eGFP amino groups were unmasked, and up to 70% after a shorter time period of 4 h. MALDI-TOF-MS analysis of conjugate D after cleavage confirmed that the

main peak of released eGFP showed almost identical molecular weight as free eGFP, a strong support for the traceless release (**Figure 4.20**).

a)

b)
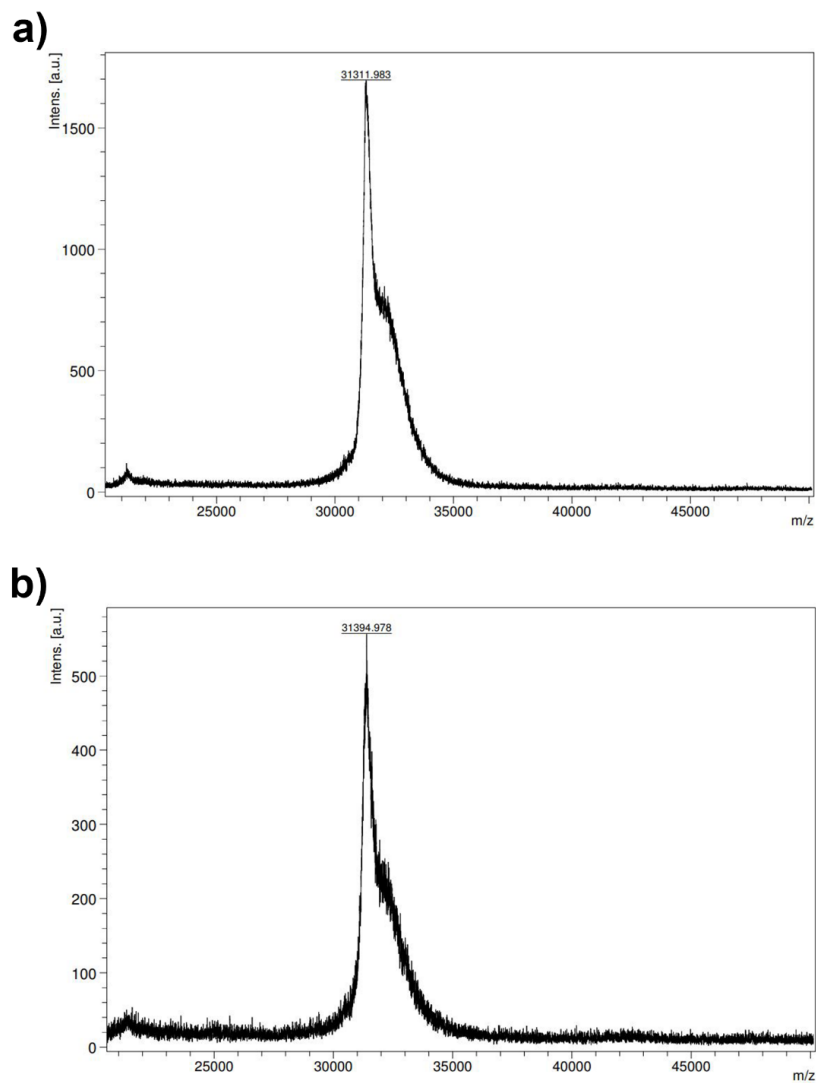
Figure 4.20 MALDI-TOF-MS spectra of **a)** free eGFP and **b)** traceless released eGFP from eGFP conjugate D (with N-melittin but without TPAn masking) at pH 5.5 for 24 h at 37°C. The broad peak of eGFP and traceless released eGFP is almost identical, with the difference of the top peak only 83 mass units which is less than one AzMMMan (MW 167).

These data confirm that the current dual-responsive system can fulfill the requirements of stability at neutral pH, a charge reversal at weakly acidic pH but without causing prominent

cleavage of AzMMMan bonds, and a traceless release under slightly more acidic endosomal pH (mainly in the first 4 h), all owing to the dual pH-responsive design of the eGFP conjugates.

4.12 Cellular uptake of active-targeted pH-responsive eGFP conjugates

Flow cytometry analysis was carried out to obtain quantitative information about the cellular uptake behavior of the different eGFP conjugates. Several criteria were considered in the evaluation procedure to properly address the impact of GE11-mediated targeting and pH-triggered charge conversion on the cellular uptake. To show the role of active targeting, the HeLa-derived carcinoma cell line KB overexpressing EGFR (**Figure 4.21a**) was considered as suitable cell target for the peptide ligand GE11.[103, 104] The results were verified by testing the neuroblastoma N2A cell line (**Figure 4.21b**) as a negative control due to the no/low expression levels of EGFR.[131] For charge reversal to occur *in vitro*, the acidic condition of the tumor microenvironment was mimicked by adjusting the pH of the cell culture medium to 6.5 to provide the pH-induced cleavage of TPAn from melittin (in situ cleavage of eGFP conjugates). Of note, the acidic condition had no significant effect on the cell viability (data not shown). In parallel to this, two culture control groups were run in the standard pH 7.4 culture medium, where cells were treated either with non-cleaved conjugates (TPAn-covered melittin) or with pre-cleaved eGFP conjugates as positive controls, respectively. To verify the efficiency of the conjugate-based delivery system, the free eGFP was applied for comparison. For the pre-cleaved eGFP conjugate samples, the cleavage of the melittin-TPAn bond was performed at pH 6.5 for 4 h before incubation with cells. Prior to flow cytometry, the KB cells were incubated with different eGFP conjugates (A–E, 2 µM) in non-cleaved or pre-cleaved form or under in situ cleavage condition for 4 h. HEPES-treated cells were used to set the gating. As shown in **Figure 4.21a**, a significant cellular uptake could be observed for all pre-cleaved and in situ-cleaved eGFP conjugates A–D containing TPAn-unmasked melittin, while uptake was low for non-cleaved ones and, surprisingly, for the melittin-free but EGFR-targeted conjugate E.

a)

b)
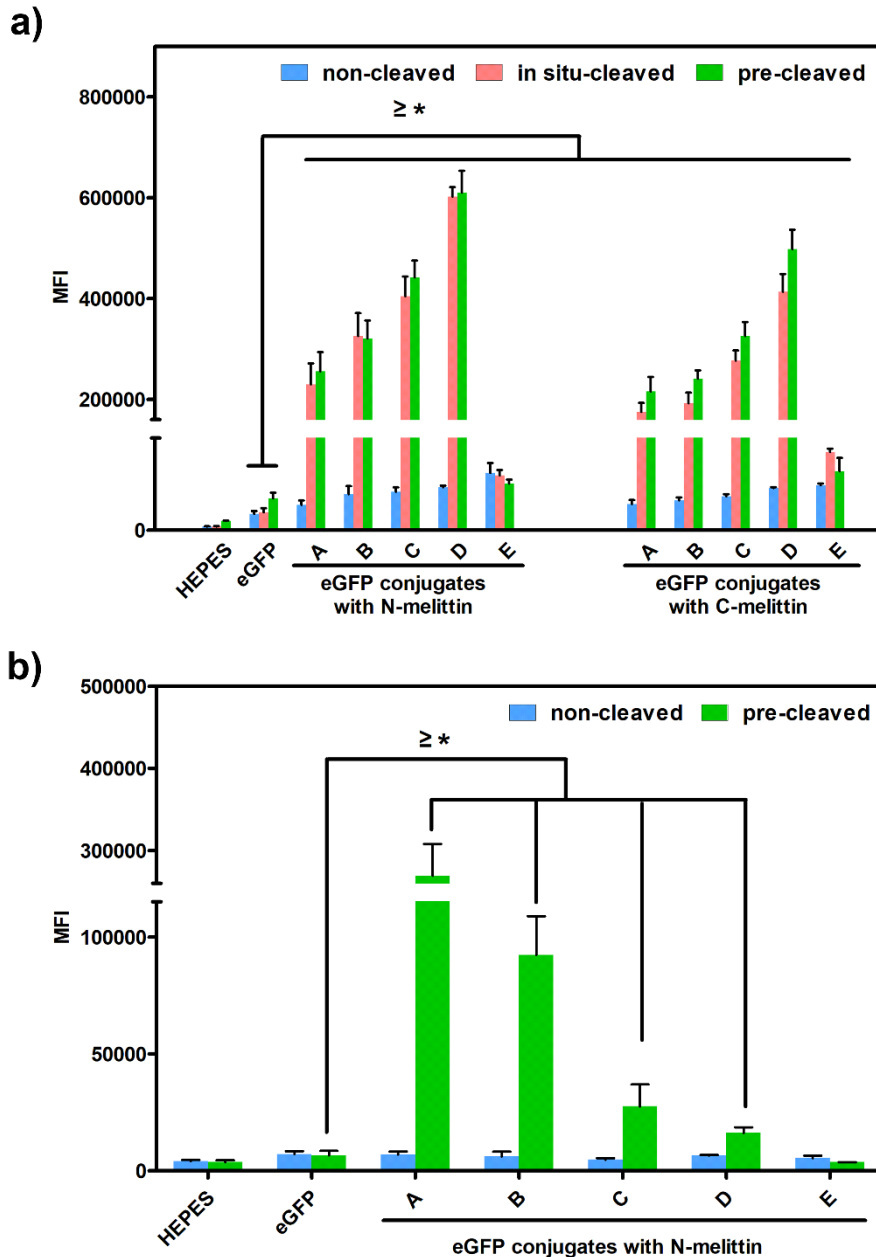
Figure 4.21 EGFR-specific cellular uptake of eGFP conjugates. **a)** Cellular uptake of eGFP conjugates A–E with N- or C-melittin (with/without TPAn) into the receptor-positive KB cells after 4 h incubation at 37°C acquired by flow cytometry. **b)** Analogous uptake control study of eGFP conjugates containing N-melittin (with/without TPAn) on the receptor-negative cell line N2A. Unmodified eGFP was considered as negative control. The HEPES-treated control cells were used to set up gating. eGFP conjugates were applied to cells at 2 µM either in their intact form (non-cleaved), or after *in vitro* pre-incubation at pH 6.5 for 4 h (pre-cleaved), both under standard cell culture conditions of pH 7.4. Additionally, the conjugate cleavage under tumor

50

microenvironment conditions was simulated by adding intact conjugates to cell culture medium with adjusted pH to 6.5 (in situ-cleaved) (n = 3, mean ± SD). Significant differences between the groups were calculated as *p < 0.05, **p < 0.01, and ***p < 0.001. Experiments were carried out by Mina Yazdi (PhD student at Pharmaceutical Biotechnology, LMU München).

The minor differences between the pre- and in situ-cleaved samples signify that the charge reversal of eGFP conjugates can occur in pH 6.5 cell culture medium mimicking the mild acidic tumor microenvironmental pH *in vitro*. Expectedly, unmodified eGFP and TPAn-capped eGFP conjugates (without any acidic exposure) had no significant affinity toward cell membrane, likely attributed to their lack of positive charge.

In contrast to the non-cleaved eGFP conjugate A (melittin: 22 equiv, GE11: 0 equiv), the pH-dependent detachment of TPAn from melittin and subsequent charge reversal of conjugate A could promote the electrostatic attraction to the cell membrane leading to enhanced cellular uptake which is the main aim of the surface modification strategy. When comparing pre- or in situ-cleaved eGFP conjugates A to D, it can be found that the cellular uptake was influenced by the ratio of cationic melittin and peptide ligand GE11 in the delivery system. The more GE11 peptide, the higher cellular entry could be obtained in receptor-positive KB cells (**Figure 4.21a**), which is highlighted in the highest uptake of eGFP conjugate D (melittin: 6, GE11:16 equiv). In contrast, evaluation of the cellular uptake into EGFR-negative N2A cells demonstrated the most increased uptake for conjugate A with the highest TPAn-unmasked melittin content, and lowered uptake (conjugates B to D) with increasing PEG_{2kDa}-GE11/reducing melittin content (**Figure 4.21b**). In these non-target cells, uptake strictly correlated with the surface charge of conjugates after charge reversal upon melittin unmasking as displayed in **Figure 4.17**. The comparison of **Figure 4.21a** and **4.21b** well documents that the uptake of conjugate A is only charge reversal-mediated, whereas conjugate D is strongly dependent on receptor-ligand interaction. In agreement with several studies, our delivery system benefits from active targeting via EGFR-mediated uptake of protein cargo.[63] Data confirm that for KB target tumor cells, the GE11-EGFR interaction is necessary to increase the transfection efficiency in a synergistic fashion with charge reversal-induced electrostatic endocytosis. Interestingly, the conjugation of PEG_{2kDa}-GE11 units alone (without melittin-

TPAn units) in eGFP conjugate E (slightly negative zeta potential, see **Figure 4.17**) could not provide a similar uptake efficacy as for eGFP conjugates B to D, emphasizing the effective role of both GE11 ligand and melittin-related positive charge (**Figure 4.21a**). The favorable cellular uptake results imply to the combined effect of receptor-ligand and electrostatic targeting of eGFP conjugates also facilitated by the protein transduction domain octa-arginine compensating the negative charges of eGFP-AzMMMan.

4.13 Cellular internalization and endosomal escape of eGFP conjugates

The cellular uptake and endosomal escape of the eGFP conjugates were concurrently imaged by confocal microscopy using HeLa cells stably expressing Gal8-mRuby3 reporter. Like its subclone KB, HeLa cells overexpress EGFR. Cells were treated with different eGFP conjugates (A–E, 2 µM) for 24 h. Before the experiment, the conjugates underwent pH-induced charge transition via unmasking TPAn from melittin (pre-cleaved conjugates). The nuclei of cells were stained with DAPI. As is seen in **Figure 4.22**, cellular internalization varies with different eGFP conjugates. Conjugates A to D showed an increasing trend in uptake consistent with the flow cytometry results. The observed structure-function relationship further supports our conclusion that a higher ratio of GE11 could amplify the cellular internalization, but requires the presence of unmasked positively charged melittin. This also explains why no cell entry was observed for conjugate E. Therefore, of the five tested eGFP conjugates, conjugate D is appreciated regarding its highest uptake and distribution inside the cells.
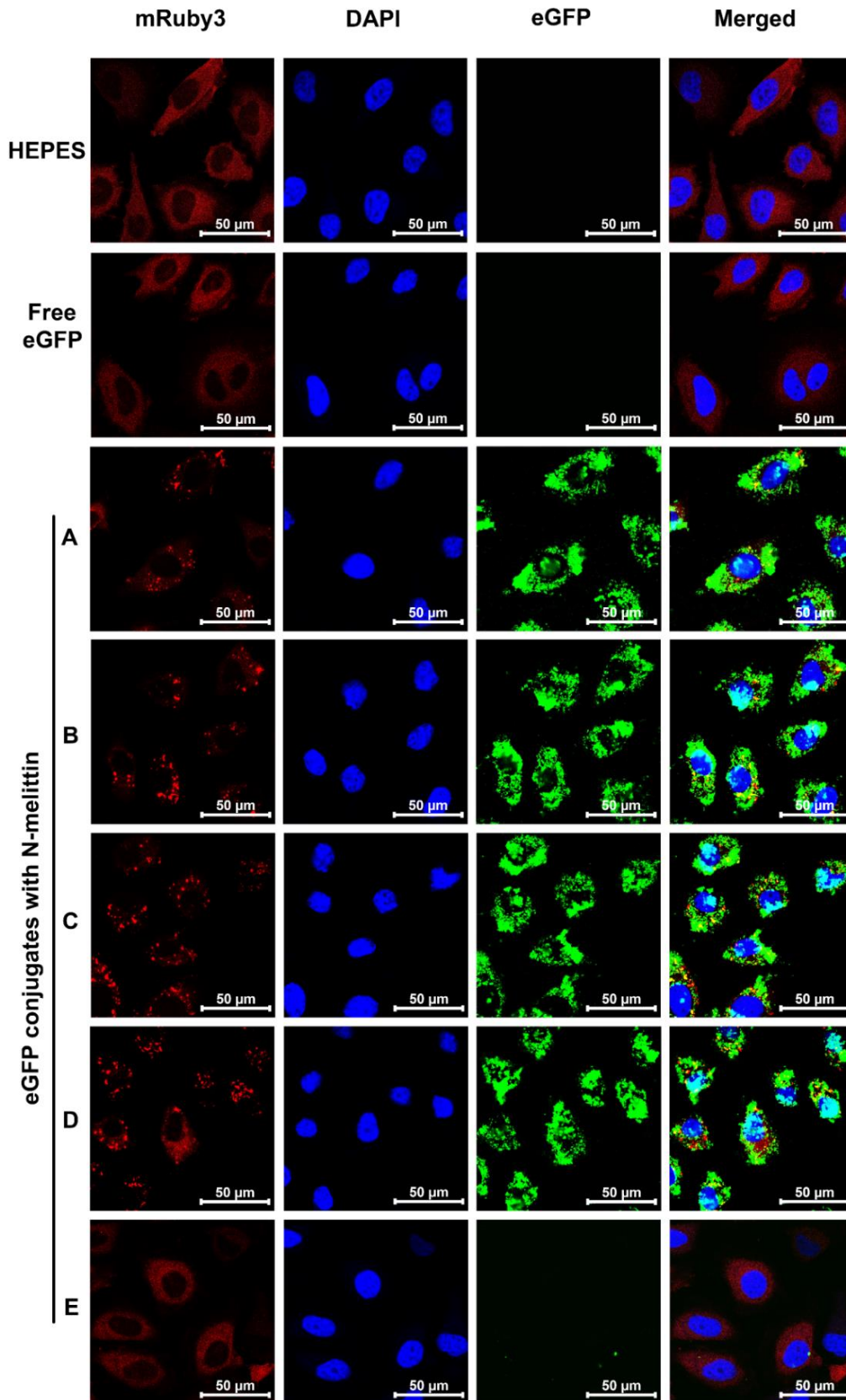
Figure 4.22 The simultaneous visualization of intracellular delivery, endosomal escape, and nuclear delivery of eGFP conjugates (with N-melittin) imaged by confocal laser scanning microscopy (CLSM). The pre-cleaved eGFP conjugates A–E (2 µM) and unmodified eGFP were incubated with HeLa cells stably expressing Galectin8-mRuby3 (HeLa-Gal8-mRuby3) for 24 h at 37°C before imaging. The colors were defined as follows: the diffused cytosolic mRuby3 distribution (red), endosomal-membrane disruption (bright red spot), nucleus (blue, stained by DAPI), and eGFP protein bearing a nuclear localization signal (nls) (green). The scale bars represent 50 µm. Experiments were performed by Miriam Höhn (Pharmaceutical Biotechnology, LMU München) and Mina Yazdi (PhD student at Pharmaceutical Biotechnology, LMU München).

What makes a delivery system sufficiently ideal for protein delivery is an optimal endosomolysis profile correlated with the cytosolic release of the cargo.[132] The HeLa-Gal8-mRuby3 cell line also enables the characterization of the endosomal escape performance of the conjugates.[133, 134] In the absence of endosomal membrane destabilization, cells showed a diffused cytosolic mRuby3 distribution pattern as revealed in the HEPES-treated control cells (**Figure 4.22**). Following endosome membrane disruption, Gal8-mRuby3 interacts with glycosylation moieties on the intra-endosomal surface leading to punctate fluorescent spots. **Figure 4.22** illustrates the apparent endosomal disruption events for all eGFP conjugates except for conjugate E. The reason is ascribed to the pH-dependent lytic role of melittin after the AzMMMan cleavage to induce rupture in the endosome membrane. eGFP conjugates A to D contain melittin contributing to their endosomal escape. The conjugate E lacking melittin is not effective for protein delivery, suffering from low uptake and lack of subsequent endosomal escape. The successful endosomal release can be confirmed not only by fluorescent spots but also by the subsequent nuclear localization of the eGFP protein. Since the eGFP model in our system is tagged with a lysine-containing SV40 LTA nuclear localization signal (nls), trafficking into the nucleus requires a traceless cleavage from the conjugates and endosomal escape of the active form of the protein. We conclude from our results regarding conjugate D that the traceless cleavage of acid-labile bonds provided by AzMMMan linker resulted in the unmodified eGFP escape from the endosome into the cytosol followed by nuclear accumulation (**Figure 4.22**).

4.14 Controllable lytic activity of melittin in eGFP conjugates

Melittin is a major part of the bee venom with a sequence of 26 amino acids. It has been utilized in various forms for the delivery of different cargos (e.g. drug, gene and protein).[84, 95, 96, 106, 122, 135-140] Due to its positive charge, melittin is involved in the electrostatic interaction with the negatively charged cell membrane, which is advantageous to enhance cell entry. The potent lytic activity of natural melittin is not pH-specific; therefore, the concentration of melittin plays a critical role at the site of action, inducing membrane disruption in the endosome or at the cell surface. Although melittin is an attractive candidate in the cargo delivery context, its undesired cytolysis ability hampering clinical application requires control. Boeckle et al. previously observed that blocking the N-terminus of melittin by linkage to a carrier reduced lysis activity at neutral pH but not at endosomal pH, providing a preferred specificity over C-terminal coupling.[95] Meyer et al. introduced a methodology in which melittin lysine residues were masked by DMMAn, blocking lytic activity. Upon endosomal acidification at around pH 5.5, DMMAn is cleaved off the lysines and melittin restores its lytic effect required for an endosomal escape; this was successfully applied for an improved nucleic acid transfer.[84, 96, 106] In the current work, we applied the more labile TPAn to mask melittin through a pH-responsive bond at the tumor microenvironment.

In order to check any unfavorable lytic activity of N- or C-melittin, we evaluated cell viability of KB cells after treatment with escalating doses of eGFP conjugates in various states (non-cleaved, in situ-cleaved, pre-cleaved). Based on 48 h MTT results (**Figure 4.23**), no cytotoxicity of intact (non-cleaved) eGFP conjugates was observed even at an extremely high concentration of 8 µM (**Figure 4.23a** for N-melittin, **Figure 4.23b** for C-melittin). This is well explained by TPAn activity covering the positive charges of melittin and preventing interaction with the cell membrane.

a)

b)
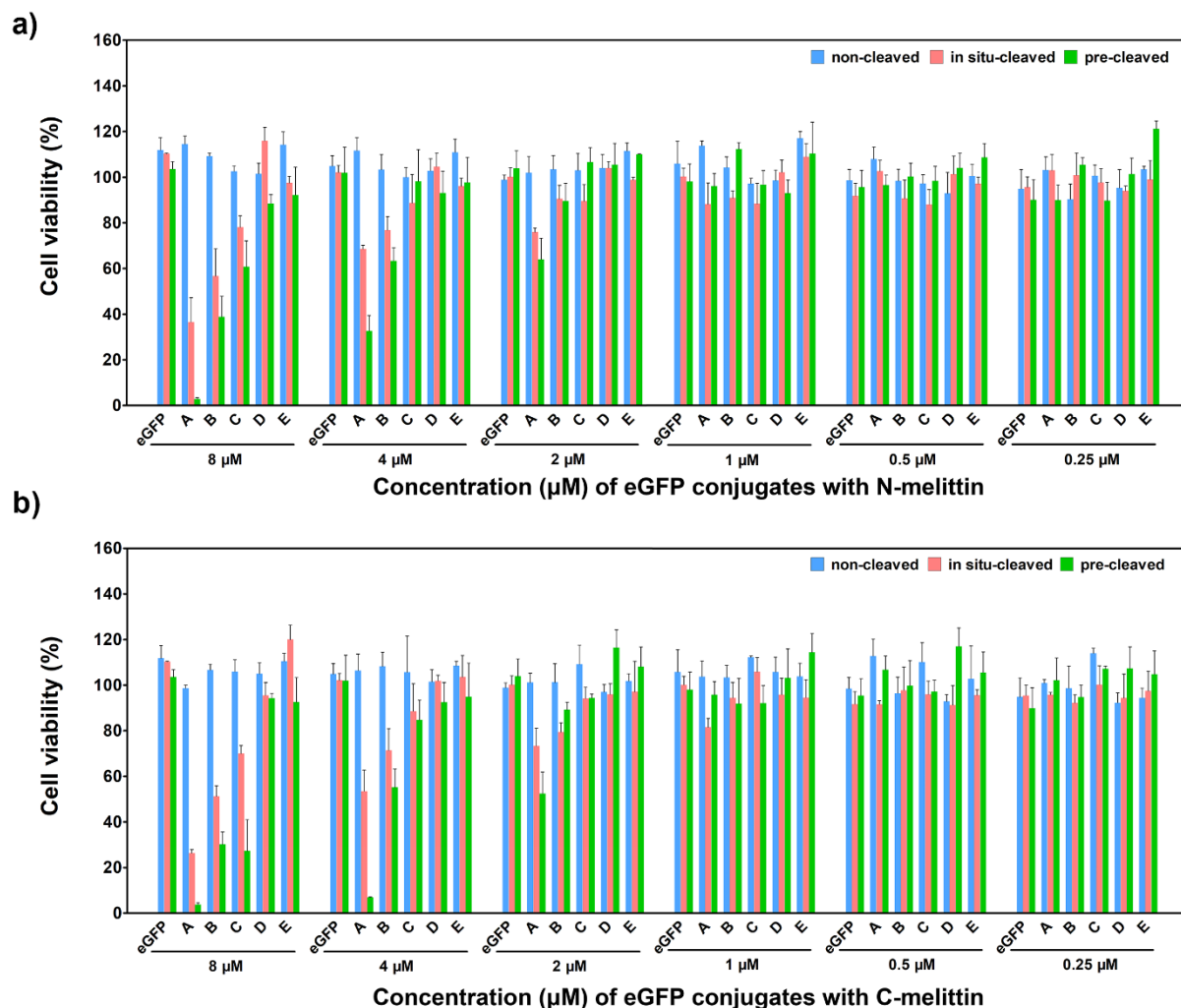
Figure 4.23 The cell viability after treatment with eGFP conjugates A–E with **a)** N-melittin and **b)** C-melittin (with or without TPAn masking) determined by MTT assay according to a standardized protocol. Different concentrations (0.25, 0.5, 1, 2, 4, and 8 µM) of eGFP conjugates (in non-, in situ-, and pre-cleaved states), and unmodified eGFP were added to the culture medium of KB cells at their defined corresponding pH (either pH 7.4 for non- and pre-cleaved forms, or 6.5 for in situ cleavage) for 48 h incubation at 37°C. The cell viability was calculated as a percentage relative to HEPES-treated control wells (n = 3, mean ± SD). Experiments were carried out by Mina Yazdi (PhD student at Pharmaceutical Biotechnology, LMU München).

In contrast, when TPAn is detached at pH 6.5 by either pre-cleavage or in situ cleavage in cell culture, moderate toxicities were observed in a concentration- and conjugate-dependent manner. No significant toxicities of eGFP conjugates were observed at ≤ 2 µM

implying their good tolerability by KB cells. At the high concentration of 4 or 8 µM, toxicities increased with increasing melittin content from conjugates C to A. Consistent with previous work,[95] eGFP conjugates containing N-melittin (**Figure 4.23a**) displayed lower cytotoxicity than those containing C-melittin (**Figure 4.23b**). It should be noted that conjugates D with the best EGFR-specific uptake of eGFP did not show cytotoxicity even at the highest dose of 8 µM.

4.15 Characterization and cytotoxic activity of analogous Cyt C conjugate

Owing to the potential advantages of efficient intracellular delivery and controlled release of protein cargo, the feasibility of our established system for cytosolic delivery of therapeutic Cyt C in active form was also tested in cancer cells using MTT and apoptosis assays. Cyt C has inspired great interest in anticancer strategies for its key role in triggering apoptosis-related enzymatic cascade leading to programmed cell death. However, the large size and cell membrane-impermeability are major obstacles limiting the cytosolic import.[110, 141] Herein, the Cyt C conjugate was synthesized based on the eGFP conjugate D formulation benefitting from higher efficacy and good cell tolerability. The TNBS assay demonstrated the modification of at least 16 out of the 20 primary amines of Cyt C (19 lysines plus one terminal amino group) with AzMMMan. The analytical results confirmed the pH-triggered charge reversal property of the conjugate and traceless release of Cyt C (**Figure 4.24**).
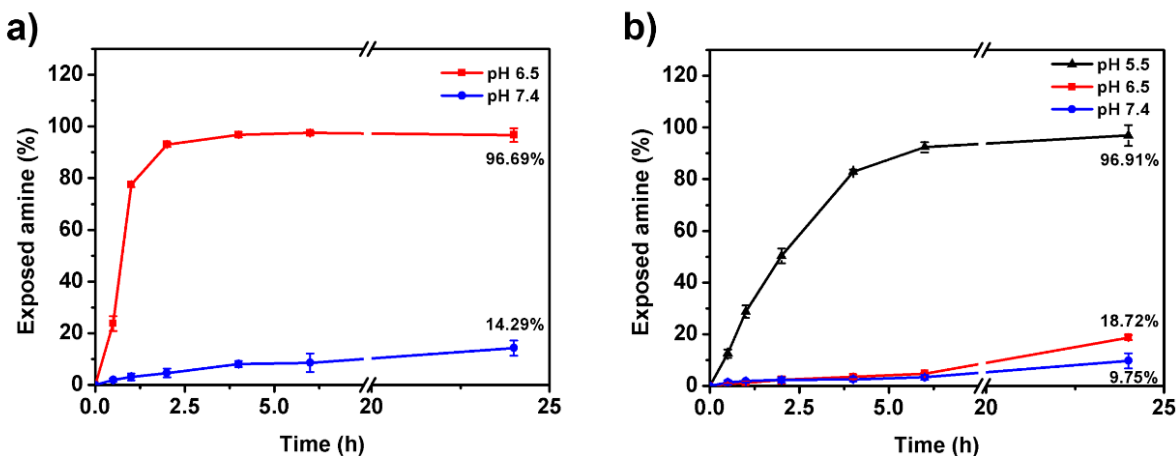
Figure 4.24 The pH-sensitive charge reversal of cytochrome c (Cyt C) conjugate and traceless release of Cyt C. **a)** The exposed amine changes of Cyt C conjugate with N-melittin in HEPES buffer (pH 7.4 or 6.5) at different incubation time points at 37°C were measured using TNBS assay. **b)** Traceless release of Cyt C from analogs of conjugate (with N-melittin but without TPAn masking) was evaluated upon incubation at different pH (5.5, 6.5, and 7.4) at 37°C via TNBS assay (n = 3, mean ± SD).

To confirm the charge reversal property finding, the unmasked amino groups of melittin in the Cyt C conjugate were quantified through TNBS assay over 24 h at 37°C. As seen in **Figure 4.24a**, the results showed an increasing trend in the exposed amino groups of Cyt C conjugate by over 90% in the first 2 h and the ratio over 95% after 24 h incubation at pH 6.5. It indicates that the charge reversal occurred at a pH of 6.5, and that the majority of the amino groups were exposed within a time period of 2 h. To the contrary, when the pH was adjusted to 7.4, it was discovered that the amino group exposure ratio of the Cyt C conjugate did not exceed 15% after being incubated for 24 h. This also suggested that the Cyt C conjugate was very stable at physiological pH for a period of 24 h.

In addition, the TNBS test was used to establish that the traceless release of Cyt C occurred as a result of the reversal of the AzMMMan linkage at a slightly more acidic endosomal pH of 5.5. This experiment was carried out using a Cyt C conjugate with N-melittin, but it did not include TPAn. This was done to prevent any complications that may have been caused by the unmasking of melittin-TPAn. Cyt C conjugate was observed for

a 24 h-monitoring of unmasked Cyt C amino groups exposed at pH 5.5, 6.5, or 7.4 at 37°C (**Figure 4.24b**). In order to identify the exposed amino groups of Cyt C using the TNBS test, the lysine amino groups of melittin were removed as background. The unmasking of amino groups in Cyt C was minimal at pH 7.4 and 6.5, even after 24 hours, it did not reach 10% at pH 7.4 and 19% at pH 6.5. More than 96% of Cyt C amino groups were unmasked during the same time period but at a pH of 5.5, and up to 80% after a shorter time period of 4 h.

Due to the dual pH-responsive design of the Cyt C conjugate, these results also show that the system can meet the requirements of stability at neutral pH, a charge reversal at weakly acidic pH without causing noticeable cleavage of AzMMMan bonds, and a traceless release under slightly more acidic endosomal pH just like eGFP conjugates performed.

The bioactivity of Cyt C was evaluated on KB cells for 48 h after exposure with in situ-cleaved state of the Cyt C conjugate (2, 4, and 8 µM) compared to free Cyt C at the same dose levels. According to the results in **Figure 4.25a**, cell viability decreased significantly in a dose-dependent manner in Cyt C conjugate-treated cells, whereas no cell killing was induced by free Cyt C. These data highlighted that Cyt C based on our covalent modification strategy could be delivered intracellularly and induce cell killing. Further evidence on important features of our conjugation strategy supporting cytosolic Cyt C delivery, while maintaining its pro-apoptotic activity, was obtained on KB cells by Annexin-V assay. **Figure 4.25b** displays representative flow cytometry plots of all treated cells. Although Cyt C could reduce the number of viable cells and promote apoptosis, the percentage of early and late apoptotic cells shows a clear difference between conjugated and free Cyt C-treated groups, as observed in MTT results. These findings re-confirmed the qualification of our system for efficient cytosolic delivery of proteins in active form.

a)

b)
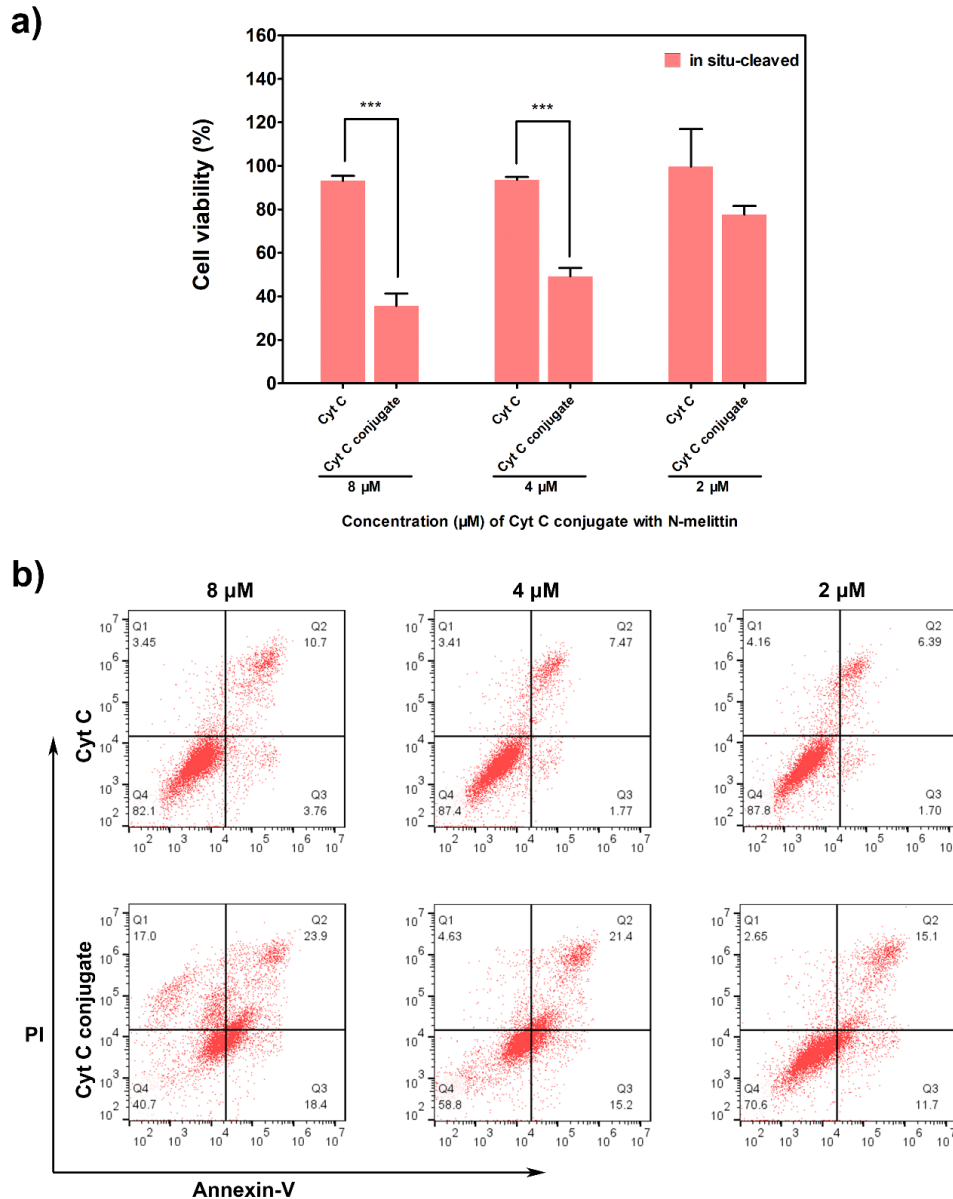
Figure 4.25 Antitumoral effect of cytochrome c (Cyt C) conjugate. Different concentrations (2, 4, and 8 μM) of Cyt C conjugate (with N-melittin) as well as unmodified Cyt C were added to the cell culture of KB cells at pH 6.5 (in situ-cleaved state) for 48 h. **a)** The cell viability after treatment determined by MTT assay. The cell viability was calculated as percentage relative to HEPES-treated control well (n = 3, mean ± SD). Significant differences between the groups were calculated as ***p < 0.001. **b)** Dose dependency of cellular apoptosis determined flow cytometrically by Annexin V-FITC/PI staining. HEPES-treated cells were used to set the gating. Q1: necrotic cells, Q2: late apoptosis, Q3: early apoptosis, and Q4: living cells. Experiments were carried out by Mina Yazdi (PhD student at Pharmaceutical Biotechnology, LMU München).

5 Summary

Protein therapeutics are of widespread interest due to their successful performance in the current pharmaceutical and medical fields, even though their broad applications have been hindered by the lack of an efficient intracellular delivery approach. Herein, we fabricated an active-targeted dual pH-responsive delivery system with favorable tumor cell entry augmented by extracellular pH-triggered charge reversal and tumor receptor targeting and pH-controlled endosomal release in a traceless fashion.

In this thesis, we established an efficient dynamic system for protein delivery by pH-sensitive traceless conjugation. As a traceable model protein, the enhanced green fluorescent protein (eGFP) bearing a nuclear localization signal was covalently coupled with a pH-responsive traceless bifunctional azidomethyl-methylmaleic anhydride (AzMMMan) linker followed by functionalization with different molar equivalents of two cationic dibenzocyclooctyne-octa-arginine-cysteine (DBCO-R_8C)-modified moieties: polyethylene glycol (PEG$_{2kDa}$)-GE11 peptide for epidermal growth factor receptor (EGFR)-mediated targeting and cationic melittin (either attached in N-terminal or C-terminal form) peptide for endosomal escape. The cationic melittin domain was masked with pH-labile tetrahydrophthalic anhydride (TPAn) for a programmed charge reversal in tumor microenvironment (mild acidic pH 6.5). Peptide GE11 was incorporated via a PEG$_{2kDa}$ spacer to enhance the tumor-specific uptake into EGFR-overexpressing cells.

Therefore, eGFP conjugates with five different ratios A–E (functional units N/C-melittin to PEG$_{2kDa}$-GE11 at 22:0, 16:6, 11:11, 6:16, 0:22 equiv) were evaluated, searching for an optimized balanced ratio of both targeting GE11 unit and endosomolytic melittin unit. The SDS-PAGE experiment showed that all the eGFP conjugates were stable at physiological pH, but the free eGFP can be traceless released in the acidic endosomal pH (~ 5.5). Upon incubation at pH 6.5, similar to a mildly acidic tumor environment for 4 h, TPAn detachment and resulted in an increased positive charge to eGFP conjugates A–D except for conjugate E (without TPAn covered melittin). The TNBS assay by testing the exposed amino groups also confirmed that the TPAn were more sensitive than AzMMMan, so the charge reversal of TPAn from melittin and traceless release of eGFP could happen at pH

6.5 and 5.5, respectively. The cell viability was evaluated by MTT assay to KB cells. The results showed that all the conjugates had no toxicity at physiological pH, but the toxicities increased with the increasing ratio of melittin from conjugates C to A at pH 6.5. However, conjugates D and E had no toxic at acidic pH. Based on this, the cellular uptake efficiency was tested with receptor-positive KB cells and receptor-negative N2A cells. At sub-toxic doses 2 µM, all the conjugates significate increased the cellular uptake efficiency due to the electrostatic attraction of melittin with the cell membrane in close collaboration with GE11, alongside with additional promoting effect of the R_8C as the cell-penetrating peptide. After all the evaluations, the N-melittin showed a slightly favorable conjugate delivery profile over C-melittin. Among them, the eGFP conjugate D containing eGFP linked with 6 equiv of TPAn-masked N-melittin and 16 equiv of PEG_{2kDa}-GE11 performed best. About the conjugate D, eGFP linkage with AzMMMan was found to be highly stable at pH 7.4 (92% stability after 24 h at 37°C) but cleaved traceless at endosomal pH of 5.5 (95% cleavage after 24 h). The charge reversal at pH 6.5 resulted in a change of zeta potential from negative -5 mV to +7 mV. Conjugate D revealed the highest receptor-specific uptake into EGFR-rich HeLa and KB cells, potent endosomal escape and intracellular delivery of nls-tagged eGFP into the nucleus. Meanwhile, the conjugate D did not show any cytotoxicity at the highest tested dose of 8 µM, and insignificant uptake into EGFR-negative non-target N2A cells. The therapeutic potential of the conjugation system was demonstrated by successful cytosolic delivery of analogous cytochrome c protein conjugates with cell killing of tumor cells reported by an apoptosis assay.

In summary, our findings hold promise for a safe and efficient approach to intracellular protein delivery.

6 Appendix

6.1 Abbreviations

ACN	Acetonitrile
AzMMMan	3-(Azidomethyl)-4-methyl-2,5-furandione
BrMMMan	3-(Bromomethyl)-4-methyl-2,5-furandione
BSA	Bovine serum albumin
$CDCl_3$	Deuterated chloroform
CLSM	Confocal laser scanning microscopy
cm	Centimeter
CPP	Cell-penetrating peptide
Cyt C	Cytochrome c
D_2O	Deuterium oxide
Da	Dalton
DAPI	4',6-Diamidino-2-phenylindole
DBCO	Azadibenzylcyclooctyne
DCM	Dichloromethane
DIPEA	N,N-diisopropylethylamine
DMEM	Dulbecco's modified Eagle's medium
DMF	Dimethylformamide
DMMAn	2,3-Dimethylmaleic anhydride
DMSO	Dimethylsulfoxide

DTNB	5,5'-Dithio-bis(2-nitrobenzoic acid)
DTT	DL-Dithiothreitol
e.g.	Exempli gratia, for example
EDT	Ethanedithiol
EDTA	Ethylendiaminetetraacetic acid
eGFP	Enhanced green fluorescent protein
EGFR	Epidermal growth factor receptor
etc.	Et cetera
FBS	Fetal bovine serum
FDA	Food and drug administration
Fmoc	Fluorenylmethyloxycarbonyl
HBTU	2-(1H-Benzotriazol-1-yl)-1,1,3,3-tetramethyluronium-hexafluorophosphate
HCl	Hydrochloric acid
HEPES	N-(2-hydroxethyl) piperazine-N'-(2-ethansulfonic acid)
HOBt	1-Hydroxy-benzotriazole
INF7	Influenza hemagglutinin HA-2 terminal peptide derivative 7
IPTG	Isopropyl β-D-1-thiogalactopyranoside
g	Gram
kDa	Kilodalton
MeOH	Methanol
mg	Milligram
MHz	Megahertz

mL	Milliliter
mM	Millimolar
mmol	Millimole
MTBE	Methyl tert-butyl ether
MTT	3-(4,5-Dimethylthiazol-2-yl)-2,5-diphenyltetrazolium bromide
mV	Millivolt
MWCO	Molecular weight cut off
Na_2HPO_4	Sodium hydrogen phosphate
NaCl	Sodium chloride
NaN_3	Sodium azide
NaOH	Sodium hydroxide
NHS	*N*-Hydroxysuccinimide
NLS	Nuclear localization signal
nm	Nanometer
NMR	Nuclear magnetic resonance
PAGE	Poly acrylamide gel electrophoresis
PBS	Phosphate buffered saline
PEG	Polyethylene glycol
pH	Potentia Hydrogenii
RNase A	Ribonuclease A
RP-HPLC	Reversed-phase high performance liquid chromatography
RPMI	Roswell park memorial institute medium

RT	Room temperature
SD	Standard deviation
SDS	Sodium dodecyl sulfate
SEC	Size exclusion chromatography
SPPS	Solid-phase assisted peptide synthesis
SV40	Simian virus 40
TFA	Trifluoroacetic acid
TIS	Triisopropylsilane
TNBS	2,4,6-Trinitrobenzenesulfonic
TPAn	3,4,5,6-Tetrahydrophthalic anhydride
UV Vis	Ultraviolett visible
µM	Micromolar
µmol	Micromole

6.2 MALDI-TOF-MS

MALDI-TOF-MS of R$_8$C
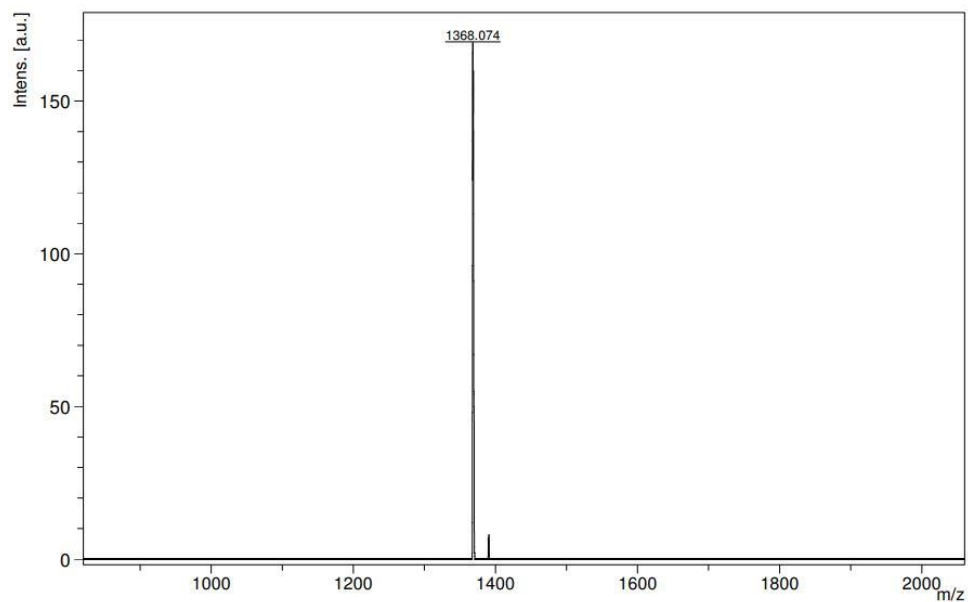
MALDI-TOF-MS of N-melittin
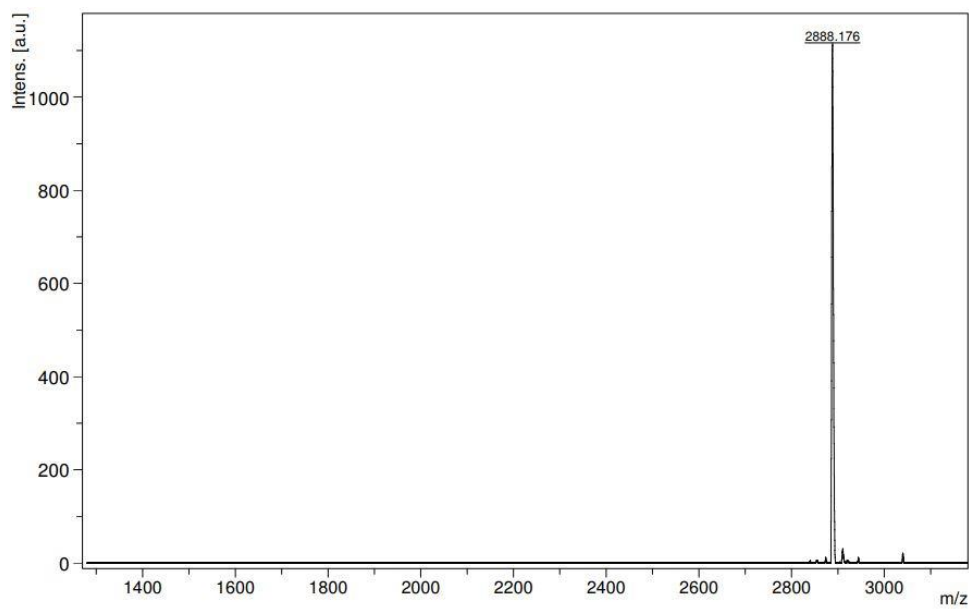
MALDI-TOF-MS of C-melittin
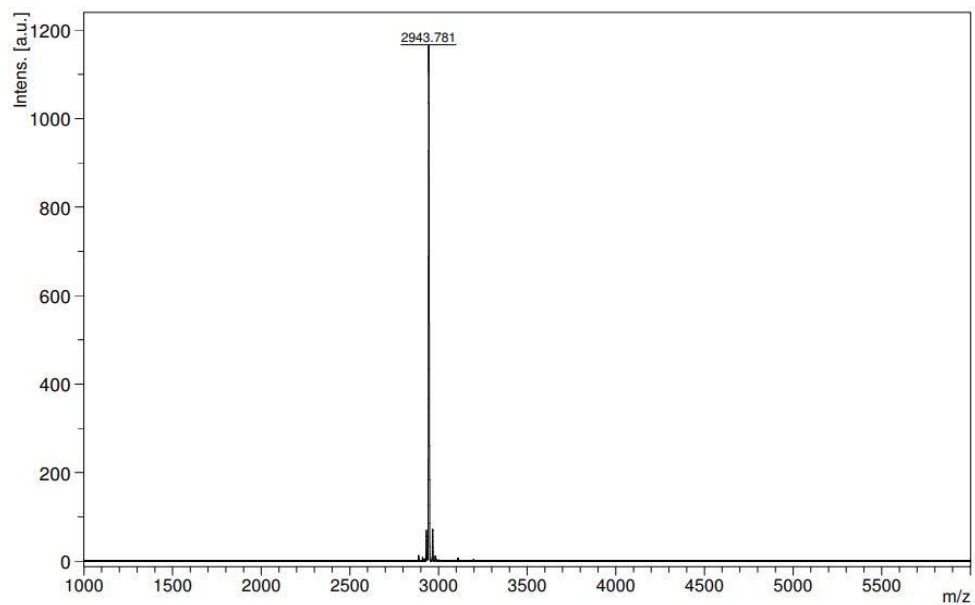
MALDI-TOF-MS of GE11
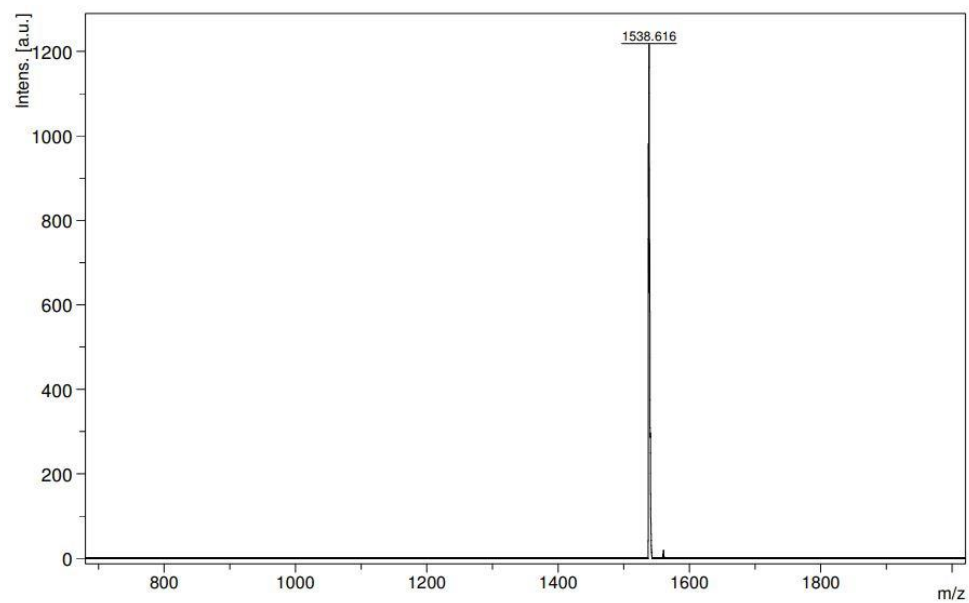
7 References

(1) Vaishya, R.; Khurana, V.; Patel, S.; Mitra, A. K. Long-term delivery of protein therapeutics. *Expert Opin. Drug Delivery* **2015**, *12* (3), 415-440.

(2) Mitragotri, S.; Burke, P. A.; Langer, R. Overcoming the challenges in administering biopharmaceuticals: formulation and delivery strategies. *Nat. Rev. Drug Discovery* **2014**, *13* (9), 655-672.

(3) Lee, K.; Rafi, M.; Wang, X.; Aran, K.; Feng, X.; Lo Sterzo, C.; Tang, R.; Lingampalli, N.; Kim, H. J.; Murthy, N. In vivo delivery of transcription factors with multifunctional oligonucleotides. *Nat. Mater.* **2015**, *14* (7), 701-706.

(4) Both , L.; White, J.; Mandal, S.; Efstratiou, A. Access to diphtheria antitoxin for therapy and diagnostics. *Eurosurveillance* **2014**, *19* (24), 20830.

(5) Leader, B.; Baca, Q. J.; Golan, D. E. Protein therapeutics: a summary and pharmacological classification. *Nat. Rev. Drug Discovery* **2008**, *7* (1), 21-39.

(6) Carter, P. J. Introduction to current and future protein therapeutics: A protein engineering perspective. *Exp. Cell Res.* **2011**, *317* (9), 1261-1269.

(7) Chan, A. C.; Carter, P. J. Therapeutic antibodies for autoimmunity and inflammation. *Nat. Rev. Immunol.* **2010**, *10* (5), 301-316.

(8) O'Flaherty, R.; Bergin, A.; Flampouri, E.; Mota, L. M.; Obaidi, I.; Quigley, A.; Xie, Y.; Butler, M. Mammalian cell culture for production of recombinant proteins: A review of the critical steps in their biomanufacturing. *Biotechnol. Adv.* **2020**, *43*, 107552.

(9) Pakulska Malgosia, M.; Miersch, S.; Shoichet Molly, S. Designer protein delivery: From natural to engineered affinity-controlled release systems. *Science* **2016**, *351* (6279), aac4750.

(10) Timin, A. S.; Litvak, M. M.; Gorin, D. A.; Atochina-Vasserman, E. N.; Atochin, D. N.; Sukhorukov, G. B. Cell-Based Drug Delivery and Use of Nano-and Microcarriers for Cell Functionalization. *Adv. Healthcare Mater.* **2018**, *7* (3), 1700818.

(11) Gu, Z.; Biswas, A.; Zhao, M.; Tang, Y. Tailoring nanocarriers for intracellular protein delivery. *Chem. Soc. Rev.* **2011**, *40* (7), 3638-3655.

(12) Zhang, Q.; Zhang, J.; Song, J.; Liu, Y.; Ren, X.; Zhao, Y. Protein-Based Nanomedicine for Therapeutic Benefits of Cancer. *ACS Nano* **2021**, *15* (5), 8001-8038.

(13) Jiskoot, W.; Randolph, T. W.; Volkin, D. B.; Middaugh, C. R.; Schöneich, C.; Winter, G.; Friess, W.; Crommelin, D. J.; Carpenter, J. F. Protein instability and immunogenicity: roadblocks to clinical application of injectable protein delivery systems for sustained release. *J. Pharm. Sci.* **2012**, *101* (3), 946-954.

(14) Schwarze, S. R.; Ho, A.; Vocero-Akbani, A.; Dowdy, S. F. In vivo protein transduction: delivery of a biologically active protein into the mouse. *Science* **1999**, *285* (5433), 1569-1572.

(15) Lu, Y.; Sun, W.; Gu, Z. Stimuli-responsive nanomaterials for therapeutic protein delivery. *J. Controlled Release* **2014**, *194*, 1-19.

(16) Zuris, J. A.; Thompson, D. B.; Shu, Y.; Guilinger, J. P.; Bessen, J. L.; Hu, J. H.; Maeder, M. L.; Joung, J. K.; Chen, Z.-Y.; Liu, D. R. Cationic lipid-mediated delivery of proteins enables efficient protein-based genome editing in vitro and in vivo. *Nat. Biotechnol.* **2015**, *33* (1), 73-80.

(17) Nischan, N.; Herce, H. D.; Natale, F.; Bohlke, N.; Budisa, N.; Cardoso, M. C.; Hackenberger, C. P. Covalent attachment of cyclic TAT peptides to GFP results in protein delivery into live cells with immediate bioavailability. *Angew. Chem., Int. Ed. Engl.* **2015**, *54* (6), 1950-1953.

(18) Zelikin, A. N.; Ehrhardt, C.; Healy, A. M. Materials and methods for delivery of biological drugs. *Nat. Chem.* **2016**, *8* (11), 997-1007.

(19) Du, S.; Liew, S. S.; Li, L.; Yao, S. Q. Bypassing endocytosis: direct cytosolic delivery of proteins. *J. Am. Chem. Soc.* **2018**, *140* (47), 15986-15996.

(20) Chiper, M.; Niederreither, K.; Zuber, G. Transduction methods for cytosolic delivery of proteins and bioconjugates into living cells. *Adv. Healthcare Mater.* **2018**, *7* (6), e1701040.

(21) Lee, Y. W.; Luther, D. C.; Kretzmann, J. A.; Burden, A.; Jeon, T.; Zhai, S.; Rotello, V. M. Protein Delivery into the Cell Cytosol using Non-Viral Nanocarriers. *Theranostics* **2019**, *9* (11), 3280-3292.

(22) Postupalenko, V.; Desplancq, D.; Orlov, I.; Arntz, Y.; Spehner, D.; Mely, Y.; Klaholz, B. P.; Schultz, P.; Weiss, E.; Zuber, G. Protein Delivery System Containing a Nickel-Immobilized Polymer for Multimerization of Affinity-Purified His-Tagged Proteins Enhances Cytosolic Transfer. *Angew. Chem., Int. Ed. Engl.* **2015**, *54* (36), 10583-10586.

(23) Lv, J.; Fan, Q.; Wang, H.; Cheng, Y. Polymers for cytosolic protein delivery. *Biomaterials* **2019**, *218*, 119358.

(24) Modzelewski, A. J.; Chen, S.; Willis, B. J.; Lloyd, K.; Wood, J. A.; He, L. Efficient mouse genome engineering by CRISPR-EZ technology. *Nat. Protoc.* **2018**, *13* (6), 1253-1274.

(25) Mukherjee, P.; Nathamgari, S. S. P.; Kessler, J. A.; Espinosa, H. D. Combined numerical and experimental investigation of localized electroporation-based cell transfection and sampling. *ACS Nano* **2018**, *12* (12), 12118-12128.

(26) Pan, S.; Jeon, T.; Luther, D. C.; Duan, X.; Rotello, V. M. Cytosolic Delivery of Functional Proteins In Vitro through Tunable Gigahertz Acoustics. *ACS Appl. Mater. Interfaces* **2020**, *12* (13), 15823-15829.

(27) Shalek, A. K.; Robinson, J. T.; Karp, E. S.; Lee, J. S.; Ahn, D.-R.; Yoon, M.-H.; Sutton, A.; Jorgolli, M.; Gertner, R. S.; Gujral, T. S.; MacBeath, G.; Yang, E. G.; Park, H. Vertical silicon nanowires as a universal platform for delivering biomolecules into living cells. *Proc. Natl. Acad. Sci.* **2010**, *107* (5), 1870-1875.

(28) Sharei, A.; Zoldan, J.; Adamo, A.; Sim, W. Y.; Cho, N.; Jackson, E.; Mao, S.; Schneider, S.; Han, M.-J.; Lytton-Jean, A.; Basto, P. A.; Jhunjhunwala, S.; Lee, J.; Heller, D. A.; Kang, J. W.; Hartoularos, G. C.; Kim, K.-S.; Anderson, D. G.; Langer, R.; Jensen, K. F. A vector-free microfluidic platform for intracellular delivery. *Proc. Natl. Acad. Sci.* **2013**, *110* (6), 2082-2087.

(29) Lee, J.; Sharei, A.; Sim, W. Y.; Adamo, A.; Langer, R.; Jensen, K. F.; Bawendi, M. G. Nonendocytic delivery of functional engineered nanoparticles into the cytoplasm of live cells using a novel, high-throughput microfluidic device. *Nano Lett.* **2012**, *12* (12), 6322-6327.

(30) Horn, J. M.; Obermeyer, A. C. Genetic and Covalent Protein Modification Strategies to Facilitate Intracellular Delivery. *Biomacromolecules* **2021**, *22* (12), 4883-4904.

(31) Liu, X.; Wu, F.; Ji, Y.; Yin, L. Recent Advances in Anti-cancer Protein/Peptide Delivery. *Bioconjugate Chem.* **2019**, *30* (2), 305-324.

(32) Mout, R.; Rotello, V. M. Cytosolic and Nuclear Delivery of CRISPR/Cas9-ribonucleoprotein for Gene Editing Using Arginine Functionalized Gold Nanoparticles. *Bio-Protoc.* **2017**, *7* (20), e2586.

(33) Yuan, P.; Zhang, H.; Qian, L.; Mao, X.; Du, S.; Yu, C.; Peng, B.; Yao, S. Q. Intracellular delivery of functional native antibodies under hypoxic conditions by using a biodegradable silica nanoquencher. *Angew. Chem., Int. Ed. Engl.* **2017**, *56* (41), 12481-12485.

(34) Roder, R.; Preiss, T.; Hirschle, P.; Steinborn, B.; Zimpel, A.; Hohn, M.; Radler, J. O.; Bein, T.; Wagner, E.; Wuttke, S.; Lachelt, U. Multifunctional Nanoparticles by Coordinative Self-Assembly of His-Tagged Units with Metal-Organic Frameworks. *J. Am. Chem. Soc.* **2017**, *139* (6), 2359-2368.

(35) Chen, T.-T.; Yi, J.-T.; Zhao, Y.-Y.; Chu, X. Biomineralized metal–organic framework nanoparticles enable intracellular delivery and endo-lysosomal release of native active proteins. *J. Am. Chem. Soc.* **2018**, *140* (31), 9912-9920.

(36) Ju, E.; Li, T.; Ramos da Silva, S.; Gao, S.-J. Gold Nanocluster-Mediated Efficient Delivery of Cas9 Protein through pH-Induced Assembly-Disassembly for Inactivation of Virus Oncogenes. *ACS Appl. Mater. Interfaces* **2019**, *11* (38), 34717-34724.

(37) Su, S.; Wang, Y. Y.; Du, F. S.; Lu, H.; Li, Z. C. Dynamic covalent bond-assisted programmed and traceless protein release: high loading nanogel for systemic and cytosolic delivery. *Adv. Funct. Mater.* **2018**, *28* (48), 1805287.

(38) Chen, J.; Ouyang, J.; Chen, Q.; Deng, C.; Meng, F.; Zhang, J.; Cheng, R.; Lan, Q.; Zhong, Z. EGFR and CD44 dual-targeted multifunctional hyaluronic acid nanogels boost protein delivery to ovarian and breast cancers in vitro and in vivo. *ACS Appl. Mater. Interfaces* **2017**, *9* (28), 24140-24147.

(39) Lee, Y.; Ishii, T.; Cabral, H.; Kim, H. J.; Seo, J. H.; Nishiyama, N.; Oshima, H.; Osada, K.; Kataoka, K. Charge-Conversional Polyionic Complex Micelles—Efficient Nanocarriers for Protein Delivery into Cytoplasm. *Angew. Chem., Int. Ed. Engl.* **2009**, *48* (29), 5309-5312.

(40) Lee, Y.; Ishii, T.; Kim, H. J.; Nishiyama, N.; Hayakawa, Y.; Itaka, K.; Kataoka, K. Efficient delivery of bioactive antibodies into the cytoplasm of living cells by charge-conversional polyion complex micelles. *Angew. Chem., Int. Ed. Engl.* **2010**, *49* (14), 2552-2555.

(41) Maier, K.; Martin, I.; Wagner, E. Sequence Defined Disulfide-Linked Shuttle for Strongly Enhanced Intracellular Protein Delivery. *Mol. Pharmaceutics* **2012**, *9* (12), 3560-3568.

(42) Zhang, P.; He, D.; Klein, P. M.; Liu, X.; Röder, R.; Döblinger, M.; Wagner, E. Enhanced Intracellular Protein Transduction by Sequence Defined Tetra-Oleoyl Oligoaminoamides Targeted for Cancer Therapy. *Adv. Funct. Mater.* **2015**, *25* (42), 6627-6636.

(43) Liu, X.; Zhang, P.; He, D.; Rödl, W.; Preiß, T.; Rädler, J. O.; Wagner, E.; Lächelt, U. pH-reversible cationic RNase A conjugates for enhanced cellular delivery and tumor cell killing. *Biomacromolecules* **2016**, *17* (1), 173-182.

(44) Roder, R.; Helma, J.; Preiss, T.; Radler, J. O.; Leonhardt, H.; Wagner, E. Intracellular Delivery of Nanobodies for Imaging of Target Proteins in Live Cells. *Pharm. Res.* **2017**, *34* (1), 161-174.

(45) Liu, C.; Wan, T.; Wang, H.; Zhang, S.; Ping, Y.; Cheng, Y. A boronic acid-rich dendrimer with robust and unprecedented efficiency for cytosolic protein delivery and CRISPR-Cas9 gene editing. *Sci. Adv.* **2019**, *5* (6), eaaw8922.

(46) Lee, Y. W.; Luther, D. C.; Goswami, R.; Jeon, T.; Clark, V.; Elia, J.; Gopalakrishnan, S.; Rotello, V. M. Direct Cytosolic Delivery of Proteins through Coengineering of Proteins and Polymeric Delivery Vehicles. *J. Am. Chem. Soc.* **2020**, *142* (9), 4349-4355.

(47) Kretzmann, J. A.; Luther, D. C.; Evans, C. W.; Jeon, T.; Jerome, W.; Gopalakrishnan, S.; Lee, Y. W.; Norret, M.; Iyer, K. S.; Rotello, V. M. Regulation of Proteins to the Cytosol

Using Delivery Systems with Engineered Polymer Architecture. *J. Am. Chem. Soc.* **2021**, *143* (12), 4758-4765.

(48) Zhang, P.; Steinborn, B.; Lächelt, U.; Zahler, S.; Wagner, E. Lipo-oligomer nanoformulations for targeted intracellular protein delivery. *Biomacromolecules* **2017**, *18* (8), 2509-2520.

(49) Hirai, Y.; Hirose, H.; Imanishi, M.; Asai, T.; Futaki, S. Cytosolic protein delivery using pH-responsive, charge-reversible lipid nanoparticles. *Sci. Rep.* **2021**, *11* (1), 19896.

(50) Yim, N.; Ryu, S.-W.; Choi, K.; Lee, K. R.; Lee, S.; Choi, H.; Kim, J.; Shaker, M. R.; Sun, W.; Park, J.-H.; Kim, D.; Heo, W. D.; Choi, C. Exosome engineering for efficient intracellular delivery of soluble proteins using optically reversible protein–protein interaction module. *Nat. Commun.* **2016**, *7* (1), 1-9.

(51) Saalik, P.; Elmquist, A.; Hansen, M.; Padari, K.; Saar, K.; Viht, K.; Langel, U.; Pooga, M. Protein cargo delivery properties of cell-penetrating peptides. A comparative study. *Bioconjugate Chem.* **2004**, *15* (6), 1246-1253.

(52) Nakase, I.; Tadokoro, A.; Kawabata, N.; Takeuchi, T.; Katoh, H.; Hiramoto, K.; Negishi, M.; Nomizu, M.; Sugiura, Y.; Futaki, S. Interaction of arginine-rich peptides with membrane-associated proteoglycans is crucial for induction of actin organization and macropinocytosis. *Biochemistry* **2007**, *46* (2), 492-501.

(53) Brock, R. The uptake of arginine-rich cell-penetrating peptides: putting the puzzle together. *Bioconjugate Chem.* **2014**, *25* (5), 863-868.

(54) Kawaguchi, Y.; Takeuchi, T.; Kuwata, K.; Chiba, J.; Hatanaka, Y.; Nakase, I.; Futaki, S. Syndecan-4 Is a Receptor for Clathrin-Mediated Endocytosis of Arginine-Rich Cell-Penetrating Peptides. *Bioconjugate Chem.* **2016**, *27* (4), 1119-1130.

(55) Derakhshankhah, H.; Jafari, S. Cell penetrating peptides: A concise review with emphasis on biomedical applications. *Biomed. Pharmacother.* **2018**, *108*, 1090-1096.

(56) Palm-Apergi, C.; Dowdy, S. F. Protein Delivery by PTDs/CPPs. *Methods Mol. Biol.* **2022**, *2383*, 257-264.

(57) Ferhan, A. R.; Park, S.; Park, H.; Tae, H.; Jackman, J. A.; Cho, N.-J. Lipid Nanoparticle Technologies for Nucleic Acid Delivery: A Nanoarchitectonics Perspective. *Adv. Funct. Mater.* **2022**, 2203669.

(58) Wadia, J. S.; Dowdy, S. F. Transmembrane delivery of protein and peptide drugs by TAT-mediated transduction in the treatment of cancer. *Adv. Drug Delivery Rev.* **2005**, *57* (4), 579-596.

(59) Pesce, D.; Wu, Y.; Kolbe, A.; Weil, T.; Herrmann, A. Enhancing cellular uptake of GFP via unfolded supercharged protein tags. *Biomaterials* **2013**, *34* (17), 4360-4367.

(60) Hu, S.; Chen, X.; Lei, C.; Tang, R.; Kang, W.; Deng, H.; Huang, Y.; Nie, Z.; Yao, S. Charge designable and tunable GFP as a target pH-responsive carrier for intracellular functional protein delivery and tracing. *Chem. Commun.* **2018**, *54* (56), 7806-7809.

(61) Liu, X.; Zhang, P.; Rödl, W.; Maier, K.; Lächelt, U.; Wagner, E. Toward artificial immunotoxins: traceless reversible conjugation of RNase A with receptor targeting and endosomal escape domains. *Mol. Pharmaceutics* **2017**, *14* (5), 1439-1449.

(62) Rouet, R.; Thuma, B. A.; Roy, M. D.; Lintner, N. G.; Rubitski, D. M.; Finley, J. E.; Wisniewska, H. M.; Mendonsa, R.; Hirsh, A.; de Onate, L.; Compte Barron, J.; McLellan, T. J.; Bellenger, J.; Feng, X.; Varghese, A.; Chrunyk, B. A.; Borzilleri, K.; Hesp, K. D.; Zhou, K.; Ma, N.; Tu, M.; Dullea, R.; McClure, K. F.; Wilson, R. C.; Liras, S.; Mascitti, V.; Doudna, J. A. Receptor-Mediated Delivery of CRISPR-Cas9 Endonuclease for Cell-Type-Specific Gene Editing. *J. Am. Chem. Soc.* **2018**, *140* (21), 6596-6603.

(63) Lieser, R. M.; Li, Q.; Chen, W.; Sullivan, M. O. Incorporation of Endosomolytic Peptides with Varying Disruption Mechanisms into EGFR-Targeted Protein Conjugates: The Effect on Intracellular Protein Delivery and EGFR Specificity in Breast Cancer Cells. *Mol. Pharmaceutics* **2022**, *19* (2), 661-673.

(64) Derossi, D.; Joliot, A. H.; Chassaing, G.; Prochiantz, A. The third helix of the Antennapedia homeodomain translocates through biological membranes. *J. Biol. Chem.* **1994**, *269*, 10444-10450.

(65) Prochiantz, A. Messenger proteins: homeoproteins, TAT and others. *Curr. Opin. Cell Biol.* **2000**, *12* (4), 400-406.

(66) Hoffman, A. S.; Stayton, P. S.; Press, O.; Murthy, N.; Lackey, C. A.; Cheung, C.; Black, F.; Campbell, J.; Fausto, N.; Kyriakides, T. R.; Bornstein, P. Design of "smart" polymers that can direct intracellular drug delivery. *Polym. Adv. Technol.* **2002**, *13* (10-12), 992-999.

(67) Wagner, E. Programmed drug delivery: nanosystems for tumor targeting. *Expert Opin. Biol. Ther.* **2007**, *7* (5), 587-593.

(68) Sun, M.; Wang, K.; Oupický, D. Advances in Stimulus-Responsive Polymeric Materials for Systemic Delivery of Nucleic Acids. *Adv. Healthcare Mater.* **2018**, *7* (4), 1701070.

(69) Abuchowski, A.; van Es, T.; Palczuk, N. C.; Davis, F. F. Alteration of immunological properties of bovine serum albumin by covalent attachment of polyethylene glycol. *J. Biol. Chem.* **1977**, *252* (11), 3578-3581.

(70) Kontermann, R. E. Strategies to Extend Plasma Half-Lives of Recombinant Antibodies. *BioDrugs* **2009**, *23* (2), 93-109.

(71) Jevševar, S.; Kunstelj, M.; Porekar, V. G. PEGylation of therapeutic proteins. *Biotechnol. J.* **2010**, *5* (1), 113-128.

(72) Veronese, F. M.; Mero, A. The Impact of PEGylation on Biological Therapies. *BioDrugs* **2008**, *22* (5), 315-329.

(73) Chapman, A. P.; Antoniw, P.; Spitali, M.; West, S.; Stephens, S.; King, D. J. Therapeutic antibody fragments with prolonged in vivo half-lives. *Nat. Biotechnol.* **1999**, *17* (8), 780-783.

(74) Thordarson, P.; Le Droumaguet, B.; Velonia, K. Well-defined protein–polymer conjugates—synthesis and potential applications. *Appl. Microbiol. Biotechnol.* **2006**, *73* (2), 243-254.

(75) Gauthier, M. A.; Klok, H.-A. Peptide/protein–polymer conjugates: synthetic strategies and design concepts. *Chem. Commun.* **2008**, (23), 2591-2611.

(76) Johnson, D. S.; Weerapana, E.; Cravatt, B. F. Strategies for discovering and derisking covalent, irreversible enzyme inhibitors. *Future Med. Chem.* **2010**, *2* (6), 949-964.

(77) Lonsdale, R.; Ward, R. A. Structure-based design of targeted covalent inhibitors. *Chem. Soc. Rev.* **2018**, *47* (11), 3816-3830.

(78) Heredia, K. L.; Maynard, H. D. Synthesis of protein–polymer conjugates. *Org. Biomol. Chem.* **2007**, *5* (1), 45-53.

(79) Kuan, S. L.; Wu, Y.; Weil, T. Precision Biopolymers from Protein Precursors for Biomedical Applications. *Macromol. Rapid Commun.* **2013**, *34* (5), 380-392.

(80) Schmaljohann, D. Thermo- and pH-responsive polymers in drug delivery. *Adv. Drug Delivery Rev.* **2006**, *58* (15), 1655-1670.

(81) Murthy, N.; Campbell, J.; Fausto, N.; Hoffman, A. S.; Stayton, P. S. Bioinspired pH-Responsive Polymers for the Intracellular Delivery of Biomolecular Drugs. *Bioconjugate Chem.* **2003**, *14* (2), 412-419.

(82) Walker, G. F.; Fella, C.; Pelisek, J.; Fahrmeir, J.; Boeckle, S.; Ogris, M.; Wagner, E. Toward Synthetic Viruses: Endosomal pH-Triggered Deshielding of Targeted Polyplexes Greatly Enhances Gene Transfer in vitro and in vivo. *Mol. Ther.* **2005**, *11* (3), 418-425.

(83) Knorr, V.; Allmendinger, L.; Walker, G. F.; Paintner, F. F.; Wagner, E. An Acetal-Based PEGylation Reagent for pH-Sensitive Shielding of DNA Polyplexes. *Bioconjugate Chem.* **2007**, *18* (4), 1218-1225.

(84) Meyer, M.; Philipp, A.; Oskuee, R.; Schmidt, C.; Wagner, E. Breathing Life into Polycations: Functionalization with pH-Responsive Endosomolytic Peptides and Polyethylene Glycol Enables siRNA Delivery. *J. Am. Chem. Soc.* **2008**, *130* (11), 3272-3273.

(85) Pang, X.; Jiang, Y.; Xiao, Q.; Leung, A. W.; Hua, H.; Xu, C. pH-responsive polymer–drug conjugates: design and progress. *J. Controlled Release* **2016**, *222*, 116-129.

(86) Dirisala, A.; Uchida, S.; Li, J.; Van Guyse, J. F. R.; Hayashi, K.; Vummaleti, S. V. C.; Kaur, S.; Mochida, Y.; Fukushima, S.; Kataoka, K. Effective mRNA Protection by Poly(l-ornithine) Synergizes with Endosomal Escape Functionality of a Charge-Conversion Polymer toward Maximizing mRNA Introduction Efficiency. *Macromol. Rapid Commun.* **2022**, *14*, e2100754.

(87) Maier, K.; Wagner, E. Acid-labile traceless click linker for protein transduction. *J. Am. Chem. Soc.* **2012**, *134* (24), 10169-10173.

(88) Wickner, W.; Schekman, R. Protein Translocation Across Biological Membranes. *Science* **2005**, *310* (5753), 1452-1456.

(89) Dobson, C. M. Protein misfolding, evolution and disease. *Trends Biochem. Sci.* **1999**, *24* (9), 329-332.

(90) Stewart, M. P.; Sharei, A.; Ding, X.; Sahay, G.; Langer, R.; Jensen, K. F. In vitro and ex vivo strategies for intracellular delivery. *Nature* **2016**, *538* (7624), 183-192.

(91) Takayama, K.; Nakase, I.; Michiue, H.; Takeuchi, T.; Tomizawa, K.; Matsui, H.; Futaki, S. Enhanced intracellular delivery using arginine-rich peptides by the addition of penetration accelerating sequences (Pas). *J. Controlled Release* **2009**, *138* (2), 128-133.

(92) Jiang, Q.-Y.; Lai, L.-H.; Shen, J.; Wang, Q.-Q.; Xu, F.-J.; Tang, G.-P. Gene delivery to tumor cells by cationic polymeric nanovectors coupled to folic acid and the cell-penetrating peptide octaarginine. *Biomaterials* **2011**, *32* (29), 7253-7262.

(93) Khalil, I. A.; Kimura, S.; Sato, Y.; Harashima, H. Synergism between a cell penetrating peptide and a pH-sensitive cationic lipid in efficient gene delivery based on double-coated nanoparticles. *J. Controlled Release* **2018**, *275*, 107-116.

(94) Sakamoto, K.; Morishita, T.; Aburai, K.; Ito, D.; Imura, T.; Sakai, K.; Abe, M.; Nakase, I.; Futaki, S.; Sakai, H. Direct entry of cell-penetrating peptide can be controlled by maneuvering the membrane curvature. *Sci. Rep.* **2021**, *11* (1), 1-9.

(95) Boeckle, S.; Wagner, E.; Ogris, M. C- versus N-terminally linked melittin-polyethylenimine conjugates: the site of linkage strongly influences activity of DNA polyplexes. *J. Gene Med.* **2005**, *7* (10), 1335-1347.

(96) Meyer, M.; Dohmen, C.; Philipp, A.; Kiener, D.; Maiwald, G.; Scheu, C.; Ogris, M.; Wagner, E. Synthesis and biological evaluation of a bioresponsive and endosomolytic siRNA− polymer conjugate. *Mol. Pharmaceutics* **2009**, *6* (3), 752-762.

(97) Wang, A.; Zheng, Y.; Zhu, W.; Yang, L.; Yang, Y.; Peng, J. Melittin-Based Nano-Delivery Systems for Cancer Therapy. *Biomolecules* **2022**, *12* (1), 118.

(98) Li, Z.; Zhao, R.; Wu, X.; Sun, Y.; Yao, M.; Li, J.; Xu, Y.; Gu, J. Identification and characterization of a novel peptide ligand of epidermal growth factor receptor for targeted delivery of therapeutics. *FASEB J.* **2005**, *19* (14), 1978-1985.

(99) Schafer, A.; Pahnke, A.; Schaffert, D.; van Weerden, W. M.; de Ridder, C. M.; Rodl, W.; Vetter, A.; Spitzweg, C.; Kraaij, R.; Wagner, E.; Ogris, M. Disconnecting the yin and yang relation of epidermal growth factor receptor (EGFR)-mediated delivery: a fully synthetic, EGFR-targeted gene transfer system avoiding receptor activation. *Hum. Gene Ther.* **2011**, *22* (12), 1463-1473.

(100) Mickler, F. M.; Mockl, L.; Ruthardt, N.; Ogris, M.; Wagner, E.; Brauchle, C. Tuning nanoparticle uptake: live-cell imaging reveals two distinct endocytosis mechanisms mediated by natural and artificial EGFR targeting ligand. *Nano Lett.* **2012**, *12* (7), 3417-3423.

(101) Müller, K.; Klein, P. M.; Heissig, P.; Roidl, A.; Wagner, E. EGF receptor targeted lipo-oligocation polyplexes for antitumoral siRNA and miRNA delivery. *Nanotechnology* **2016**, *27* (46), 464001.

(102) Schmohl, K. A.; Gupta, A.; Grunwald, G. K.; Trajkovic-Arsic, M.; Klutz, K.; Braren, R.; Schwaiger, M.; Nelson, P. J.; Ogris, M.; Wagner, E.; Siveke, J. T.; Spitzweg, C. Imaging and targeted therapy of pancreatic ductal adenocarcinoma using the theranostic sodium iodide symporter (NIS) gene. *Oncotarget* **2017**, *8* (20), 33393-33404.

(103) Wang, Y.; Luo, J.; Truebenbach, I.; Reinhard, S.; Klein, P. M.; Höhn, M.; Kern, S.; Morys, S.; Loy, D. M.; Wagner, E.; Zhang, W. Double click-functionalized siRNA polyplexes for gene silencing in epidermal growth factor receptor-positive tumor cells. *ACS Biomater. Sci. Eng.* **2020**, *6* (2), 1074-1089.

(104) Genta, I.; Chiesa, E.; Colzani, B.; Modena, T.; Conti, B.; Dorati, R. GE11 Peptide as an Active Targeting Agent in Antitumor Therapy: A Minireview. *Pharmaceutics* **2017**, *10* (1), 2.

(105) Zhou, C.; Xia, Y.; Wei, Y.; Cheng, L.; Wei, J.; Guo, B.; Meng, F.; Cao, S.; van Hest, J. C. M.; Zhong, Z. GE11 peptide-installed chimaeric polymersomes tailor-made for high-efficiency EGFR-targeted protein therapy of orthotopic hepatocellular carcinoma. *Acta Biomater.* **2020**, *113*, 512-521.

(106) Meyer, M.; Zintchenko, A.; Ogris, M.; Wagner, E. A dimethylmaleic acid–melittin-polylysine conjugate with reduced toxicity, pH-triggered endosomolytic activity and enhanced gene transfer potential. *J. Gene Med.* **2007**, *9* (9), 797-805.

(107) Jin, Q.; Deng, Y.; Chen, X.; Ji, J. Rational design of cancer nanomedicine for simultaneous stealth surface and enhanced cellular uptake. *ACS Nano* **2019**, *13* (2), 954-977.

(108) Zhou, Z.; Shen, Y.; Tang, J.; Fan, M.; Van Kirk, E. A.; Murdoch, W. J.; Radosz, M. Charge-reversal drug conjugate for targeted cancer cell nuclear drug delivery. *Adv. Funct. Mater.* **2009**, *19* (22), 3580-3589.

(109) Mei, C.; Wang, N.; Zhu, X.; Wong, K. H.; Chen, T. Photothermal-controlled nanotubes with surface charge flipping ability for precise synergistic therapy of triple-negative breast cancer. *Adv. Funct. Mater.* **2018**, *28* (45), 1805225.

(110) Lee, Y.; Ishii, T.; Cabral, H.; Kim, H. J.; Seo, J.-H.; Nishiyama, N.; Oshima, H.; Osada, K.; Kataoka, K. Charge-Conversional Polyionic Complex Micelles—Efficient Nanocarriers for Protein Delivery into Cytoplasm. *Angew. Chem., Int. Ed. Engl.* **2009**, *48* (29), 5309-5312.

(111) Grebenok, R. J.; Pierson, E.; Lambert, G. M.; Gong, F. C.; Afonso, C. L.; Haldeman-Cahill, R.; Carrington, J. C.; Galbraith, D. W. Green-fluorescent protein fusions for efficient characterization of nuclear targeting. *Plant J.* **1997**, *11* (3), 573-586.

(112) Patel, S. G.; Sayers, E. J.; He, L.; Narayan, R.; Williams, T. L.; Mills, E. M.; Allemann, R. K.; Luk, L. Y.; Jones, A. T.; Tsai, Y.-H. Cell-penetrating peptide sequence and modification dependent uptake and subcellular distribution of green florescent protein in different cell lines. *Sci. Rep.* **2019**, *9* (1), 1-9.

(113) Rosenblum, D.; Joshi, N.; Tao, W.; Karp, J. M.; Peer, D. Progress and challenges towards targeted delivery of cancer therapeutics. *Nat. Commun.* **2018**, *9* (1), 1-12.

(114) Li, R.; Ma, Y.; Dong, Y.; Zhao, Z.; You, C.; Huang, S.; Li, X.; Wang, F.; Zhang, Y. Novel paclitaxel-loaded nanoparticles based on human H chain ferritin for tumor-targeted delivery. *ACS Biomater. Sci. Eng.* **2019**, *5* (12), 6645-6654.

(115) Sadhukhan, P.; Kundu, M.; Chatterjee, S.; Ghosh, N.; Manna, P.; Das, J.; Sil, P. C. Targeted delivery of quercetin via pH-responsive zinc oxide nanoparticles for breast cancer therapy. *Mater. Sci. Eng.: C* **2019**, *100*, 129-140.

(116) Müller, K.; Kessel, E.; Klein, P. M.; Höhn, M.; Wagner, E. Post-PEGylation of siRNA lipo-oligoamino amide polyplexes using tetra-glutamylated folic acid as ligand for receptor-targeted delivery. *Mol. Pharmaceutics* **2016**, *13* (7), 2332-2345.

(117) Kos, P.; Lächelt, U.; He, D.; Nie, Y.; Gu, Z.; Wagner, E. Dual-targeted polyplexes based on sequence-defined peptide-PEG-oligoamino amides. *J. Pharm. Sci.* **2015**, *104* (2), 464-475.

(118) Morys, S.; Urnauer, S.; Spitzweg, C.; Wagner, E. EGFR targeting and shielding of pDNA lipopolyplexes via bivalent attachment of a sequence-defined PEG agent. *Macromol. Biosci.* **2018**, *18* (1), 1700203.

(119) Du, J.-Z.; Sun, T.-M.; Song, W.-J.; Wu, J.; Wang, J. A Tumor-Acidity-Activated Charge-Conversional Nanogel as an Intelligent Vehicle for Promoted Tumoral-Cell Uptake and Drug Delivery. *Angew. Chem., Int. Ed. Engl.* **2010**, *49* (21), 3621-3626.

(120) Kim, A.; Miura, Y.; Ishii, T.; Mutaf, O. F.; Nishiyama, N.; Cabral, H.; Kataoka, K. Intracellular delivery of charge-converted monoclonal antibodies by combinatorial design of block/homo polyion complex micelles. *Biomacromolecules* **2016**, *17* (2), 446-453.

(121) Lee, E. S.; Gao, Z.; Bae, Y. H. Recent progress in tumor pH targeting nanotechnology. *J. Controlled Release* **2008**, *132* (3), 164-170.

(122) Boeckle, S.; Fahrmeir, J.; Roedl, W.; Ogris, M.; Wagner, E. Melittin analogs with high lytic activity at endosomal pH enhance transfection with purified targeted PEI polyplexes. *J. Controlled Release* **2006**, *112* (2), 240-248.

(123) Wang, Y.; Shen, N.; Sakurai, K.; Tang, Z. Multi-stimuli-responsive polymeric prodrug for enhanced cancer treatment. *Macromol. Biosci.* **2019**, *19* (12), e1900329.

(124) Peeler, D. J.; Sellers, D. L.; Pun, S. H. pH-Sensitive Polymers as Dynamic Mediators of Barriers to Nucleic Acid Delivery. *Bioconjugate Chem.* **2019**, *30* (2), 350-365.

(125) Braakman, I.; Lamriben, L.; van Zadelhoff, G.; Hebert, D. N. Analysis of disulfide bond formation. *Curr. Protoc. Protein Sci.* **2017**, *90* (1), 14.11.11-14.11.22.

(126) Dunker, A. K.; Kenyon, A. J. Mobility of sodium dodecyl sulphate - protein complexes. *Biochem. J.* **1976**, *153* (2), 191-197.

(127) Rawat, S.; Suri, C. R.; Sahoo, D. K. Molecular mechanism of polyethylene glycol mediated stabilization of protein. *Biochem. Biophys. Res. Commun.* **2010**, *392* (4), 561-566.

(128) Kanamala, M.; Wilson, W. R.; Yang, M.; Palmer, B. D.; Wu, Z. Mechanisms and biomaterials in pH-responsive tumour targeted drug delivery: a review. *Biomaterials* **2016**, *85*, 152-167.

(129) Mao, J.; Li, Y.; Wu, T.; Yuan, C.; Zeng, B.; Xu, Y.; Dai, L. A simple dual-pH responsive prodrug-based polymeric micelles for drug delivery. *ACS Appl. Mater. Interfaces* **2016**, *8* (27), 17109-17117.

(130) Tangsangasaksri, M.; Takemoto, H.; Naito, M.; Maeda, Y.; Sueyoshi, D.; Kim, H. J.; Miura, Y.; Ahn, J.; Azuma, R.; Nishiyama, N.; Miyata, K.; Kataoka, K. siRNA-loaded polyion complex micelle decorated with charge-conversional polymer tuned to undergo stepwise response to intra-tumoral and intra-endosomal pHs for exerting enhanced RNAi efficacy. *Biomacromolecules* **2016**, *17* (1), 246-255.

(131) Pham, T. C.; Jayasinghe, M. K.; Pham, T. T.; Yang, Y.; Wei, L.; Usman, W. M.; Chen, H.; Pirisinu, M.; Gong, J.; Kim, S.; Peng, B.; Wang, W.; Chan, C.; Ma, V.; Nguyen, N. T. H.; Kappei, D.; Nguyen, X.-H.; Cho, W. C.; Shi, J.; Le, M. T. N. Covalent conjugation of extracellular vesicles with peptides and nanobodies for targeted therapeutic delivery. *J. Extracell. Vesicles* **2021**, *10* (4), e12057.

(132) Ahmad, A.; Khan, J. M.; Haque, S. Strategies in the design of endosomolytic agents for facilitating endosomal escape in nanoparticles. *Biochimie* **2019**, *160*, 61-75.

(133) Kilchrist, K. V.; Dimobi, S. C.; Jackson, M. A.; Evans, B. C.; Werfel, T. A.; Dailing, E. A.; Bedingfield, S. K.; Kelly, I. B.; Duvall, C. L. Gal8 visualization of endosome disruption predicts carrier-mediated biologic drug intracellular bioavailability. *ACS Nano* **2019**, *13* (2), 1136-1152.

(134) Rui, Y.; Wilson, D. R.; Tzeng, S. Y.; Yamagata, H. M.; Sudhakar, D.; Conge, M.; Berlinicke, C. A.; Zack, D. J.; Tuesca, A.; Green, J. J. High-throughput and high-content

bioassay enables tuning of polyester nanoparticles for cellular uptake, endosomal escape, and systemic in vivo delivery of mRNA. *Science advances* **2022**, *8* (1), eabk2855.

(135) Ogris, M.; Carlisle, R. C.; Bettinger, T.; Seymour, L. W. Melittin enables efficient vesicular escape and enhanced nuclear access of nonviral gene delivery vectors. *J. Biol. Chem.* **2001**, *276* (50), 47550-47555.

(136) Oude Blenke, E.; Sleszynska, M.; Evers, M.; Storm, G.; Martin, N.; Mastrobattista, E. Strategies for the activation and release of the membranolytic peptide melittin from liposomes using endosomal pH as a trigger. *Bioconjugate Chem.* **2017**, *28* (2), 574-582.

(137) Cheng, Y.; Yumul, R. C.; Pun, S. H. Virus-Inspired Polymer for Efficient In Vitro and In Vivo Gene Delivery. *Angew. Chem., Int. Ed. Engl.* **2016**, *55* (39), 12013-12017.

(138) Feldmann, D. P.; Cheng, Y.; Kandil, R.; Xie, Y.; Mohammadi, M.; Harz, H.; Sharma, A.; Peeler, D. J.; Moszczynska, A.; Leonhardt, H.; Pun, S. H.; Merkel, O. M. In vitro and in vivo delivery of siRNA via VIPER polymer system to lung cells. *J. Controlled Release* **2018**, *276*, 50-58.

(139) Peeler, D. J.; Thai, S. N.; Cheng, Y.; Horner, P. J.; Sellers, D. L.; Pun, S. H. pH-sensitive polymer micelles provide selective and potentiated lytic capacity to venom peptides for effective intracellular delivery. *Biomaterials* **2019**, *192*, 235-244.

(140) Paray, B. A.; Ahmad, A.; Khan, J. M.; Taufiq, F.; Pathan, A.; Malik, A.; Ahmed, M. Z. The role of the multifunctional antimicrobial peptide melittin in gene delivery. *Drug Discovery Today* **2021**, *26* (4), 1053-1059.

(141) Delinois, L. J.; De León-Vélez, O.; Vázquez-Medina, A.; Vélez-Cabrera, A.; Marrero-Sánchez, A.; Nieves-Escobar, C.; Alfonso-Cano, D.; Caraballo-Rodríguez, D.; Rodriguez-Ortiz, J.; Acosta-Mercado, J.; Benjamín-Rivera, J. A.; González-González, K.; Fernández-Adorno, K.; Santiago-Pagán, L.; Delgado-Vergara, R.; Torres-Ávila, X.; Maser-Figueroa, A.; Grajales-Avilés, G.; Méndez, G. I. M.; Santiago-Pagán, J.; Nieves-Santiago, M.; Álvarez-Carrillo, V.; Griebenow, K.; Tinoco, A. D. Cytochrome c: Using Biological Insight toward Engineering an Optimized Anticancer Biodrug. *Inorganics* **2021**, *9* (11), 83.

8 Publication

9 Acknowledgements

When I started writing the acknowledgement, I just realized that my PhD journey was coming to an end. These four years trained me to be an early career researcher with generous support from my supervisors, colleagues, friends and family. The thesis would not be possible to be accomplished without your help and I owe my deepest debt of gratitude to all of you!

I would like to initially express my heartfelt gratitude to Prof. Dr. Ernst Wagner, my supervisor, for giving me the opportunity to do my PhD in his research group. I greatly appreciate his scientific support, vital encouragement and professional guidance. He has walked me through all the stages of my PhD life. Without his consistent and illuminating instruction, this thesis could not have reached its present form.

Then, my special thanks go to my collaborator Mina who has given me great support for the cell culture experiments and helpful discussion when we face problems. I would also like to thank Yi for giving me generous support and helpful suggestions for the biology experiment.

I want to thank Ulrich for the good suggestions and comments on my project and thank Miriam for helping with the microscopy experiments. I would also like to thank Teoman, Simone and Tobias for the mass spectrometry measurement, and Bianca for the gel experiment. Many thanks to Xiaowen and Peng for giving me good experiences with synthesis.

Many thanks to Wolfgang for the support with our technical equipment, for repairing almost any broken instrument or computer and for ensuring the technical maintenance, as well as Olga, Miriam, Ursula and Melinda for keeping the lab running, so that we could focus on science issues due to their contributions to the group.

I would also like to thank our lunch group (Jie, Yanfang, Yi, Lun, Faqian, Fengrong and Xianjin) for the interesting and extensive discussions about science and life.

I also owe my sincere gratitude to my friends (Zhong Guo, Sha Li, Hongcheng Mai, Zhouyi Rong, Binhao Teng, Haijie Zhao, Qiao Tang and Xin Ma) who gave me their help and time by listening to me and helping me work out my problems during the difficulties in my PhD study.

Many thanks to all the AK Wagner members for giving me a comfortable learning atmosphere and an unforgettable time we spent together. Special thanks to Oversea Study Program of Guangzhou Elite Project (China) for supporting my study and life in Munich.

Then, my thanks would go to my beloved family for their loving consideration and great confidence in me all through these years. Their silent support gave me the courage and confidence to face whatever happens.

Finally, I really want to thank my wife who created a comfortable environment that allowed me to focus on my work without any worries, and also gave me some great advice in study and life.

These were the most memorable four years I have had. While challenging, it was undoubtedly exciting. I believe that what does not kill me makes me stronger and a better man.